STUDIES ON GROWTH AND CHARACTERIZATION OF SWIFT HEAVY ION IRRADIATED 2-AMINO-5-NITROPYRIDINE FAMILY OF CRYSTALS

A THESIS

Submitted by

M. AMBROSE RAJKUMAR

(Reg. No. 11657)

PHYSICS

in partial fulfillment of the requirements for the degree of

DOCTOR OF PHILOSOPHY

MANONMANIAM SUNDARANAR UNIVERSITY

TIRUNELVELI- 627012

NOVEMBER 2017

MANONMANIAM SUNDARANAR UNIVERSITY
TIRUNELVELI - 627 012

CERTIFICATE

The research work embodied in the present Thesis entitled **"STUDIES ON GROWTH AND CHARACTERIZATION OF SWIFT HEAVY ION IRRADIATED 2-AMINO-5-NITROPYRIDINE FAMILY OF CRYSTALS"** has been carried out in the **Department of Physics, St. Xavier's College (Autonomous), Palayamkottai – 627 002, Tamil Nadu**. The work reported herein is original and does not form part of any other thesis or dissertation on the basis of which a degree or award was conferred on an earlier occasion or to any other scholar.

I understand the University's policy on plagiarism and declare that the thesis and publications are my own work, except where specifically acknowledged and has not been copied from other sources or been previously submitted for award or assessment.

M. AMBROSE RAJKUMAR
RESEARCH SCHOLAR

Dr. D. PREM ANAND,
Head of the Department,
Department of Physics,
St. Xavier's College (Autonomous),
Palayamkottai – 627 002,
Tamil Nadu

ACKNOWLEDGEMENT

First and foremost, I would like to thank **God almighty** who blessed me and given wisdom to complete my research work.

I express my heartfelt gratitude to my guide **Dr. D. Prem Anand,** Head of the Department of Physics, St. Xavier's College (Autonomous), Palayamkottai, who has given an opportunity to do research under his guidance. He motivated and encouraged me in each and every step of my research work. He supported me, and constantly helped to shape my research work. It was a great privilege, and pleasure to work under his guidance.

I am thankful to **Rev. Dr. V. Britto, S.J.** Principal, and, **Rev. Dr. Gilburt Camillus, S.J.** former Principal, St. Xavier's College (Autonomous), Palayamkottai for their blessings and permission to pursue research in Physics research centre at St. Xavier's College (Autonomous), Palayamkottai.

My sincere thanks to **Rev. Dr. Danis Ponniah, S.J.** Provincial, Jesuit Madurai Province and former Rector of our college for his blessings, support and encouragement. I also extend my thanks to **Rev. Dr. D. Thomas Alexander, S.J.** Rector for his encouragement.

I express my deep gratitude to **Rev. Fr. Arul Ravi, S.J.** Director, St. Xavier's Hostel, St. Xavier's College (Autonomous), Palayamkottai for his motivation, encouragement and permission to stay in our college hostel to carry out my research work.

I offer my sincere thanks to **Prof. P. Ramasamy,** Director -Research, SSN College of Engineering and **Dr. M. Senthil Pandian,** Research Scientist, SSN College of Engineering, Chennai who gave me an opportunity to learn about Sankaranarayanan- Ramasamy (SR) method and valuable discussions about my research work.

I record my thanks to **Board of Research in Nuclear Sciences- Department of Atomic Energy (BRNS-DAE)** (File no: 2012/34/63/BRNS/2865 dt: 01 March 2013) for funding this major research project.

I am thankful to **Dr. P.K. Bajpai,** Research scientist National Centre for Accelerator based Research (NCAR), and Head of the Department of Pure and Applied Physics, Guru Ghasidas Vishwavidyalaya, Bilaspur, **Dr. S.P. Patel and Dr. T. Trivedi,** Assistant professor of Department of Pure and Applied Physics, Guru Ghasidas Vishwavidyalaya, Bilaspur, Chhattisgarh for their valuable guidance and help during irradiation.

I offer my sincere thanks to **Prof. S. Stanly John Xavier,** Co-Investigator, Board of Research in Nuclear Sciences- Department of Atomic Energy (BRNS-DAE) (File no: 2012/34/63/BRNS/2865 dt: 01 March 2013) major research project, **Dr. M. Julias Ceasar** (Department of Commerce), **Prof. M. Selvakumar** (HOD of Chemistry) and **Prof. C. Maria Magdalane** (Department of Chemistry) for their valuable guidance and motivation during my research work.

I thank **Dr. S. Paulraj**, **Dr. V. Sivashankar**, **Dr. G. David Rathinavelu, Dr. B. Helina, Dr. R. Mary Jenila (Vice principal), Dr. S. Anna Venus (Co- ordinator), Dr. S. G. Rejith, Prof. M. Augustin,** and **Dr. L. Arun Jose**

faculties, Department of physics, St. Xavier's College (Autonomous), Palayamkottai for their motivation and support.

I also grateful to my co researchers **Prof. Y. Samson, Dr. M.J. Jarald Brigth Gilda, Dr. S. Anbarasu, Dr. K. Daries Bella, Mrs. Muthurani, Ms. S. Sathya** and lab assistants **Mr. T. Joseph, Mr. Rajaguru @ Rex, Mr. Albin Jerome** for their timely help and support throughout my research work.

I am thankful to my friends **Dr. Manimuthu , Dr. Lenin, Dr. T. Mathivanan, Mr. M. Kumar, Mr. F. Patrick, and Bro. Karunakar, S.J. (Andhra Province**) for their valuable help, motivation, support and affectionate attitude and incomparable understanding.

I express my heartfelt gratitude to my parents **S. Mariadass, J. Esther Rani and my brother Rev. Fr. M. Devanesan** for their boundless love, motivation, constant support and encouragement. I am extremely grateful to them for the successful completion of the thesis and this research work would not be possible without their sacrifice.

I also extend my thanks to my relatives and friends who have directly and indirectly motivated and encouraged during my research.

The services rendered by SAIF, IIT Madras, St. Joseph's College, IISC, Bangalore, Noorul Islam University, Kumarakoil, Loyola College, and NCAR, Bilaspur, Manonmaniam Sundaranar University, Tirunelveli are gratefully acknowledged.

M. AMBROSE RAJKUMAR

CONTENTS

LIST OF TABLES

LIST OF FIGURES

LIST OF ABBREVIATIONS

2A5NPCl	2-amino-5-nitropyridinium chloride
2A5NPDP	2-amino-5-nitropyridinium dihydrogen phosphate
2A5NPHO	2-amino-5-nitropyridinium hydrogen oxalate
2A5NPS	2-amino-5-nitropyridinium sulfamate
α	Alpha
β	Beta
γ	Gamma
ε_r	Dielectric constant
θ	Theta
λ	Wavelength
μ	Micro
μ m	Micrometer
ν	Frequency
A	Ampere
Å	Angstrom
a, b, c	Unit cell parameters
ATR	Assembled Temperature Reduction
Au^+	Gold ion
d	Diagonal length of indentation
dE/dx	Electronic energy loss
dN/dx	Nuclear energy loss
DTA	Differential thermal analysis
FTIR	Fourier Transform Infra Red
H_v	Vickers hardness

Hz	Hertz
M eV	Million electron volt
mg	Milligram
MHz	Mega Hertz
n	Hardness coefficient
NLO	Nonlinear optics
nm	Nanometer
pnA	Particle nano Ampere
ppm	Parts per million
Real	Real part impedance
SONLO	Second Order Nonlinear Optics
TG	Thermogravimetric
UV	Ultra Violet
XRD	X- ray Diffraction

CHAPTER I
INTRODUCTION TO CRYSTAL GROWTH BY SOLUTION METHODS AND SWIFT HEAVY ION IRRADIATION

1.1 Introduction

Crystals are all around us everyday and we use them many ways ranging from ornaments to even to develop cutting edge technologies. Crystal is highly ordered atoms or microscopic particles in three dimensional manners. The uniformity of the single crystal allows transmission of electromagnetic waves without scattering. Developments have been done in science and technology, especially in the field of electronics, fiber optics and lasers since crystal plays a vital role in solid state devices. Progress in crystal growth and epitaxy technology is highly demanded. Conventional and modern method of single crystal growth plays an essential role for the development of production of high efficiency photovoltaic cells and detectrors for alternative energy and medicine and long life time light emitting diode (LED). Now a days a variety of crystals are needed to meet some very important gaps in conventional production engineering and finds application in lasers, nonlinear optics (NLO), light emitting diode (LED), pyroelectric detectors and optical components for communications. Semiconductor lasers, piezoelectric, ferroelectric and infrared sensitive crystals are part of several solid state devices in use today (Nalwa and Miyata 1996)**.** One of the new worlds created by laser is the field of nonlinear optics. Now, nonlinear optics (NLO) has become very important and an indispensable in the field of science, engineering and technology. It has become vast research in international arena. Nonlinear optical (NLO) materials have received much attention due to their potential applications such as optical data storage, colour display, optical communications, laser fusion etc (Haja Hameed et al 2006, X. Wang 2002).

Nonlinear optical materials exhibit prominent characteristics in terms of the fast and parallel processing of a signal, which are required for the applications of optical communications. Materials with large nonlinear optical coefficients and a wide transparency range have been investigated for a few decades. Thus the nonlinear optical crystals have played an important role in the field of engineering and technology. New nonlinear optical crystal, particularly for the ultraviolet (UV) and infrared (IR) spectral regions is still very active. Even though, scientist, researchers have been modified to enhance the properties of existing nonlinear optical materials by irradiation.

Ion induced modifications of solid has emerged as an area to quantify the properties of solids up to shallow depth in physics, chemistry, material science etc. Ion beam irradiation used in industrial, technical and medical applications for the compound formation, nano structure, thin film, biological diagnosis etc. One can modify materials using heavy ions of high energetic beams and we can acquire desired optical, electrical and mechanical properties. Researchers have been used energetic ion beam in different ways in material science. Effect of high energetic ion beam depends on the ion energy, fluence, and ion species. The interaction of the ion with materials is the deciding factor in the ion beam induced material modifications.

1.2 Nucleation

Nucleation, the initial process that occurs in the formation of a crystal from a solution, a liquid, (or) a vapour in which the series of atomic (or) molecular processes by which the atom (or) molecules of a reactant phase rearrange into a cluster of the product phase large enough as have to ability to grow irreversibly to a macroscopically larger size. The cluster is known as nucleus. Nucleation is one of the two major mechanisms of the first order phase transition, the process of generating a

new phase from an old phase whose free energy has become higher than that of emerging a new phase (Hohenberg and Halperin 1977; Chaikin and Lubensky 1995). Nucleation occurs vial the formation of small embryos of the new phase inside the large volume of the old phase. Nucleation can be classified into two types, (i) Primary (ii) Secondary. Further, primary nucleation is classed into two kinds (i) heterogeneous (ii) homogeneous. Surface of some different substance, such as a dust particle (or) the wall of the container, acts as the center upon which the first atoms, ions or molecules of the crystal become properly oriented. It is more common, it can be said simply heterogeneous nucleation would take place in the presence of foreign particles in the solution. Secondary nucleation takes place when nucleation is induced by the presence of crystals of the same substance. Most of the chemical industries, fertilizer industries, sugar industries and petro- chemical industries produce their products following the principle of secondary nucleation. The rate of nucleation is the number of nuclei formed per unit time per unit volume. Nucleation rate is virtually zero until a critical value of supersaturation is achieved, after which the rate increases exponentially.

1.3 Crystal growth techniques

Based on phase transformation, crystal growth techniques can be classed onto three types

(i) Solid growth (solid- solid phase transformation)

(ii) Solution growth (Liquid- solid phase transformation)

(iii) Vapour growth (Vapour – solid phase transformation)

1.3.1 Crystal growth from solution:

Crystal growth from solution is widely used than growth from melt and vapour phase. This method is widely used to grow the crystals, which have high solubility

and have variation in solubility with temperature (Chernov 1984). In this process, a saturated solution of the material in an appropriate solvent is used from which crystallization takes place as the solution becomes critically supersaturated. The supersaturated can be achieved either by lowering the temperature of the solution (or) by slow evaporation. The advantage of the method is that crystals can be prepared from a solution at temperatures well below its melting point, perhaps even at room temperature and therefore it turns out to be easily applicable in many cases (Pamplin 1980).

Crystal growth from solution can divides into two types.

(i) High temperature solution growth (ii) Low temperature solution growth. Further, low Temperature solution growth is classed into four types,

(i) Slow evaporation method (ii) Slow cooling method

(iii) Temperature gradient method (iv) Gel method

1.3.2 Advantageous of Solution Growth

(i) The growth process occurs near the ambient temperature.

(ii) Growth apparatus is relatively simple and cheap.

(iii) The concentration of structural imperfections in solution grown crystals is relatively low.

(iv) Sometimes, impurities may slow down the crystallization process by being adsorbed on the growing face of the crystal which changes the crystal habit.

(v) Low temperature introduces small thermal stress in the grown crystals.

(vi) The crystals obtained usually have well-developed faces which enable to investigate crystal growth process including insitu observations and capture impurities.

1.4 Solutions and Solvents

A solution is a homogeneous mixture of a solute in a solvent. Solute is the component, which is present in a smaller quantity and that one which gets dissolved in the solution. A good solvent should possess the following characteristics:

a. Moderate solubility

b. Positive temperature coefficient of solubility

c. A small vapour pressure

d. Non-corrosiveness

e. Non-toxicity

f. Non-flammability

g. Less volatility

1.5 Solubility and Supersolubility

Solubility of the material in a solvent decides the amount of the material, which is available for the growth and hence defines the total size limit. If the solubility is too high, it is difficult to grow bulk single crystals and too small a solubility restricts the size and growth rate of the crystals. Solubility gradient is another important parameter, which dictates the growth procedure. Neither a flat nor a steep solubility curve will enable the growth of bulk crystals from solution; while the level of supersaturation could not be varied by reducing the temperature in the former, even a small fluctuation in the temperature will affect the supersaturation to growth of good quality bulk crystals in both cases. If the solubility gradient is very small, slow evaporation of the solvent is the other option for crystal growth to maintain the supersaturation in the solution. Growth of crystals from solution is mainly a diffusion-controlled process; the medium must not be viscous to enable faster transference of the growth units from the bulk solution by diffusion (Santhanaraghavan and

Ramasamy 2001). Hence, a solvent with less viscosity is preferable. Supersaturation is an important parameter for the solution growth process. The crystal grows by the accession of the solute in the solution as a degree of supersaturation is maintained. The solubility data at various temperatures are essential to determine the level of supersaturation. Hence, the solubility of the solute in the chosen solvent must be determined before starting the growth process. The solubility of the solute may be determined by dissolving the solute in the solvent maintained at a constant temperature with continuous stirring. On reaching saturation, the equilibrium concentration of the solute may be determined gravimetrically. A sample of the clear supernatant liquid is withdrawn by means of warmed pipette and a weighted quantity of the sample is analysed. By repeating the above procedure for different temperatures, the solubility curve can then be plotted. The whole concentration-temperature field is separated by the saturated-solution line (solubility curve) into two regions; unsaturated and supersaturated solutions. Saturated solutions are those mixtures, which can retain their equilibrium indefinitely in contact with the solid phase with respect to which they are saturated. The solubility of most substances increases with temperature (the temperature coefficient of the solubility is positive). Crystals can be grown only from supersaturated solutions, which contain an excess of the solute above the equilibrium value. The region of supersaturated solutions can be divided into two sub-regions; metastable (stable) and labile (unstable) zones. Nucleation will occur spontaneously in the labile zone. Metastable zone refers to the level of supersaturation where spontaneous nucleation cannot occur and a seed crystal is essential to facilitate growth. The diagram is divided into three zones, which are termed as region stable (I), region metastable (II) and region labile (III). Region I corresponds to the undersaturated zone, where crystallisation is not possible. This

region is thermodynamically stable. The region II between the supersolubility curve and the solubility curve is termed as metastable zone where spontaneous crystallization is improbable. Seeded crystal growth can be achieved in this region. The unstable or labile zone where the spontaneous nucleation is more probable is termed as region III (Figure 1.1).

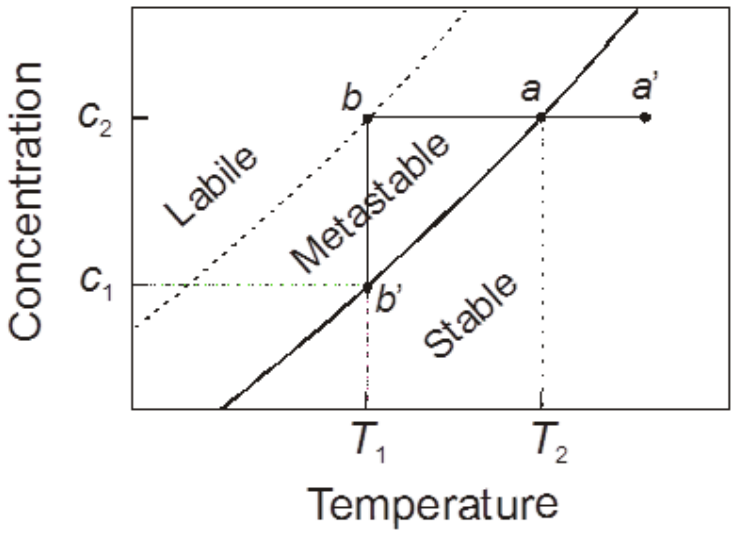

Fig. 1.1 Solubility diagram showing different levels of saturation

1.6 Slow evaporation method

In this method, an excess of a given solute is established by utilizing the difference between the rates of evaporation of the solvent and the solute. In contrast to the cooling method, in which the total mass of the system remains constant, in the solvent evaporation method, the solution loses particles, which are weakly bound to other components, and, therefore, the volume of the solution decreases. In almost all cases, the vapour pressure of the solvent above the solution is higher than the vapour pressure of the solute and, therefore, the solvent evaporates more rapidly and the solution becomes supersaturated. Usually, it is sufficient to allow the vapour formed above the solution to escape freely into the atmosphere. This is the oldest method of crystal growth and technically, it is very simple.

1.7 Slow cooling method

This is the best method among others to grow bulk single crystals from solution. In this method, supersaturation is produced by a change in temperature usually throughout the whole crystallizer. The crystallization process is carried out in such a way that the point on the temperature dependence of the concentration moves into the metastable region along the saturation curve in the direction of lower solubility. Since the volume of the crystallizer is finite and the amount of substance placed in it is limited, the supersaturation requires systematic cooling. It is achieved by using a thermostated crystallizer and volume of the crystallizer is selected based on the desired size of the crystals and the temperature dependence of the solubility of the substance.

1.7.1 Preparation of Solutions

Preparation of solution to grow the desired crystals by solution growth technique is an important stage of crystal growth. The solution is saturated as per the solubility data obtained from the solubility diagram (accurate solubility-temperature data). The saturated solution is filtered using the filter paper. The filtered solution is transferred into the growth beaker and placed in the Constant temperature bath (CTB). The desired supersaturation required is obtained by just lowering the temperature. Extreme care is to be taken to avoid undersaturation, which results in the dissolution of seed crystal. Similarly high supersaturation is also to be avoided` to prevent the formation of spurious nucleation. The growth vessel is hermetically sealed to avoid the evaporation of the solvent. The solution is tested for saturation by suspending small test seed crystal in the solution. If the system is not in equilibrium, the seed crystal either dissolves or the solute will crystallize on the seed. By adjusting the

temperature, the necessary equilibrium condition is achieved and the test seed crystal is removed and a fresh seed crystal is introduced for crystal growth.

1.7.2 Seed Preparation

The quality of the crystal grown very much depends on the quality of the seed crystals used. Small seed crystals can be obtained by spontaneous nucleation in the labile region of the supersaturated solution. A seed used to grow a large uniform crystal must be single crystal free of inclusions, cracks, block boundaries, sharp cleaved edges, twinning and any other obvious defects. It should be of minimum size, compatible with other requirements. When larger crystals of the same material are already available, they can be cut in the required orientation to fabricate the seed crystal. Since the growth rate of the crystal depends on the crystallographic orientation, the seed crystal must be cut in such a way that it has larger cross-section in the fast growing direction.

1.7.3 Cooling Rate

To obtain the required supersaturation, a driving force for the growth of crystal, the temperature of the growth solution is lowered. The cooling rate is to be employed according to the growth rate of the crystals. A large cooling rate changes the solubility beyond metastable limit and fluctuations in the supersaturation may encourage inclusions. A proper balance between temperature lowering rate and growth rate will yield good quality crystal.

1.8 Sankaranarayanan-Ramasamy (SR) Method

Sankaranarayanan and Ramasamy method has been developed to grow large size single crystal in a particular direction. It is one of the methods to grow the crystals from solution. In comparison with other methods for single crystal preparation this method easily controlled the orientation and it achieves a higher

crystallization rate. Simple and less expensive experimental set up of this method can be easily installed in any laboratory. At present, there is a lot of literature available which made use of SR method to grow crystals of different kinds like organics, inorganics and semiorganics.

1.8.1 Experimental Setup

1.2 Experimental setup of Sankaranarayanan- Ramasamy (SR) method

The experimental setup is shown in Figure 1.2. It consists of a growth ampoule made out of glass. An outer glass shield tube protects and holds the inner growth ampoule. It consists of two ring heaters, growth ampoule, water bath, temperature controllers, ammeters, transformers and sensors. The ring heaters were controlled by temperature controller arrangement to maintain the heater voltage and it provides the necessary temperature for solvent evaporation and for growing crystals. The ring heater was playing a major role in this novel unidirectional SR method. A ring heater positioned at the top of the growth ampoule was connected to the temperature controller and it provides the necessary temperature for solvent evaporation. The temperature around the growth ampoule was selected based on the solvent used and was controlled with the aid of the temperature controller. Depending on the growth rate of the crystal, the ring heater was moved downwards using a translation mechanism. The entire arrangement was placed in the water bath to reduce

the temperature fluctuation. Thermometers show the temperatures near the heating coils. In SR method the following main points have to be considered i.e. concentration of the solution, ampoule size, selection of seed crystal orientation, seed mounting, temperature at top and bottom portion and growth rate. According to the solubility data, saturated solution was prepared and transferred to glass ampoule for collecting the seed crystal by slow evaporation solution technique (SEST). A thin plate like seed crystal was selected for unidirectional growth with specific direction. The saturation solution was fed into the glass ampoule. In the freshly prepared solution, the solute concentration was deliberately kept slightly under saturated in order to avoid any possible physical instability at the growth interface. In contrast to the conventional SEST method, in the SR method the crystal was restricted to grow with a specific orientation inside a glass ampoule. To achieve the constant growth rate, the solvent lost due to evaporation was compensated by adding freshly prepared solution.

1.9 NONLINEAR OPTICS (NLO)

Nonlinear optics (NLO) is the study of the interaction of intense electromagnetic fields with materials to produce modified fields that are different from the input field in phase, frequency, amplitude and polarization. Nonlinear optics holds the key for the future technology of photonics which would utilize optical frequency conversion, optical signal processing and image processing using ultra fast laser pulses. The advantages of photonics as compared to electronics are the gain in speed, band width and interconnectivity. The most commonly used nonlinear optical effects are of second order: frequency doubling and linear electro-optics. For these second order nonlinear optical effects, which also include optical sum and difference

frequency generation, optical parametric amplification and in most cases also photorefractive effects, noncentrosymmetry is required.

NLO processes can be viewed as dielectric phenomena. Electric fields that an applied dc field or a propagating electromagnetic wave when passes through the medium induces electron displacement. Electron that is bound to the nearby nuclei in the medium gets slightly perturbed by the external applied electromagnetic field and begins oscillating at the applied frequency. The magnitude of such an induced polarization (P) at modest field strengths will be proportional to the applied field and expressed as (Zernike and Midwinter 1973)

$$P = \chi E \qquad (1.1)$$

where E is the magnitude of the applied electric field and χ is the linear susceptibility of the material. The NLO phenomena occur at sufficiently intense fields. As the applied field strength increases (e.g., lasers) the polarization response of the medium is no longer linear as shown by the equation (1.1). The induced polarization (P) becomes a function of the applied field and is given by

$$P = \chi^{(1)} E^{(1)} + \chi^{(2)} E^{(2)} + \chi^{(3)} E^{(3)} + \ldots.$$

Where, $\chi^{(2)}$ and $\chi^{(3)}$ coefficients represent the second and third order susceptibilities of the medium respectively. Williams and Yariv put forth a chemically oriented picture to describe the connection between the nonlinear propagation response and applied electric field in medium. This description considers an individual molecular unit rather than a collection of molecular units to describe the NLO optical phenomena. The applied electric field competes with the interatomic binding forces, thereby permitting the electrons to move further away from the equilibrium positions giving rise to microscopic polarizability. The explanation of nonlinear optics lies in the way in which a beam of light propagates through a solid. The nuclei and the

associated electrons of the atoms in the solid are form electric dipoles. The electromagnetic radiation interacts with these dipoles causing them to oscillate, results in the dipoles themselves acting as sources of electromagnetic radiation. As the intensity of the incident radiation increases, the relation between the radiation and the amplitude of the vibration becomes nonlinear; this results in generation of frequencies that is different from those of incident fields. Thus second and higher harmonic generations occur. The properties like processibility and interfacing ability with other materials led to the way of study of NLO effects and introduction of new concepts.

1.9.1 General Requirements of NLO Crystals

An ideal nonlinear optical material should possess the following characteristics:

1. large nonlinear figure of merit for frequency conversion
2. high laser damage threshold
3. fast optical response time
4. wide phase matchable angle
5. architectural flexibility for molecular design and morphology
6. ability to process into crystals, thin films
7. optical transparency (no absorption at fundamental and SH wave lengths)
8. ease of fabrication
9. nontoxicity and good environmental stability
10. high mechanical strength and thermal stability
11. non- hygroscopic nature.

1.10 Inorganic crystals

Inorganic crystals are mostly ionic bonded; it is always easier to synthesize inorganic materials. Often these have high melting point and high degree of chemical inertness. High temperature oxide materials are well studied for diverse applications like piezoelectric, ferroelectricity and electro- optics. Some of the useful crystals discovered are Lithium Niobate ($LiNbO_3$), Potassium Niobate ($KNbO_3$), and its analogues, Potassium Titanyl phosphate (KTP) and its analogues; and β- Barium Borate. Many of these materials have been successfully used in commercial frequency doublers, mixers and parametric generators to provide coherent laser radiation at high efficiency in new regions of the spectrum inaccessible by other nonlinear optical crystal and conventional laser sources. The search for novel crystals with nonlinear optical (NLO) property is still challenge for scientists to fulfill molecular engineering application as the nonlinear optical crystals should possess high absorption edge, large birefringence and molecular hyperpolarizabilities. Second order nonlinear optical materials are used in optical switching (modulation), frequency conversion, and electro optical applications and material frequently used for these commercial purposes are inorganic. Generally the inorganic NLO crystals possess very good thermal and mechanical stability.

1.11 Organic Nonlinear Optical (NLO) Crystals

Organic materials are attracting a great deal of attention, as they have large optical susceptibilites, inherent ultrafast response time and high- optical thresholds for laser power compared with inorganic materials for laser power compared with inorganic materials. The search for organic NLO materials has been of great interest in the recent years, because of their significant impact in electro- optic effect and second harmonic generation, optical bistability, laser remote sensing, optical disc data

stroage, laser driven fusion, medical and spectroscopic image processing, colour display and optical communication. (Franken et al 196; D. Ulrich et al 1989; D.S. Chemla and J. Zyss 1987)**.** Organic materials with large hyperpolarizabilities have been widely used because of their donor and acceptor strength of π- electron conjugation path through charge transfer axis. The most widely used organic crystal for this type of applications is nitrophenol family such as NPNa, NPLi, NPk, 3-methyl-4-nitropyridine-1-oxide (POM), N- 4- nitrophenyl -(L)- prolinol (NPP) and 3- methyl- 4- methoxy- 4'-nitrostibene etc., (Chemla and Zyss 1987).

The advantages of organic nonlinear optical materials are

High second order nonlinear optical efficiency

Birefringence used for phase matching

Possibility to chemically engineer the molecular properties

However there are some drawbacks with organic NLO materials. **Disadvantages of organic crystals are**

- poor chemical, thermal and mechanical stability
- low damage threshold
- low optical transparency
- Lack of quality and lack growth as bulk size.

This can have important consequences for the structural perfection of the crystals.

1.12 Semiorganic nonlinear optical crystals

The most efficient crystalline organic materials exhibit large quadratic susceptibilities (χ^2) associated with a target transparency limit (λ= 500 nm cut off), in contrast to the cases on the inorganic materials, where weaker (χ^2) values are combined with a large transparency range (160-2000 nm). Therefore, two crystal-engineering routes (i) inorganic and organic may be suggested with a view to obtain

an optimal transparency and efficiency trade-off. In order to improve on these drawbacks a new type of hybrid organic- inorganic crystal was propsed in 1999. This type of material is composed of organic and inorganic ions. These organic- inorganic crystal are tried to combine the advantages of both organic and inorganic compounds to have convenient mechanical and thermal stabilities through the inorganic subnetwork and to exhibit large nonlinear optical efficient due to the grafted organic molecules (Manivannan et al 2005, Horiuchi et al 2002). Semiorganics are primarily classified into two categories, type I and type II. Type I semiorganics are inorganic salts of large conjugated organic molecules. The organic part in type I are generally chiral compounds like tartrates, oxalates and a host of amino acids. L-Arginine phosphate monohydrate (LAP) is a typical example of this class. Type II semiorganics are coordination complexes of polarizable organics bonded to metal atoms. The metal atoms help in forming relatively strong coordinate bonds resulting in better thermal and mechanical stability. Zinc tris (thiourea) sulphate belongs to this class, with zinc bonded to three thiourea molecules and a sulphate ion. One of the advantages of semiorganics is that the bonding schemes are three dimensional, unlike polar organic crystals and hence result in stubbier habit. Presently, inorganic and organic materials are replaced by semiorganic materials.

1.13 2-amino-5-nitropyridine

2-amino-5-nitropyridine has an interesting molecular structure, which has a nitro group as an electron donor and amino group as an electron acceptor. Further, the pyridine ring acts as a cationic bonding site, the nitro group as hydrogen acceptor, and the amino group as a hydrogen donor. Because of this special molecular structure, it has been commonly used as molecular building blocks of nonlinear optical materials, which have been the subject of very intensive studies in the last few years for their

potential applicability in image processing and optical communications. It has also been used within hydrogen- bonded organic anionic networks, or as counterions in organic- inorganic salts. 2-amino-5-nitropyridine has a nitro group as an electron acceptor and an amino group as an electron donor to induce high NLO character. 2-amino-5-notropyridine is an organic chromophore known for its second- order non-linear optical properties due to its high hyperpolarizability (27.0 x 10^{-30} esu). The protonated cation of this organic base can form compounds with several types of anions, and, in some cases, materials exhibiting second harmonic generation SHG. The association of 2- amino- 5-nitropyridine with some specific anions has resulted in compounds with improved chemical and thermal stability and mechanical resistance which are important factors to consider for the design of the nonlinear optical materials. 2-amino-5-nitropyrine has high hyperpolarizability (27.0 x 10^{-30} esu) along with specific interest such as the presence of at least three hydrogen nonding sotes owing to the amino group and the easily protonated nitrogen atom which provide strong anchoring to the counter anions and the blue- shifted absorption relative to p- nitroaniline- like molecules resulting from a heteroatom in the α-position with respect to the amino group, suggesting applications in blue light second- harmonic generation. Through several crystal structure determinations, it has been observed that shielding effect originating from anionic matrixes is responsible for the acentric packing of the 2-amino-5-nitropyrine cation.

1.14 Review of 2-amino-5-nitropyrine derivative crystals

Busby and Creighton (1982) evaluated the SERS (surface enhanced Raman spectrum) enhancement factor with particular interest in the contribution from high surface coverage. 2-mino-5-nitropyridine was used as convenient electrochemical probe since it could be shown to form a strongly bond complex. Masse and Zyss

(1991) designed new polar crystal which combines the advantages of both organic and inorganic materials. 2-amino-5-nitropyridinium used as a cation. 2-amino-5-nitropyridinium dihydrogen monophosphate (2A5NPDP) crystal structure was solved. Properties of 2-amino-5-nitropyridinium dihydrogen monophosphate (2A5NPDP) was studied and was displayed high NLO efficiency with crystal nonlinear co-efficients are d_{15} = 7.2 p m/V and d_{24}= 1.3 p m/V (Koter et al 1992) Zyss et al (1993) had studied perfection of polar alignment of nonlinear chromophores in a crystalline H- bonded guest-host structure: 2-amino-5-nitropyridinium-L-monohydrogentartrate. 2-amino-5-nitropyridine- L-(+)- tartrate, a new secomd harmonic generation crystal was synthsised by Osamu watanable et al (1993). Second harmonic generation was found to be very low because of the use of basic compounds with low hyperpolaeizability (β). Pecaut and Masse (1993) provided a step towards a new route to obtain non-linear optical crystals which containing a highly polarizable 2-amino-5-nitropyridinium cation and inorganic anionic host matrices and new structure of semiorganic crystal of bis 2-amino-5-nitropyridinium dichromate was solved. Pecaut et al (1993) were prepared 2-amino-5-nitropyridinium halides (Cl^-, Br^-). The non-centrosymmetry frame work was shown high second harmonic generation. Relation between surface enhanced Raman intensity and surface concentration for 2-amino-5-nitropyridine adsorbed on roughened polycrystalline silver electrodes were studied and stability of surface was studied by Foresti et al (1994). A new nonlinear optical crystal of 2-amino-5-nitropyridinium acetophosphate was designed using molecular stimulation program containing the 2-amino-5-nitropyridinium chromophores Pecaut and Masse at al 1994. Foresti et al (1994) explained adsorption of 2-amino-5-nitropyridine on the (111) and (210) solver faces and elucidated the surface concentration obtained by stepping the applied potential. Maurzio Muniz- Miranda et

al (1995) explained experimentally the effect of halide anion on surface enhanced Raman scattering of 2-amino-5-nitropyridineadsorbed on solver sols. New noncentro symmetric structures containing herringbone motifs of molecular entities engineered using 2-amino-5-nitropyridine and n- chloroacetic acid assemblies by Yvette Le Fur et al (1996). Oussaid at al (1996) have been studied Raman scattering in 2-amino-5-nitropyridine – L- (+) tartrate single crystals at room temperature and at 10 K. They explained crystal of monoclinic symmetry space group ($P2_1$) underwent to detectable structural phase transition between these two temperatures. The potonation effect on the first hyperpolarizability (β) of 2-amino-5-nitropyridine was examined by Hyper-Rayleigh scattering technique and hyperpolarizability (β) value of the protonated 2-amino-5-nitropyridine in acetone was determined by Horiuchi et al (1997). Anna Puig- Molina et al (1998) studied experimentally electron density distribution and topological analysis of 2-amino-5-nitropyridinium dihydrogen phosphate (2A5NPDP). They showed that the crystal H- bond frame work involved four anions and one cation. Zaccaro et al (1998) explained the synthesis and structural characterization by X- ray diffraction of 2-amino-5-nitropyridinium dihydrogen phosphate (2A5NPDP) by using a continuous hybrid solid solution. This leads to the production of large and optically clear crystal using an original vertical temperature-gradient method. Feve et al (1999) presented a comparative study of the linear and nonlinear optical properties of two semiorganic crystals of 2-amino-5-nitropyridinium dihydrogen phosphate (2A5NPDP) and 2-amino-5-nitropyridinium dihydrogen arcenates (2A5NPDAs). Refractive indices from direct prism and angular noncritically phase- matched second harmonic generation (SHG) were determined experimentally. Horiuchi et al (1999) shown 2-amino-5-nitropyridinium chloride (2A5NPCl) crystal was efficient to convert the frequency of the incident beam up to

440 nm by using phase matching second harmonic generation. Horiuchi et al (2002) experimentally determined the quadratic nonlinear coefficients of the organic-inorganic 2-amino-5-nitropyridinium chloride (2A5NPCl) crystal by second harmonic generation. By comparing 2-amino-5-nitropyridinium chloride (2A5NPCl) crystal with other crystals of the P- notroaniline family, it was found that 2-amino-5-nitropyridinium chloride (2A5NPCl) crystal was advantageous for the generation of the short wavelength until 410 nm and its figure of merit was superior to that of the 2-amino-5-nitropyridinium dihydrogen phosphate (2A5NPDP) crystal. The optical power limiting properties of a 2-amino-5-nitropyridinium dihydrogen phosphate (2A5NPDP) crystal and two steps nonlinear process were described by Morel et al (2002). Turnbull Mark et al (2002) explained the synthesis, structure and magnetic susceptibility of two 5-nitro-2- aminopyridinium cuprates: $(5\text{-NAP})_2$ Cu Cl_4 and the quantum magnetic ladder $(5\text{-NAP})_2$ $CuBr_4$ H_2O. Cocrystals were prepared for second order nonlinear optical materials by using 2-amino-5-nitropyridine with benzenesulfonic acids by Hideko Koshima et al (2004). Dhanuskodi and Manikandan (2004) studied single crystal EPR study on γ-irradiated nonlinear optical material of 2-amino-5-nitropyridinium chloride (2A5NPCl) and principal values of the g- tensor and A-tensor were also determined. Semiorganic nonlinear optical material for short wavelength generation, 2-amino-5-nitropyridinium bromide (2A5NPBr) was prepared and it was proved experimentally that it is suitable for short wavelength generation by Dhanuskodi et al (2005). Manivannan et al (2005) designed a new semiorganic nonlinear crystal for short wavelength generation: 2-amino-5-nitropyridinium tetrafluoroborate (2A5NPFB). The large poeder second harmonic generation efficiency of 2-amino-5-nitropyridinium tetrafluoroborate (2A5NPFB) is due to the sinsity of chromophores and it is the highest observed among the herringbone

structures built with the $2A5NP^+$ entity was also reported. Gamelas et al reported first time novel change transfer supramolecular assemblies with Keggin anions and 2-amino5-nitropyridine. Aakeroy et al studied intermolecular forces and polymorphism of 2-amino- 5-nitropyridine structure. Pricilla Jayakumari et al (2007) have reported spectral and optical studies of 2-amino-5-nitropyridinium dihydrogen phosphate (2A5NPDP). 2-amino-5-nitropyridinium dihydrogen phosphate (2A5NPDP) has a good optical transmittance it is suitable for frequency doubling applications were also elucidated. Manikandan and Dhanuskodi (2007) modified 2-amino-5-nitropyridinium –L- tartrate using γ-ray. Alteration was done in such a way that the unpaired electron was coupled equivalently by three protons. Quanshi et al (2007) measured low- temperature heat capacity of 2-amino-5-nitropyridine, themal anomaly and thermodynamical function. Thermodynamical properties were further investigated through differential scanning calorimeter (DSC) and the themogravimetric (TG) analysis. The new organic- inorganic salt, 2-amino-5-nitropyridinium hydrogen selenate has been synthesized and its properties were also measured by Lorenc et al (2008). Surface- enhanced Raman scattering (SERS) spectra of 2-amino-5-nitropyridine (ANP) adsorbed on colloidal silver triangular nanoplates were obtained using samples with different meansize and surface plasma frequencies. Anandha Babu et al (2009) synthesized a new second harmonic generation (SHG) crystal of 2-amino-5-nitropyridinium toluenesulfonate. Optical and thermal properties were also measured. They were reported that 2-amino-5-nitropyridinium toluenesulfonate is a promising material for NLO applications. A new crystal of 2-amino-5-nitropyridinium hydrogen selenate was synthesized and structure was also solved by Samah Akriche and Mohamed Rzaigui (2010). Rodrigues et al (2009) synthesized and found a new structure of 2-amino-5-nitropyridinium

tetraoxidorhenate (VII) monohydrate. Anandha Babu et al (2011) synthesized a new second harmonic generation (SHG) crystal of 2-amino-5-nitropyridinium phenolsulfonate. The properties of new NLO single were also reported. Lin Chen et al (2013) synthesized and characterized a degradable polymides from (5-amino-2-pyridine). 80. Josephine Viavulamary Jovitha et al (2013) designed a new crystal of 2-amino-5- nitropyridinium trifluoroacetate and its structure was also solved. Sivasubramani et al (2015 and Sivasubramani et al 2016) elucidated the growth and properties of 2-amino-5-nitropyridinium nitrate (2A5NPN) and they explained that 2-amino-5-nitropyridinium nitrate (2A5NPN) is a promising third order nonlinear optical single crystal.

1.15 Swift heavy ions

First nuclear particle accelerator was built in 1930's. It was intended to probe into the nucleus by nuclear reactions. Since then, the particle accelerator was playing an important role in material science. Presently, accelerators which can deliver particles with an energy ranging from few kilo electron volts to several hundreds of giga electron volts are available. Particle or ion beams accelerated from these accelerators are classified into two, depending upon the energy imparted to the materials through which it passes. These are the low- energy and high energy heavy ion beams. Low energy ion beams have an energy ranging from few keV to few hundreds of keV, which losses energy to the material (up to 10 eV/ amu) through elastic collisions with the nucleus or atoms of the material. This type of energy loss is called 'nuclear energy loss' (dE/dx)n (Avasthi. D.K 2002) whereas high energy heavy ions known as "swift heavy ions (SHI)" have energy ranging from few tens of MeV to few GeV and losses energy to the target (1 MeV/amu) predominantly via inelastic collisions with the target material. These projectile ions impart energy

to the electron cloud and these electrons transfer energy to the lattice via electron-phonon interactions (Avasthi. D.K 2002). This type of energy loss is called 'electronic energy loss' (dE/dx)e, and in this case, the nuclear energy loss is very much negligible as compared to that of electronic energy loss.

1.16 Effects and use of swift heavy ions

As swift heavy ions (SHI) passes through the target material it produces electronic excitation of the atoms in the material. Effect of SHI is different in different class of materials. It is more active in insulators than in metals and semiconductors (Kraft et al 2002). Different models were proposed to explain the effect of SHI in materials, coulomb explosion (Schiwietz. et al 2001; Fleisher. R. L et al 1975; Akkermann et al 1992) and thermal spike model (Wolfgang Bolse 2002; Seitz and Koehler 1956; Wang et al 1994). During the passage of SHI through the materials, the target atoms are ionised by electronic excitation. As a result, a cylinder of positive ion was created along the path of ions. These positive ions are mutually repulsive and explode radially due to conversion of electrostatic energy to coherent radial atomic movements under coulomb forces until the ions are screened by conduction electrons. As a result, ion tracks may be formed along the path of the projectile ion due to radial coulomb explosion. This process viz., coulomb explosion, is predominant in insulators where there is little conduction electrons. According to thermal spike model, SHI transmits its energy to the electrons of target materials as kinetic energy via inelastic collision. This kinetic energy is transmitted to the lattice by electron-phonon interactions, resulting in the increase of lattice temperature above the melting point of the material, followed by rapid quenching. This leads to the formation of 'amorphous track' along the path of the projectile ion when the melt solidifies. Intense electronic energy deposition can be effectively used to modify material properties.

Electronic energy loss in the materials can be varied from few eV/Å up to few 10's of keV/Å by choosing appropriate ions and energies. This remarkable ability of SHI provides unique opportunity to engineer properties of materials. SHI irradiation is now considered as an advanced technique to modify structural, optical and optoelectronic properties of crystals through intense electronic energy deposition. Vast number of studies was reported on structural and micro structural phase transformation in poly crystalline and single crystal materials due to swift heavy ion irradiation (Schattat and Bolse 2004; Sathyavathi et al 1999; Ingram, and McCormick 1988; Benyagoub et al 2001; Gilbert- Mougel et al 2001; Nakao et al 1996; Balamurugan et al 2002; Kamboj et al 2002; Shah et al 1999, Suriya kumar et al 2009; Ramesh kumar et al 2007; Kanagasekaran et al 2010; Mythili et al 2008; Lian Zhang et al 2013; Ahlam et al 2012; Trautmann et al 2000; Kanagasekaran et al 2009; Krishnakumar et al 2007; Arun kumar et al 2012; Bhat et al 2000; Srinivasan et al 2007; Prabukanthan et al 2008; Prabha et al 2012; Bangaru 2011; Kumaresan et al 2008; Sangeetha et al 2011; Ananadha babu et al 2008). Tremendous energy deposition to the material can produce various changes in the material. It can produce columnar defect (Wolfgang and Beate 2002), point defect (Levalois and Marie1999) and even amorphous tracks along the path of its motion (Dufour et al 1993). Using ion beam irradiation, one can create new defects as well as anneal out pre- existing defects in materials (Sreekumar et al 2008; Kucheyev et al 2003). SHI are also used to produce materials with novel properties, which cannot be generated by any other means. Figure 1.3 shows Schematic diagram of swift heavy ion irradiation

The irradiation of solid materials with high energy ions is extremely important from the fundamental physics as well as from the materials engineering point of view. Interactions of energetic ions with crystalline materials induce deep buried disorder.

The dynamics of the defects are influenced by many mechanisms like creation of oxygen vacancies, interstitial cation vacancies, etc. A high energy heavy ion loses its energy in a medium through two processes, namely, electronic loss and nuclear collisions, the latter process is responsible for displacing atoms of the medium from their lattice positions (Rodrigues et al 2009). Since controlled irradiation can lead to a controlled introduction of defect states in the material system, it has been and is being beneficially used to control the materials properties. Ion beams play a significant role in engineering the properties of materials. The nature of modifications depend on the electrical, thermal, optical structural and physical properties of the target material, the mass of the projectile ion and its energy and also the type of irradiation like its fluence and beam dimension. These ions are expected to make columbic interaction between the target atom and the energetic ion beams. Ion implantation provides an alternative method of introducing dopant atoms into the lattice. In this case, a beam of dopant ions accelerated through a potential of typically MeV is allowed to impinge on the surface of the target atom. To achieve deep penetration of ions, the ions must interact and collide, individually or collectively, with atoms of the solid matrix. During these collisions, energy will be exchanged between the moving ion and the stationary lattice atoms with a concomitant energy loss by the ions and an energy gain by the atoms. The energy loss serves to slow down the ions, eventually to rest in the lattice; the atomic energy gain results in the creation of defects or disorder in the lattice. The thermal annealing can be used to re-order the lattice. The radiation damage produced by implantation often produces conductivity changes that swamp those desired by the addition of the ion. Modification on crystalline properties can be achieved by inducing electronic excitation in materials (Lesueur and Dunlop 1993). These electronic excitations can be produced by swift heavy ions (SHI) irradiation.

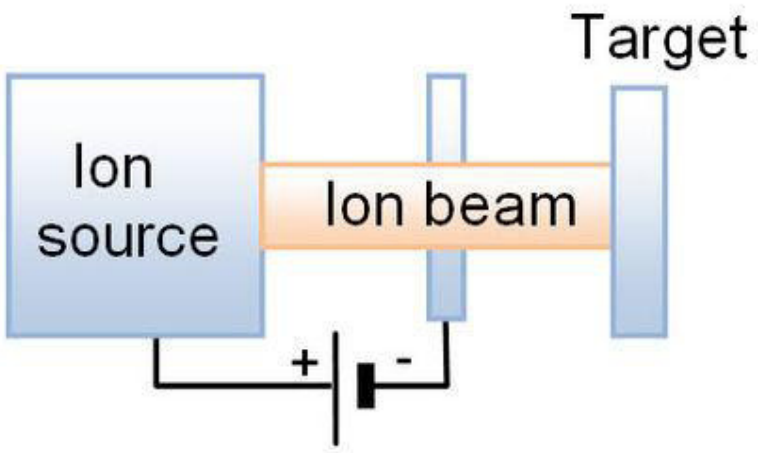

Fig. 1.3 Schematic diagram of swift heavy ion irradiation

When one such ion penetrates through single crystals, the process of nuclear energy loss $(dE/dx)_N$ or electronic energy loss $(dE/dx)_E$ can occur. The former is due to direct transfer of energy to the target through elastic collision and the later is due to inelastic collision. Depending upon the radiation behaviour, materials can be generally divided into two, first being sensitive to the energy deposited in their electronic system and the second being insensitive to the electronic part of the energy deposition. Organic solids can be jibed into the first type and metals can be fitted into the second type. This general behavior is strongly altered when swift heavy ions are used (Katz et al 1990). Energetic ions are suitable means for the qualifying of the surface or bulk structure of solids. An ion depending on its kinetic energy, mass and nuclear charge can create changes within a thin surface layer or can penetrate far into the bulk to produce long and narrow garbled zone along its trajectory (Kramer 1995). When an energetic ion beam fleets through a material, the coulomb interaction between the target atom and the implanted energetic ion causes alterations in the material. Due to this interaction, the incident ion loses its energy along its path in two ways, one by means of the inelastic collisions of the energetic ion with the atomic electrons of the

material and other by elastic scattering from the nuclei of the atoms of the material. The latter process is responsible for displacing atoms of the medium from their lattice positions. At high energy, the changes due to electronic energy loss become predominant. The mono energetic beam stops around its projected range and creates disorder in the lattice. The interaction of the ion beam with a solid is a nonequilibrium process. After the passage of the ion, the solid returns to its equilibrium, leaving behind the surface and produces modifications. These interactions result in chemical transformations in the modified crystal structure resulting in the modification of the optical, mechanical, physical and electrical properties of the material. When heavy ions with energies in the MeV range pass through a solid, they deposit their energy mainly to the electrons of the target atoms. Most of the primary excitation and ionization processes occur close to the ion trajectory in a cylindrical core region with a radius of a few nanometers. Some of the electrons are ejected with higher kinetic energies and can cause further ionizations at some hundreds of nanometers from the primary ion path. The resulting dose distribution for each individual ion follows approximately a $1/r^2$ law (where r is the radial distance from the projectile trajectory) (Singh et al 1999; Aithal et al 1997; Bhat et al 1996). In particular close to the ion path, extremely high energies are deposited in a very small volume of some hundreds of eV/nm^3 within an extremely short time, difficult to reach by any other radiation source. The high electronic excitation density in the core region has a strong influence on the resulting defect creation, whereas the damage in the larger halo is similar to effects induced by conventional radiation such as electrons, gamma- or X-rays.

Swift heavy ion (SHI) beams have become an indispensable part of the material processing schemes and in the modification of the surface layer of solids. Recent advances in the region of very high-energy physics and progress in the

experimental methods have produced some qualitative new results regarding modifications induced by high-energy ions. High-energy heavy ion irradiation is relatively a new curiosity in materials science and technology (Srivastava et al 1997). When a swift heavy ion irradiation passes through matter; it loses its energy mainly in two ways. The interaction of heavily charged ions with electrons of the target material through Coulomb forces produces a track of ionization and highly kinetic electrons along the path of the primary ion due to inelastic collision. This is known as electronic energy loss or electronic stopping (Se). Nuclear energy loss or nuclear stopping (Sn) dominates at low energies, which is caused by the elastic scattering from the screened nuclear potential of the target. Both Sn and Se give rise to various modifications of the solids. In the regime of ion energies where electronic energy loss is dominant, several interesting features of modifications of solids have been observed in recent years (Rout et al 2001). The amount of electronic energy loss in each collision varies from a few eV/A˚ to KeV/A˚. The nature of modification depends on electrical, thermal and structural properties of target material, the mass of the projectile ion and irradiation parameters (Singh et al 1995). Swift heavy ion bombardment can induce irreversible change of structure and chemical composition within a small volume surrounding the ion track (Sun et al 2006). The swift heavy ions (SHI) irradiation leads to modification of the materials through the transfer of considerable amount of energy via collision with the electrons of target which result in the formation of high energy densities along the ion path (Avasthi 2005; Dixit et 1993 and Deepthy et al 2001). The SHI significantly modify the optical properties of crystals by changing the refractive index (Sreeramana Aithal et al 1997). Heavy ions are capable to break the molecular bonds and create damage to the single crystals (Nagabhushana et al 2008). SHI induced point defects in crystals act as the color centers (Deepthy et al 2001) and

lead to the enhancement in luminescence efficiency (Nagabhushana et al 2008a; Kanagasekaran et al 2009). In the present study we used SHI irradiation to manipulate properties of 2-amino-5nitropyridine (2A5NP) family NLO crystalline derivatives.

1.17 Aim of the present study

Though semiorganic nonlinear optical (NLO) single crystal combined the advantage of both organic and inorganic crystals, the efficiency of second harmonic generation (SHG) and other physico- chemical properties are not remarkable one for efficient opto- electronic devie fabrication. Structural, optical, and electrical properties to be improved further, when devices to be fabricated for industrial applications. Thermal stability of the semiorganic crystasl is also to be improved. Modifications in the structural, optical, electrical, thermal and SHG are needed. Improved physical and chemical properties of the crystal can be achieved by Swift heavy Ion (SHI) irradiation. Swift Heavy Ion (SHI) can enhance the optical, electrical, thermal and SHG properties of the grown crystals. The main aim of present research work is

- To search and develop newer variety of organic 2-amino-5nitropyridine (2A5NP) family NLO crystalline derivatives which could replace conventional laser materials.
- To grow bulk newer variety of organic 2-amino-5nitropyridine (2A5NP) family NLO crystalline derivatives by using Assembled Temperature Reduction (ATR) method Sankaranarayanan- Ramasamy (SR) method.
- To irradiate these 2-amino-5nitropyridine (2A5NP) family NLO crystalline adducts with swift Heavy Ion (SHI) Au^{3+} with three different flences varying from 10^{12} to 10^{14} ions/cm^2 using **3 MV Pelletron Tandem Accelerator having high current beams (Typically 100-300 μA from the ion source and**

post acceleration currents ~ 50μA) facility in Pure and Applied Physics Department, Guru Ghasidas Vishwavidyalaya (a central university) at **Bilaspur, Chhattisgrah,** India.

- To investigate the physical properties of both virgin (pristine) and irradiated crystals such as crystal structure, NLO efficiency, thermal stability, mechanical strength, electrical, optical and surface topographical studies.

CHAPTER II
CHARACTERIZATION TECHNIQUES

2.1 INTRODUCTION

Characterization techniques play a vital role in crystal growth to understand the properties of grown crystal such as structure, mechanical, optical, electrical, and thermal. It is necessary to involve the crystals for the various characterizations to check its quality and chemical properties. The usage of the crystals depends on the properties and so the characterization is important part in crystal growth. It also helps to grow quality single crystal and gives crystal clear information about the grown crystal. The instrumentation details and operating procedure of important characterization techniques used in the present work are given in the following sections.

2.2 Single Crystal X-Ray Diffraction

X-ray crystallography is a tool used to determine the three-dimensional structure of molecules. The structural and conformational studies of molecules become essential to understand their function. The crystallographic studies not only provide knowledge about the conformation but also about the factors that keep the molecules in the desired conformation. The conformations of biomolecules play a major role in the design of drugs. Max von Laue, in 1912, discovered that crystalline substances act as three-dimensional diffraction gratings for X-ray wavelengths similar to the spacing of planes in a crystal lattice. X-ray diffraction is based on constructive interference of monochromatic X-rays and a crystalline sample. These X-rays are generated by a cathode ray tube, filtered to produce monochromatic radiation, collimated to concentrate, and directed toward the sample. The interaction of the incident rays with the sample produces constructive interference (and a diffracted ray)

when conditions satisfy Bragg's Law ($n\lambda = 2d \sin\theta$). This law relates the wavelength of electromagnetic radiation to the diffraction angle and the lattice spacing in a crystalline sample. These diffracted X-rays are then detected, processed and counted. By changing the geometry of the incident rays, the orientation of the centred crystal and the detector, all possible diffraction directions of the lattice should be attained. All diffraction methods are based on generation of X-rays in an X-ray tube. These X-rays are directed at the sample, and the diffracted rays are collected. A key component of all diffraction is the angle between the incident and diffracted rays.

2.3 Software used for crystal structure determination

The intensity data for the crystals were collected by Bruker AXS (SMART APEX -II) diffractometer equipped with graphite monochromator MoK_α radiation ($\lambda = 0.71073$ Å) using ω and φ scan modes. The intensities were corrected for Lorentz and polarization effects and absorption effects by using the SADABS (Bruker 2008) program. The structures were solved by direct methods using SHELXS97 (Sheldrick 2008) program. The structures were refined by full-matrix least-squares technique using SHELXL97 (Sheldrick 2008). The geometrical parameters were calculated using PLATON (Spek 2009), and the molecular and packing diagrams were drawn using programs ORTEP (Farrugia 2012), and Mercury (Macrae et al 2008).

2.4 UV-Vis NIR Spectrophotometer

The instrument used in ultraviolet, visible, near infrared spectroscopy is called a UV-Vis-NIR spectrophotometer. The basic parts of a spectrophotometer are a light source, a holder for the sample, a diffraction grating or monochromator to separate the different wavelengths of light and a detector. The radiation source is often a Tungsten filament (300-2500 nm), a deuterium arc lamp, which is continuous over the

ultraviolet region (190-400 nm) and Xenon arc lamps for the visible wavelengths. The detector is typically a photodiode or a charge coupled device. Photodiodes are used with monochromators, which filter the light so that only light as a single wavelength reaches the detector. Diffraction gratings are used with CCDs, which collect light of different wavelengths on different pixels.

A spectrophotometer can be either single or double beam. The single beam was the earliest design, but is still in common use in both teaching and research labs. In a double beam instrument, the light is split into two beams before it reaches the sample. One beam is used as the reference. The other beam passes through the sample. A narrow bandwidth was selected with the help of band pass filters. The reference beam intensity is taken as 100% transmission or 0% absorbance and the measurement displayed is the ratio of the two beam intensities. In the transmission study the intensity was recorded in terms of percentage of transmittance (%) along Y-axis and the wavelength (nm) along X-axis. In this investigation, Perkin-Elmer double beam UV-Vis NIR spectrometer was used to study the optical quality of the grown crystals in the wavelength range of 200-1100 nm at room temperature with the slit width 2 nm and scan speed 240 nm per minute. Cut and polished conventional SEST and assembled temperature reduction (ATR) method grown crystals of 1 mm and less than 1 mm thickness were used. In the present thesis work, optical transparency and band gap of grown single crystals has been analyzed by recording absorption and transmission spectra in the wavelength range of 200-1100 nm. For this purpose a UV-VIS-NIR spectrometer (PerkinElmer Lambda35) has been employed.

2.5 Microhardness

Micro-indentation hardness testing is a method for measuring the hardness of a material on a microscopic scale. A precision diamond indenter is impressed into the

material at loads from a few grams to 1 kilogram. The impression length, measured microscopically and the test load are used to calculate a hardness value. The hardness values obtained are useful indicators of a material's properties and its behaviour. The length of the hardness impressions are precisely measured with an optical microscope using an eyepiece and computer software.

A hardness number is then calculated using the test load, the impression length and a shape factor for the indenter type used for the test. Hardness value depends on the elastic and plastic behaviour of the solid and the test conditions. In an attempt to understand the mechanical behaviour of crystals, which is rarely found in literature to identify the mode of deformation, micro-indentation tests have been made on a selected surface of crystal with Vickers diamond pyramid. The indenter employed in the Vickers test is a square based pyramid whose opposite sides meet at the apex at an angle of 136°. The diamond is pressed into the surface of the material at loads ranging up to approximately 120 kilograms-force and the size of the impression is measured with the aid of a calibrated microscope. The Vickers number (H_v) is calculated using the following formula:

$$H_v = 1.854 \left(\frac{P}{d^2} \right)$$

Where, P being the applied load and d the average diagonal of the indentation. The applied load is usually specified when H_v is cited. The hardness measurement in the present investigation was carried out at Archbishop Casmir instrumentation centre, St. Joseph's college, Trichy, Tamilnadu.

2.6 Dielectric Analysis

The term dielectric was first coined by Faraday to suggest that there is something analogous to current flow through a capacitor structure during the charging

process when current introduced at one plate flows through the insulator to charge another plate. The important consequence of imposing a static external filed across the capacitor is that the positively and negatively charged species in the dielectric become polarized. Charging occurs only as the field within the insulator is changing. Electrical measurements to evaluate the dielectric behaviour of materials are usually made with cells having two identical electrodes applied to the faces of a sample in the form of a crystal. A two terminal sample holder was used for dielectric measurements. The cell was made of copper and the sample was held between the electrodes to ensure proper electrical contact at all temperatures. The whole assembly was placed in a glass container in which the heater was housed. The large thermal capacity so achieved by this arrangement gave good thermal insulation to the cell and the entire sample had uniform temperature. A thermocouple was fixed in the vicinity of lower electrode to measure the temperature of the sample. The dielectric permittivity, dielectric loss and dielectric tensor components are measured using Agilent 4284-A LCR meter available at Archbishop Casmir instrumentation centre, St. Joseph's college, Trichy, Tamilnadu. Two opposite surfaces across the breadth of the sample were treated with good quality silver or graphite paste in order to obtain good Ohmic contact. Using LCR meter, the capacitance of the grown crystals was measured for the frequencies 100 Hz to 1 MHz at the temperature range of 30°C to 150°C. The dielectric permittivity of the crystal was calculated using the relation:

$$\varepsilon_r = \frac{C_{crys}}{C_{air}}$$

where C_{crys} is the capacitance of the crystal and C_{air} is the capacitance of same dimension of air.

2.7 Thermal Analysis

Thermal analysis is an essential analytic technique to study the thermal behaviour of materials and finds widespread applications in diverse industrial and research fields. It is a general term, which covers a group of related techniques in which the temperature dependence of the parameters of any physical property of a substance is measured. In addition to providing valuable information on the thermal stability of the compounds and the decomposition products, these studies often provide an insight into their mode of decomposition. NLO materials having excellent SHG efficiency can be used for device fabrication, if they possess good thermal stability over a wide range.

2.7.1 Methods of thermal analysis

Thermo analytical methods involve the measurement of various properties of materials subjected to dynamically changing environments under predetermined conditions of heating rate, temperature range and gaseous atmosphere or vacuum. In many cases, the use of a single thermo analytical technique may not provide sufficient information to solve the problem on hand and hence, the use of other thermal techniques, either independently or simultaneously for complementary information becomes necessary. Three main analyses used for the thermal properties are as follows:

(i) Thermo gravimetric analysis (TGA), which involves monitoring weight while varying temperature

(ii) Differential thermal analysis (DTA), which involves comparing the precise temperature difference between a sample and an inert reference material, while heating both

(iii) Differential scanning calorimetry (DSC), similar to DTA except that electrical energy is used to restore the cooler of the two materials to the same temperature as the other. This allows direct measurement of energy changes

These techniques are useful for determining glass points, phase changes, water of crystallization and mixtures, where the components have different melting or decomposition points. Hence these techniques find extensive use in all fields of inorganic and organic chemistry, metallurgy, mineralogy and many other areas.

2.8 Kurtz Powder technique

Kurtz Powder technique (Kurtz & Perry 1968) is used to check the second order NLO property of the material and to classify the materials so that each falls into one of the five groups, large coefficient, small coefficient, phase matchable, non-phase matchable and centrosymmetric materials. A laser typically a Q-switched high repletion Nd: YAG laser serves to illuminate a large area of a thin layer of powder of the material to be studied. The sample was prepared by sandwiching the grinded crystalline powder with average particle size of about 90 μm between two glass slides, using copper spacers of 0.4 mm thickness. Since typical values of the coherence length are in the range of 1-10 μm, this value of average particle size yields maximum second harmonic signal independent of particle size in phase matchable crystalline powder. The powder is compacted into a thin cell to define the thickness of the layer. The cell is held within an optical system that collects all the scattered SHG from the sample over 4π radians, and the signal is monitored by a photomultiplier. The measurement technique is used to study the amount of SHG from the powder sample as a function of particle size in the sample, the powder being sieved to a small range of size for each test. It is necessary to monitor the laser power for control purposes. The required information is obtained from the measurement of SHG power verses

particle size, which is compared for an identical geometry with the results determined for KDP powder samples. The second harmonic signal generated in the crystals was confirmed by the emission of green radiation. The experimental results suggest that all the samples exhibit SHG and hence they can be used in frequency conversion for high power lasers.

2.9 Scanning electron microscope (SEM)

The scanning electron microscope (SEM) is one of the most widely used instruments in materials research laboratories and is common in various forms in fabrication plants. Scanning electron microscopy is central to microstructural analysis and therefore important to any investigation relating to the processing, properties, and behavior of materials that involves their microstructure. The SEM provides information relating to topographical features, morphology, phase distribution, compositional differences, crystal structure, crystal orientation, and the presence and location of electrical defects. The SEM is also capable of determining elemental composition of microvolumes with the addition of X-ray or electron spectrometer and phase identification through analysis of electron diffraction patterns.

Lenses in the SEM are not a part of the image formation system but are used to demagnify and focus the electron beam onto the sample surface. This gives rise to two of the major benefits of the SEM: range of magnification and depth of field in the image. Depth of field is that property of SEM images where surfaces at different distances from the lens appear in focus, giving the image three-dimensional information. The SEM has more than 300 times the depth of field of the light microscope. Another important advantage of the SEM over the optical microscope is its high resolution. Subnanometer resolution at low beam energies is now achievable from an SEM with a field emission (FE) electron gun. Magnification is a function of

the scanning system rather than the lenses, and therefore a surface in focus can be imaged at a wide range of magnifications. Sample preparation can be minimal or elaborate for SEM analysis, depending on the nature of the samples and the data required. Minimal preparation includes acquisition of a sample that will fit into the SEM chamber and some accommodation to prevent charge build-up on electrically insulating samples. Most electrically insulating samples are coated with a thin layer of conducting material, commonly carbon, gold, or some other metal or alloy. The choice of material for conductive coatings depends on the data to be acquired: carbon is most desirable if elemental analysis is a priority, while metal coatings are most effective for high resolution electron imaging applications. Alternatively, an electrically insulating sample can be examined without a conductive coating in an instrument capable of "low vacuum" operation.

Accelerated electrons in an SEM carry significant amounts of kinetic energy, and this energy is dissipated as a variety of signals produced by electron-sample interactions when the incident electrons are decelerated in the solid sample. These signals include secondary electrons (that produce SEM images), backscattered electrons (BSE), diffracted backscattered electrons (EBSD that are used to determine crystal structures and orientations of minerals), photons (characteristic X-rays that are used for elemental analysis and continuum X-rays), visible light (cathode luminescence-CL), and heat. Secondary electrons and backscattered electrons are commonly used for imaging samples: secondary electrons are most valuable for showing morphology and topography on samples and backscattered electrons are most valuable for illustrating contrasts in composition in multiphase samples (i.e. for rapid phase discrimination). X-ray generation is produced by inelastic collisions of the incident electrons with electrons in discrete orbitals (shells) of atoms in the sample.

As the excited electrons return to lower energy states, they yield X-rays that are of a fixed wavelength (that is related to the difference in energy levels of electrons in different shells for a given element). Thus, characteristic X-rays are produced for each element in a mineral that is "excited" by the electron beam. SEM analysis is considered to be "non-destructive"; that is, x-rays generated by electron interactions do not lead to volume loss of the sample, so it is possible to analyze the same materials repeatedly.

2.10 Fluorescence spectroscopy

If an atom or molecule first absorbs energy– for instance a photon-, this is called excitation. Very shortly (in the order of nanoseconds) after excitation it emits a photon of a longer wavelength. It is called fluorescence. In fluorescence spectroscopy, a beam with a wavelength varying between 180 and ~800 nm passes through a solution in a cuvette. We then measure from an angle the light that is emitted by the sample. In fluorescence spectrometry both an excitation spectrum (the light that is absorbed by the sample) and/or an emission spectrum (the light emitted by the sample) can be measured. The concentration of the analyte is directly proportional with the intensity of the emission.

There are several parameters influencing the intensity and shape of the spectra. When recording an emission spectrum the intensity is dependent on the:

- Excitation wavelength
- Concentration of the analyte solvent
- Path length of the cuvette
- Self-absorption of the sample

A molecule can be excited from its electronic ground state. In the electronic ground state the molecule has the lowest possible electronic energy. Upon excitation

(the absorption of a photon) one of the electrons goes into a higher electronic state and the molecule is excited. The molecule will stay in its electronic excited state in the order of pico or nanoseconds (ns). Then the electron will fall back to its ground state and will emit a photon of a longer wavelength than the photon used for excitation. A fluorescence emission spectrum is recorded when the excitation wavelength of light is held constant and the emission beam is scanned as a function of wavelength. An excitation spectrum is the opposite, whereby the emission light is held at a constant wavelength, and the excitation light is scanned as a function of wavelength. The excitation spectrum usually resembles the absorbance spectrum in shape.

2.11 Fourier Transform Infrared Spectroscopy

Infrared spectroscopy deals with the study of vibrational spectra of molecules. The absorption of infra-red radiations causes an excitation of molecule from a lower to the higher vibrational level. Each vibrational level is associated with a number of closely spaced rotational levels. The infra-red spectrum is considered as vibrational-rotational spectra. All the bonds in a molecule are not capable of absorbing infra-red energy but only those bonds which are accompanied by a change in dipole moment will absorb in the infra-red region. Such vibrational transitions which are accompanied by a change in the dipole moment of the molecule are called infra-red active transitions. Thus, these are responsible for absorption of energy in the infra-red region. On the other hand, the vibrational transitions which are not accompanied by a change in dipole moment of the molecule are not directly observed and these are infra-red inactive. Vibrational transitions of C=O, N-H, O-H, etc. bands are accompanied by a change in dipole moment and thus, absorb strongly in the infra-red region. But transitions in Carbon-Carbon bonds in symmetrical alkenes and alkynes

are not accompanied by the change in dipole moment and hence do not absorb in the infra-red region. Since the absorption in infra-red region is quantized, a molecule of the organic compound will show a number of peaks in the infra-red region.

Fourier Transform Infrared Spectroscopy (FT-IR) is a simple mathematical technique to resolve a complex wave into its frequency components. The conventional IR spectrometer is not of much use for the far IR region, as the sources are weak and the detectors are insensitive. FT-IR has made this energy limited region more accessible. It has also made the mid infra- red (4000- 400 cm^{-1}) more useful. Conventional spectroscopy, called the frequency domain spectroscopy, records the radiant power as a function of frequency. In the time domain spectroscopy, the changes in radiant power are recorded as a function of time. In the Fourier Transform Spectrometer, a time domain plot is converted into a frequency domain spectrum. The actual calculation of the Fourier transform of such systems is done by means of high-speed computers.

CHAPTER IV

STUDIES ON Au^{3+} SWIFT HEAVY ION IRRADIATED 2-AMINO-5-NITROPYRIDINIUM CHLORIDE (2A5NPCl) NONLINEAR OPTICAL (NLO) SINGLE CRYSTAL

4.1 Introduction

Second and third order nonlinear effects lead to a variety of useful applications in laser technologies and photonics and in investigating non- linear optical (NLO) properties of many classes of potentially, technologically useful materials such as organics, organometallics, inorganic, organic- inorganic, and semiconductors. There has been growing interest in fundamental and scientific research in the area of molecule based non- linear optical (NLO) materials with large second and third order nonlinearities. In particular, second order non- linear optical (NLO) materials offer many attractions, such as non resonant ultrafast response times, low dielectric constant and intrinsic architectural tailorability. The noncentro symmetric organization of chromophore is an essential requirement for efficient bulk second order non- linear optical (NLO) materials. Non- linear optical (NLO) materials have been identified as a strong candidate for emerging photonic data processing technologies. Non- linear optical (NLO) materials possess vast potential for use in a variety of photonic system, including high speed optical modulators, ultrafast optical switches and high density optical data storage media. Non- linear optical (NLO) crystals are very important for laser frequency conversion. The inorganic non- linear optical (NLO) crystals posses relatively modest optical nonlinearity due to the lack of extended π- electron delocalization. Compared with inorganic counterparts organic non- linear optical (NLO) materials have large NLO coefficient due to the presence of delocalized π- electron system linking donor and acceptor which enhances the

necessary asymmetric polarisability and synthetic flexibility but in general they have very poor thermal and chemical stabilities lower continuous wavelength radiation damage (Masse & Zyss 1991) and a poor optical transparency (Masse 1995). The search for new non- linear optical (NLO) materials with improved stability, and a wide transparency window has resulted in the development of the new class of materials called semiorganic. In semiorganic, polarisable organic molecules are stiochiometrically bonded inorganic host. It combines the advantage of both organic and inorganic materials. More recently, crystals combining the asset of semiorganic entities were developed (Masse et al 1993). One of the prominent chromophores for semiorganic materials and a successful outcome has been presented by 2-amino-5-nitropyridinium dihydrogen phosphate (2A5NPDP) (Kotler et al 1992; Ambrose Rajkumar et al 2016; Horiuchi et al 1995; and Samuel et al 1995), 2- amino-5-nitropyridinium chloride (2A5NPCl) (Pecault et al 1993), 2-amino-5-nitropyridinium sulfamate (2A5NPS) (Ambrose Rajkumar et al 2015), and 2-amino-5- nitropyridinium hydrogen oxalate (2A5NPHO) (Ambrose Rajkumar et al 2014). Using an outstanding chromophore and nonlinear optical material, the new structure of 2-amino-5-nitropyridinium hydrogen oxalate (2A5NPHO) was grown and structure solved. The mechanical and electrical properties of 2-amino-5-nitropyridinium hydrogen oxalate were reported (Ambrose Rajkumar et al 2014 a, b & c). The efficient semi organic crystals such as 2-amino-5-nitropyridinium dihydrogen monophosphate (2A5NPDP), 2-amino-5-nitropyridinium- L-monohydrogentartrate, 2- amino-5-nitropyridine –L-(+)- tartrate, 2-amino-5-nitropyridinium halides (Cl^-, Br^-), 2-amino-5-nitropyridine adsorbed on roughened polycrystalline silver electrodes, 2- amino-5-nitropyridinium acetophosphonate, 2-amino-5-nitropyridine adsorbed on silver sols, 2-amino-5nitropyridinium dihydrogen phosphate, 2- amino-5- nitropyridine and n- chloroacetic

acid assemblies, 2-amino-5-nitropyridine-L-(+)-tartrate, 2-amino-5-nitropyridinium chloride, 2-amino-5-nitropyridinium dihydrogenphosphate/arsenate, 2-amino-5-nitropyridinium chloride, two 5-nitro-2-aminopyridinium cuprates: $(5\text{-NAP})_2\ CuCl_4$ and the quantum magnetic ladder $(5\text{-NAP})_2\ CuBr_4 \bullet H_2O$, 2-amino-5-nitropyridine with benzenesulfonic acids, 2-amino-5-nitropyridinium tetrafluoroborate, 2-amino-pyridinium p-nitro-benzoate, 2-amino-5-nitropyridinium l-tartrate, 2-amino-5-chloropyridinium hydrogen selenate, 2-amino-5-nitropyridinium-toluenesulfonate, 2-amino-5-nitropyridinium hydrogen selenate, 2-amino-5-nitropyridinium tetra oxidorhenate (VII) monohydrate, quantum chemical studies on structure of 2-amino-5-nitropyrimidine, 5-amino-2-pyridine, 2-amino-5-nitropyridinium nitrate (Masse et al 1991; Horiuchi et al 1995; Anna Puig et al 1998; Morela et al 2002; Pricilla Jeyakumari et al 2007; Zyss et al 1993; Osamu Watanabe et al 1993; Oussaid et al 1996; Pecaut et al 1993; Foresti et al 1994; Pecaut and Masse 1994; Maurizio Muniz et al 1995; Yvette Le Fur et al 1996; Oussaid et al 1996; Horiuchi et al 1997; Ibanez et al 1997; Horiuchi et al 1999; Dhanuskodi et al 2004; Horiuchi et al 2004; Zaccaro et al 1998; Turnbull et al 2002; Hideko et al 2004; Manivannan et al 2005; Jebas and Balasubramanian 2006; Manikandan, and Dhanuskodi 2007; Lorenc et al 2008; Akriche et al 2009; Anandha Babu et al 2009; Rodrigues et al 2009; Arivazhagana and Subhasinib 2012; Lin Chen et al 2013; Sivasubramani et al 2015; and Sivasubramani et at 2016.) and 2-amino-5-nitropyridinium dihydrogen phosphate (2A5NPDP) were grown by using Sankaranarayanan- Ramasamy (SR) method and optical, electrical, mechanical and NLO properties were reported (Ambrose Rajkumar et al 2016; Ambrose Rajkumar et al 2014). The grown crystal of 2-amino-5-nitropyridinium sulfamate (2A5NPS) structure was solved and reported. An efficient NLO crystal of 2-amino-5-nitropyridinium sulfamate (2A5NPS) and 2-amino -5-

nitropyridinium chloride (2A5NPCl) were grown by assembled temperature reduction method and it's optical, electrical, mechanical and thermal properties were reported (Ambrose Rajkumar et al 2016a, and Ambrose Rajkumar et al 2017). Energetic ions are suitable means for the modification of the surface or bulk structure of solids. An ion, depending on its mass, nuclear charge and kinetic energy can create changes only within a thin surface layer, of is able to penetrate far into the bulk and to produce a long and narrow disordered zone along its trajectory (Ishwar Bhat et al 2002). Irradiations with energetic ion beams play a vital role in the field of defect studies in inorganic materials. The energetic ions lose their energy during their passage through the material. This energy is spent either in displacing atoms of the sample by elastic collisions or exciting the atoms by inelastic collisions. Low energy ions up to a few hundred KeV have been used in the modification of surface and interface. The loss of energy by the ions in exciting or ionizing the atoms by inelastic collisions is called as electronic energy loss. It is dominant at high energies where the displacement of atoms due to elastic collisions is insignificant (Vorobyova et al 2005; Ning Yu et al 1997). The irradiation of materials with energetic ions leads to the creation of a wide variety of defect state in the material system, which changes the physical and chemical properties such as structure, optical and electrical transport properties of the material. The changes are strongly dependent on the mass of the incident ion, the irradiation energy, fluences and temperature. The irradiation may cause ionization or excitation and possibly displacement of atoms from their sites in the lattice of the materials (Kucheyeva et al 2001; Seager et al 2007; and Sarkar et al 2008). The formation of irradiation- induced defects in materials is extremely sensitive to the irradiation temperature (Knaster et al 2016). Recent research interest is focused on the search of new semiorganic nonlinear optical (NLO) materials, as

these materials share the advantages of both inorganic (high thermal and mechanical stability) and organic (broad optical frequency and second harmonic conversion efficiency) materials. (Ravi & Subramanian 2007; Dhanuskodi et al 2007; Bright et al 2010; Justin Raj & Jerome Das 2008; Ravishankar et al 2011; Uma Devi et al 2010; Iyanar et al 2010; Iyanar et al 2009; Sethuraman et al 2008; and Chun et al 1988). After the advent of laser the nonlinear phenomena made a big revolution in the field of optics and the frequency conversion become an important and popular for laboratory lasers (Tao1 et al 1992 and Sagawa et al 1995). Understanding the effects of different radiations on solid state materials in particular NLO crystals is an important problem and has practical applications for use in radiation rich environments. New uses of this technology are developing, and one promising field is that of optical materials. The need for higher transmission speeds and densities in communications is placing ever increasing demands on materials technology. Nonlinear optics holds great potential for the development of all optical devices with the goal of providing improved performance compared with semiconductors (Bucha et al 1994). Using heavy ions of high energetic beam, one can modify materials so that they can acquire desired optical, electrical, and mechanical properties. In many cases, ion irradiation causes dramatic change in the optical absorption and luminescent properties of insulators. Hence In this chapter attempts were made on 2-amino-5-nitropyridinium chloride (2A5NPCl) with Au^{3+} ion of varying fluences.

4.2 Experimental procedure

4. 2.1Crystal growth

2-amino-5-nitropyridinium chloride (2A5NPCl), a semiorganic crystal was grown from slow evaporation method. 1: 1 equimolar ratio of 2-amino-5-nitropyridine and hydrochloric acid was dissolved in distilled water and stirred well for six hours to get homogenous saturated solution.

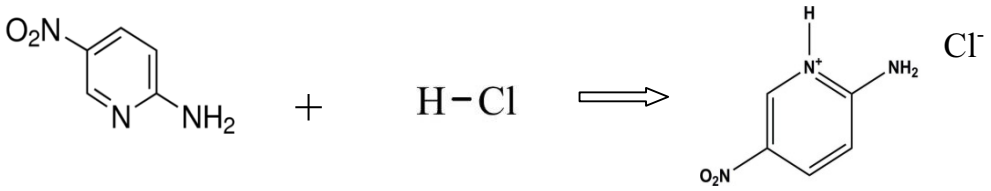

Fig. 4.1 Reaction scheme of 2-amino -5-nitropyridinium chloride (2A5NPCl)

The solution was filtered using whatman filter paper and kept at room temperature to evaporate. Nucleation of the crystal was formed after 60 days. Reaction scheme of 2-amino-5-nitropyridinium chloride (2A5NPCl) NLO single crystal is shown in Fig. 4.1. A good transparent coloured optical and defect free crystal was harvested for 120 days. The semiorganic crystal of 2-amino-5-nitropyridinium chloride (2A5NPCl) dimension of 7 × 3 × 2 mm^3 and 8 x 3x 2 mm^2 are shown in Figure 4.2 (a, b) respectively.

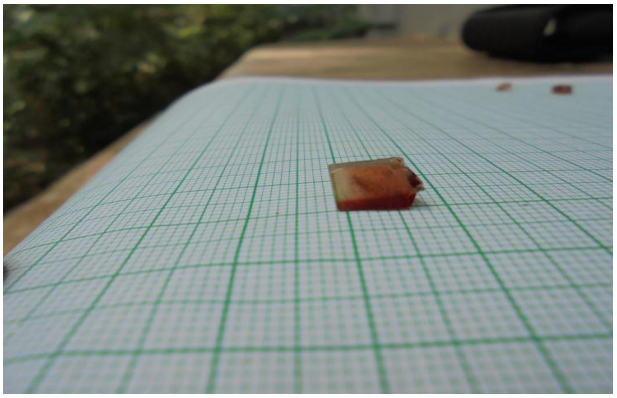

Fig.4.2 (a) Seed crystal of 2-amino-5-nitropyridinium chloride (2A5NPCl) NLO single crystal from slow evaporation

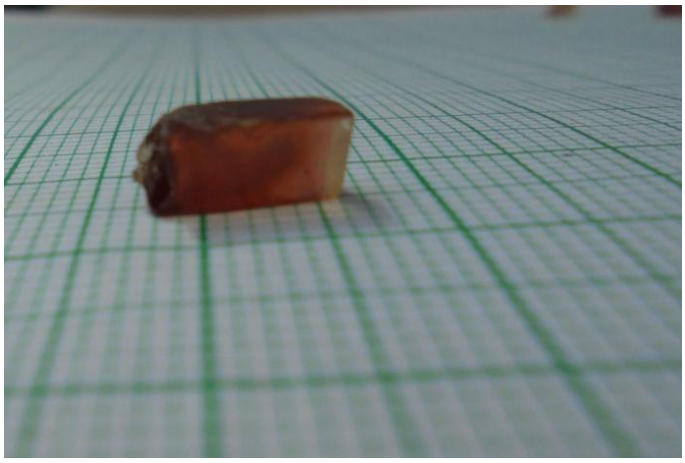

Fig. 4.2(b) Seed crystal of 2-amino-5-nitropyridinium chloride (2A5NPCl) NLO single crystal from slow evaporation

4.2.2 Solubility of 2-amino-5-nitropyridinium chloride (2A5NPCl)

The synthesized salt was used to measure the solubility of 2-amino-5-nitropyridinium chloride (2A5NPCl) in distilled water. A 250 ml glass beaker filled with 100 ml of distilled water was placed inside a constant temperature bath whose temperature was fixed at 30°C. An acrylic sheet with a circular hole at the middle through which a spindle from an electronic motor placed over a sheet was introduced into the solution. A Teflon paddle was attached at the end of the rod for stirring the solution. 2-amino-5-nitropyridinium chloride (2A5NPCl) salt was added in small amounts. The addition of the salt and stirring were continued till the formation of precipitate which confirmed the saturation of the solution. The solubility study of 2-amino-5-nitropyridinium chloride (2A5NPCl) was carried out by increasing the amount of 2-amino-5-nitropyridinium chloride (2A5NPCl) salt that dissolved in water at 30°C, 35°C, 40°C, 45°C, and 50°C. Fig. 4.3 shows the solubility of 2-amino-5-nitropyridinium chloride (2A5NPCl) in 100 ml of double distilled water at different temperatures. It is seen from the solubility curve that the solubility increases with

temperature. The solubility of 2-amino-5-nitropyridinium chloride (2A5NPCl) was found to be 16.3 g/100 ml of water at 30°C.

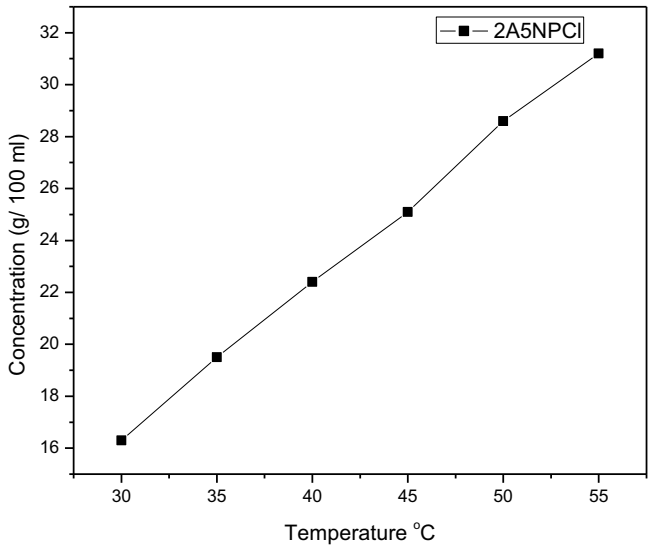

Fig. 4.3 Solubility of 2-amino -5-nitropyridinium chloride (2A5NPCl) NLO single crystal

4.2.3 Bulk crystal from assembled temperature reduction (ATR) method

Fig. 4.4 (a) As grown NLO single crystal of 2-amino -5-nitropyridinium chloride (2A5NPCl) from assembled temperature reduction (ATR) method

2-amino-5-nitropyridinium chloride (2A5NPCl) was grown as a bulk single crystal using Assembled temperature reduction (ATR) method to check its quality. First 2-amino-5-nitropyridinium chloride (2A5NPCl) was grown from slow evaporation method and a good quality and shape of a seed crystal was selected for bulk growth. This good seed from slow evaporation was mounted in a sample holder which is made up of acyrilic. Acyrilic sample holder was connected with microcontroller which was able to rotate the sample holder both clock and anticlock direction. From this bidirectional rotation in homogeneous and inclusion in the crystal would be avoided. A standard 500 crystallizer was used to grow bulk crystal. Saturated solution was prepared using distilled water and filtered using whatman paper. Temperature of saturated solution was 40°C. Then the saturated solution was over heated up to 50°C of one day. Temperature was reduced 2°C/ hour higher than the saturation temperature again temperature was reduced 1°C/ day to saturated temperature. A sample holder which had the seed crystal of 2-amino-5-nitropyridinium chloride (2A5NPCl) was introduced into the standard crystallizer. From this saturated point, temperature was reduced 0.5°C/ day. A bulk crystal of 2-amino-5-nitropyridinium chloride (2A5NPCl) was harvested after 120 days. The size of the crystal is 30×20×20 mm^3.The grown crystal is shown in Fig. 4.4 (a) and 4.4(b). Bulk crystal was cut and polished for irradiation is shown in Fig. 4.5.

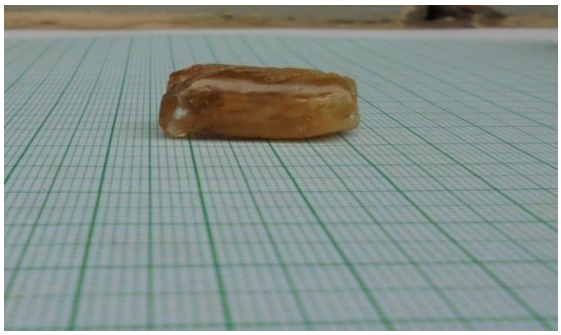

Fig. 4.4 (b) As grown NLO single crystal of 2-amino -5-nitropyridinium chloride (2A5NPCl) from assembled temperature reduction (ATR) method

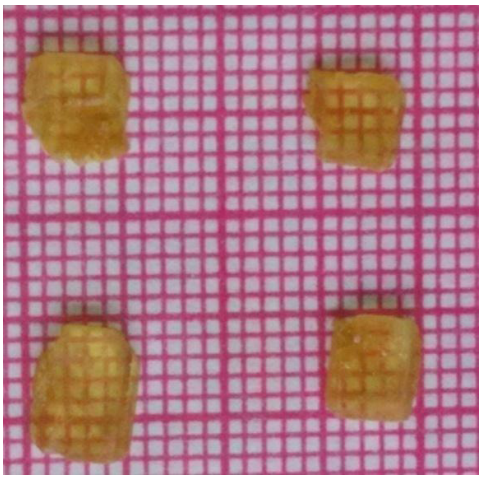

Fig. 4.5 Cut and polished crystal of 2-amino-5-nitropyridinium chloride (2A5NPCl) NLO single crystal

4.3 Au^{3+} ion irradiation

To know the importance of ions in material, 2-amino-5-nitropyridinium chloride was irradiated. 2-amino-5-nitropyridinium chloride was cut in 1mm thickness and polished for irradiation process. Au^{3+} ion was irradiated in National Centre for Accelerator based Research (NCAR) at Pure and Applied Physics Department, Guru Ghasidas Viswavidyalaya (a central university), Billaspur, Chhattisgarh using 3 MV Pelletron Tandem Accelerator. The cut and polished 2-amino-5-nitropyridinium chloride crystals were kept in a sample holder which is made up of stainless steel. Au^{3+} ion was irradiated at room temperature. Projected range of ion beam, electronic and nuclear loss was calculated using SRIM-2012. Swift heavy ion (SHI) of Au^{3+} was selected from a source of negative ions by cesium sputtering (SNICS). Au^{3+} ions of (10^{13}, 5 x10^{13} and 10^{14} ions/cm^2) different fluence irradiated on the semi organic samples. Energy of Au^{3+} ion was 10.8 MeV, 10.4 MeV and 10.8 MeV for 10^{13}, 5 x10^{13} and 10^{14} ions/cm^2 fluences respectively. The swift heavy ion (SHI) was scanned the samples normal to crystalline surface. Radiation was measured using dosimeter during the experimental work.

4.4 Result and discussion

4.4.1. Stopping and range of ions in matter (SRIM)

The projected range of swift heavy ion (SHI), electronic loss and nuclear loss were calculated using SRIM-2012. Swift heavy ion (SHI) was lost its energy, when it entered into the surface of the target atom. Incident energetic ion changed its direction by colliding with target atom. Projected range of swift heavy ion (SHI), electronic

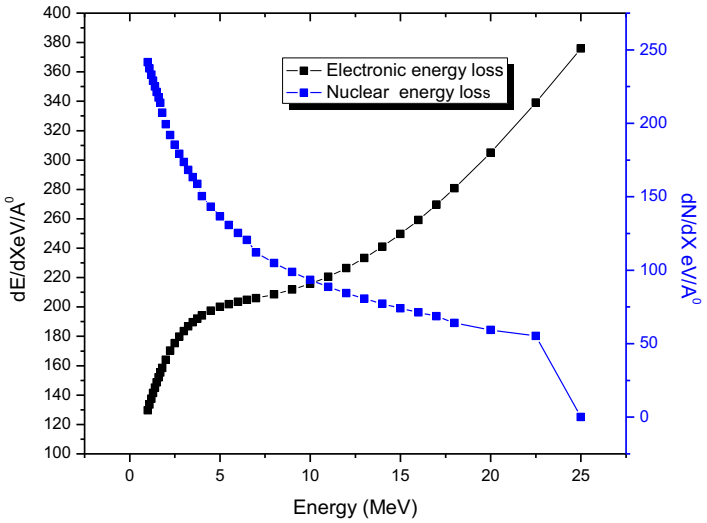

Fig. 4.6 projected range of ion Au^{3+} on 2-amino-5-nitropyridinium chloride (2A5NPCl) NLO single crystal

Ion Energy (MeV)	dE/dx Elec.	dN/dx Nuclear	Projected Range (µm)	Longitudinal Straggling(Å)	Lateral Straggling(Å)
10.00	1.259E+01	5.762E+00	2.90	2061	2090
11.00	1.287E+01	5.447E+00	3.21	2224	2274

Tab. 4.1 Electronic and nuclear energy losses and projected range for input incident Au^{3+} ion energies in 2-amino-5-nitropyridinium chloride (2A5NCl) single crystal

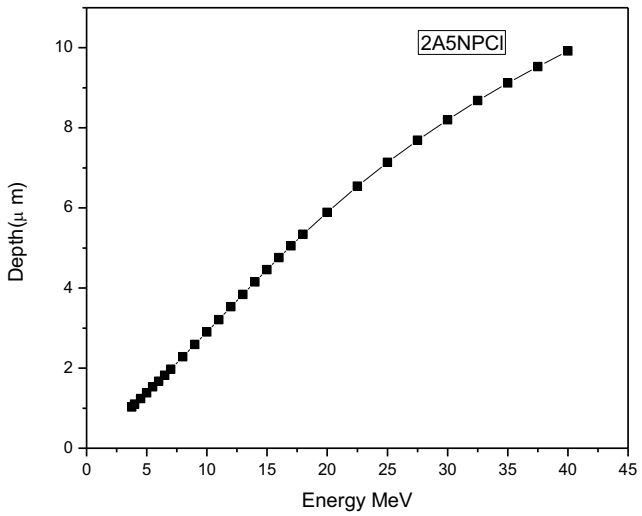

Fig. 4.7 Penetration depth of Au^{3+} ion in 2-amino-5-nitropyridinium chloride (2A5NPCl) NLO single crystal

loss and nuclear loss are presented in Tab. 4.1. Fig. 4.6 shows the electronic (dE/dx) and nuclear (dN/dX) energy losses. It is evident from the graph that electronic energy loss (dE/dx) increases with increase of ion energy (MeV), while nuclear energy ((dN/dx) loss decreases with increasing ion energy. It is also noticed from the graph that projected range of incident Au^{3+} ion is (R_P) 3.21 μm and straggle (δR_p) is 0.2274 μm. From these values, the modified surface thickness was calculated using the formula (R_P+ δR_p) and was found to be 3.4374 μm. Fig. 4.7 shows penetration depth of Au^{3+} ion in 2-amino-5-nitropyridinium chloride (2A5NPCl) NLO single crystal.

4.4.2. Single crystal X-ray diffraction

Pristine and irradiated samples of 2-amino-5-nitropyridinium chloride crystals were subjected to single crystal X-ray diffraction after swift heavy ion of Au^{3+} irradiation with different fluences. 2- amino-5-nitropyridinium chloride (2A5NPCl) is a monoclinic crystal system with a space group $P2_1$ and lattice parameters are

a= 9.957Å, b= 7.384 Å, c= 4.821Å, β= 95.85^0 and Z= 2. The measured values were concordant with reported values by Horiuchi et al **(**Horiuchi et al 1999**).** Density of 2-amino-5-nitropyridinium chloride was calculated from crystallographic data using ρ= MN/NV, where M is the molecular weight, Z is the number of molecules per unit cell, N is the Avogadro number and V is the volume of unit cell. Density was found to be 1.71g/cm^3. Fig.4.8. shows the Single crystal X-ray diffraction of pristine and irradiated crystals. The sharp nature of the peak indicated the good crystallinity of the grown crystal. It is revealed from the irradiated with different fluence (10^{13} ions/cm^2, 5 x10^{13} ions/cm^2 and 10^{14} ions/cm^2) pattern that decreased peak intensity and broadened the peak was due to defects.

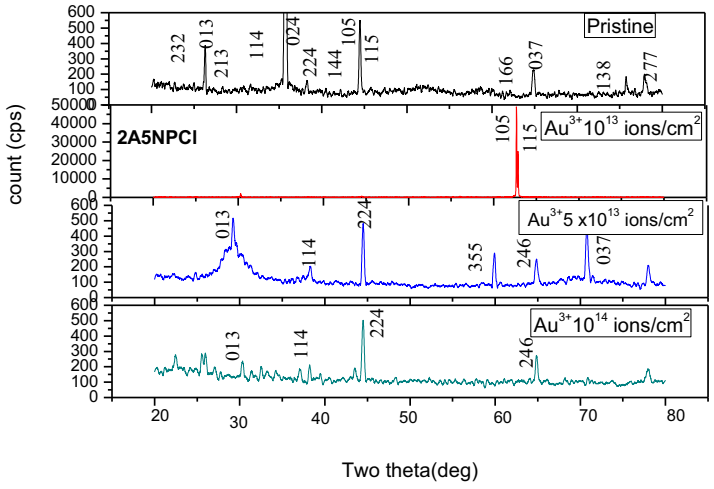

Fig. 4.8 Single crystal X-ray diffraction pattern of pristine and Au^{3+} ion irradiated crystals of 2-amino-5-nitropyridinium chloride (2A5NPCl) NLO single crystal

These decreased and broadening peak intensity shows occurrence of amorphization due to swift heavy ion (SHI). It was also noticed that the peak intensity

decreases with increase of ion fluence. At higher fluence, SHI creates cluster of defects. So peak intensity decreases due to rich defects produced in the crystalline structure. Ion projected range is 3.21 μm. In this range large amount of energy would have been dumped into relatively small volume causing electronic and avalanche and subsequently extending the damage region in the crystal.

4.4.3 FTIR

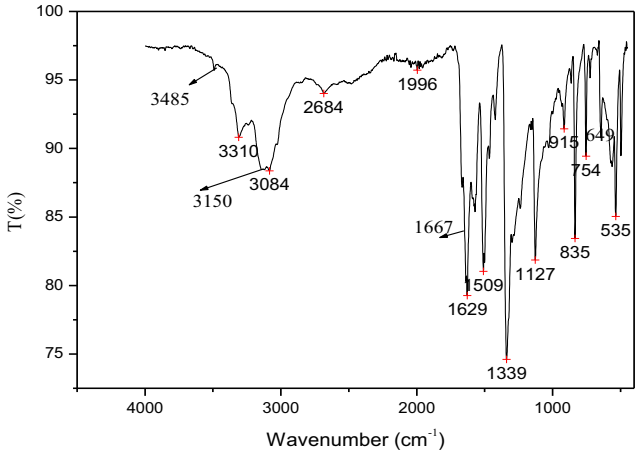

Fig. 4.9 FTIR spectral analysis of pristine 2-amino-5-nitropyridinium chloride (2A5NPCl) NLO single crystal

Pristine and irradiated samples of 2-amino-5-nitropyridinium chloride were exposed to FTIR spectrometer to analyse vibrational group in the grown crystals. FTIR spectral analysis of pristine 2-amino-5-nitropyridinium chloride (2A5NPCl) NLO single crystal is shown in figure 4.9. Strong and broad vibrational frequency observed at 3310 cm^{-1} and 3150 cm^{-1} indicate the presence of NH_2 asymmetric and symmetric modes. The symmetric and asymmetric vibrations of NO_2 occurred at 516 cm^{-1} and 1339 cm^{-1} respectively. These values are in good agreement with reported values by S. Dhanuskodi et al (Dhanuskodi et al 2005). Aromatic asymmetric stretching vibration of $2A5NP^{+}$ observed at 1648 cm^{-1}. The C-H out of plane and the

vibrational frequency 649 cm^{-1} indicates the inorganic Cl^-. The measured FT-IR and reported

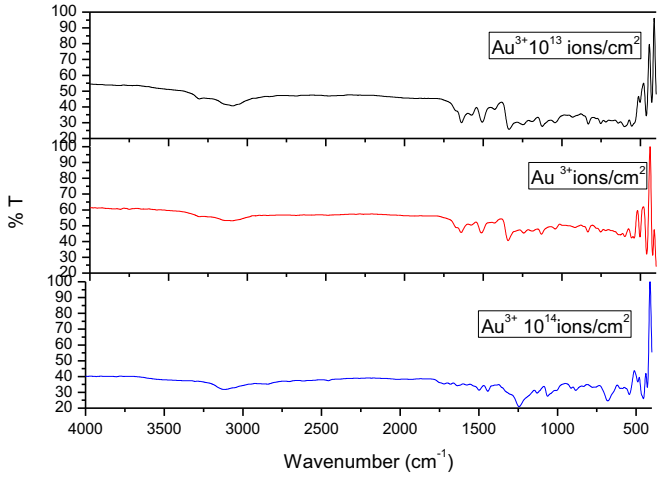

Fig.4.10 FTIR spectral analysis of Au^{3+} ion irradiated 2-amino-5-nitropyridinium chloride (2A5NPCl) NLO single crystal

Tab.4.2 The measured FTIR and reported values of 2-amino-5-nitropyridinium chloride (2A5NPCl) NLO single crystal

Reported Values (cm^{-1})	Measured values (cm^{-1})	Assignments
3296	3310	Asymmetric NH_2
3196	3150	Symmetric NH_2
1673	1667	C = N Asymmetric
1627	1629	N − H bending
1516	1509	Symmetric N − O
1352	1339	Asymmetric N − O
752	754	C − H out of plane pending
648	649	(N − H...Cl)

values are given in Tab. 4.2. It is noticed from the Fig. 4.10 that, appreciable peak or absence of peak from the pristine spectrum was observed after irradiation. When the sample is irradiated with MeV Au^{3+} ion, a large amount of energy is deposited in the system through electronic energy loss. This energy was used to break the bonds in target molecules. Vibrational frequency at 1223 cm^{-1} revealed that in- plane pending (C-H) vibrations are usually combined with pyridine (C-C) stretching mode. Vibration occurred at 3100 cm^{-1} is due to two C-H bonds in pyridine ring of the molecule. Bands observed at 531 cm^{-1} may be assigned to wagging and rocking modes of the nitro group.

4.4.4 Optical properties

Optical property of pristine and irradiated with different fluence (10^{13}, 5 x10^{13} and 10^{14} ions/cm^2) of 2-amino-5-nitropyridinium chloride was analyzed using UV-Vis-NIR analyzer. An optical spectrum of pristine and irradiated 2-amino-5-nitropyridinium chloride (2A5NPCl) is shown in Fig. 4.11. It is noticed from the absorption spectra that lower cut off value of pristine is 350.26 nm. The grown crystal almost has 99% of transmittance after the lower cut off wavelength. The absence of absorption in the region 350.26 nm and 800 nm is essential for the NLO materials. 2-amino-5-nitropyridinium is highly usable for second harmonic generation applications. Maximum absorption (λ_{max}= 350.26 nm) is due to the presence of conjugated double bond present in the sample. It is also noted from Fig.4.11 that the protonation of pyridine in the acid medium shortens the conjugated bond lengthens the C-NO_2 and shortens the conjugated bond lengths C=C, C=N and C-NH_2. This is due to alternation in the intra molecular charge transfer, ie.., NH being an electron-donor group in competition with the electron acceptor NO_2 group. The presence of the

protonated N- heteroatom in the aromatic ring is believed to account for the inclination of the molecular transition dipole moment with respect to the nitro amino direction in the non protonated molecule. This protonation modifies the transparency of the original molecule (Tao1 et al 1992). It is also observed from the absorption spectra that absorption of irradiated crystal increases with increase of ion fluences. Absorption is very high at fluence of 10^{14} ions/cm^2. It is also noticed that absorption of pristine is lesser than the irradiated crystals. Increasing of absorption is due to higher concentration of defects (Wrestbrook 1958) and the capture of excited electrons by existing ion vacancies in the irradiated 2-amino-5-nitropyridinium chloride (2A5NPCl). There is small change of absorption edge in the irradiated

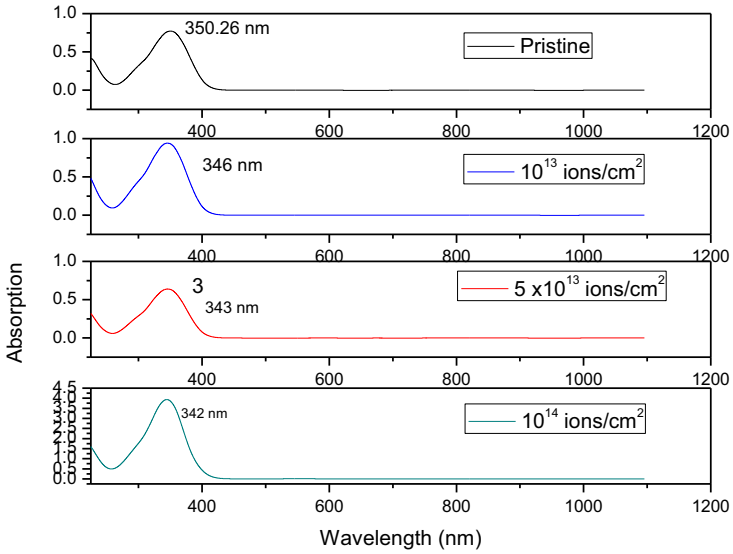

Fig. 4.11 Absorption spectra of Au^{3+}ion irradiated 2-amino-5-nitropyridinium chloride (2A5NPCl) NLO single crystal

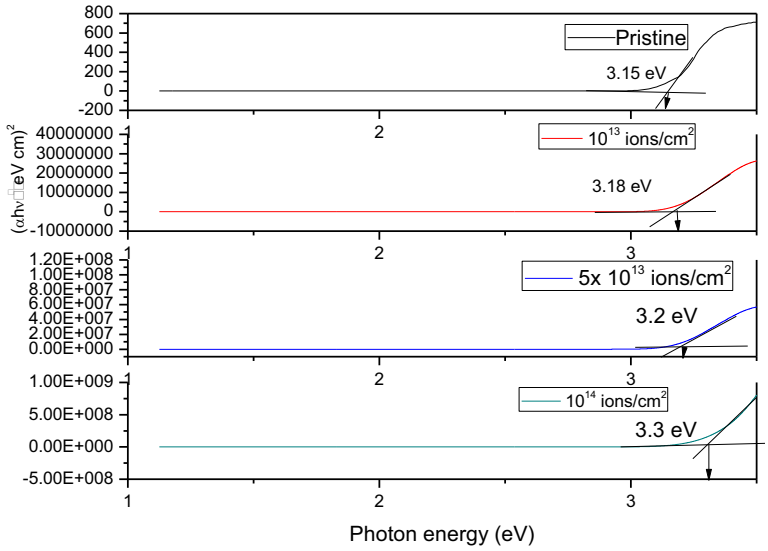

Fig. 4.12 Tauc's plot of pristine and Au^{3+} ion irradiated 2-amino-5-nitropyridinium chloride (2A5NPCl) NLO single crystal

crystals. lower cut off values are 346 nm, 343 nm, and 342 nm for Au^{3+} ion irradiated with three different fluence 10^{13} ions/cm^2, 5x 10^{13} ions/cm^2 and 10^{14} ions/cm^2 respectively. Both pristine and irradiated crystals have wide transparency window which is one of the additional key requirements for having efficient NLO character. Absorption edges were shifted towards shorter wavelength due to the formation of intermediate energy levels and change in structure after irradiation. It is also revealed that there is no additional peak absorbed in the spectra. This is due to the energy of the irradiated ion is not enough to move atoms from lattice to substitution. It is noticed that the surface of semiorganic crystal of 2-amino-5-nitropyridinium chloride (2A5NPCl) is not highly altered due to irradiation. Energy band gap of semiorganic crystals were calculated and using transmittance and absorption coefficient (α).

$$\alpha = A(Eg - h\nu)^{\frac{1}{2}}$$

where A is a constant, h is Plank's constant, E_g is the optical band gap and ν the frequency of the incident photons. Fig. 4.12 shows Tauc's plot. Energy band gap of pristine as well as irradiated samples were calculated and found to be 3.5 eV, 3.18 eV, 3.2 eV and 3.3 eV for pristine, 10^{13} ions/cm^2, 5x 10^{13} ions/cm^2 and 10^{14} ions/cm^2 respectively. Extinction coefficient (K) of the semiorganic crystal of 2-amino-5-nitropyridinium chloride (2A5NPCl) was calculated using

$$K = \frac{\lambda\alpha}{4\pi}$$

Fig. 4.13 shows extinction coefficient (K) of pristine and irradiated semiorganic NLO single crystal. It is understood from the extinction coefficient graph that there is loss of light due to interaction between incident light and electrons in pristine as well as

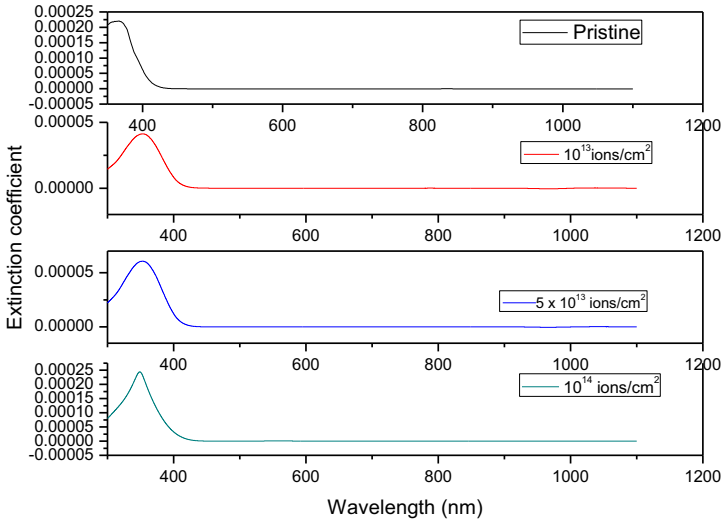

Fig.4.13 Extinction coefficient of pristine and Au^{3+}ion irradiated 2-amino-5-nitropyridinium chloride (2A5NPCl) NLO single crystal

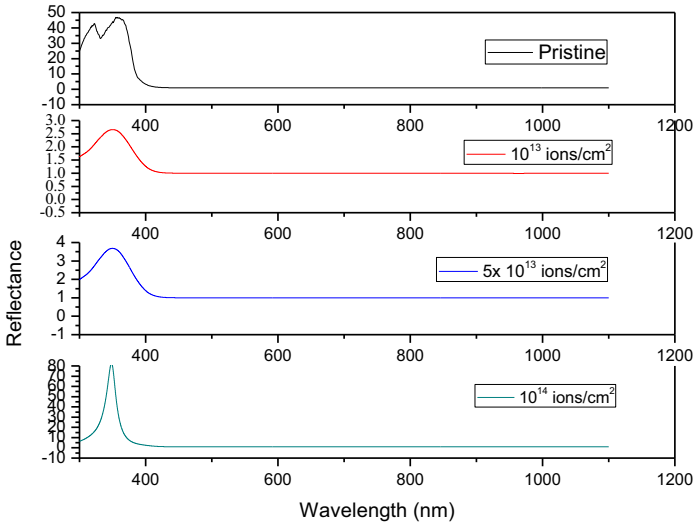

Fig. 4.14 Reflectance of pristine and Au^{3+}ion irradiated 2-amino -5-nitropyridinium chloride (2A5NPCl) NLO single crystal

Au^{3+} ion irradiated crystals. Fig. 4.14 shows reflectance of pristine and irradiated single crystals. It was calculated using

$$R = \frac{1 - \sqrt{1 - \exp(-\alpha t)}\exp(-\alpha t)}{1 - \exp(-\alpha t)}$$

It is evident that reflectance of light decreases gradually with increase of wavelength and attains constant. Decrease of reflectance shows the higher transmittance of grown crystal of pristine and irradiated using three different ion fluences.

4.4.5 Microhardness study

Vicker's hardness measurement is one of the best hardness tests. Figure 4.15 shows hardness of pristine and irradiated 2-amino-5-nitropyridinium chloride (2A5NPCl) crystals. It is clearly noticed from the graph that both pristine and irradiated semiorganic crystals respond linearly with applied load. Load was applied

on pristine and irradiated crystals in range from 25-100 g. Microhardness of the both pristine and irradiated with different fluences (10^{13}, 5 x10^{13} and 10^{14} ions/cm^2) increases with increase of applied load. It is also noticed from the graph that hardness of irradiated samples are greater than pristine sample. Microhardness increases with increase of SHI ion fluence. This is due to amorphization created in the irradiated crystals. Increase of hardness is creation of internal stress (residual surface compression stress) on the surface of the irradiated crystals additionally by swift heavy ion. At higher fluence, crystals are rich in defects. Hardening coefficient was calculated using least square fit method and it was found to be 3.3, 2.3, 2.41 and 3.62 for pristine and irradiated crystals with three different ion fluences 10^{13} ions/cm^2, 5x 10^{13} ions/cm^2 and 10^{14} ions/cm^2 respectively. Plastic deformation and stiffness of pristine and irradiated crystals were calculated. Stiffness was calculated using

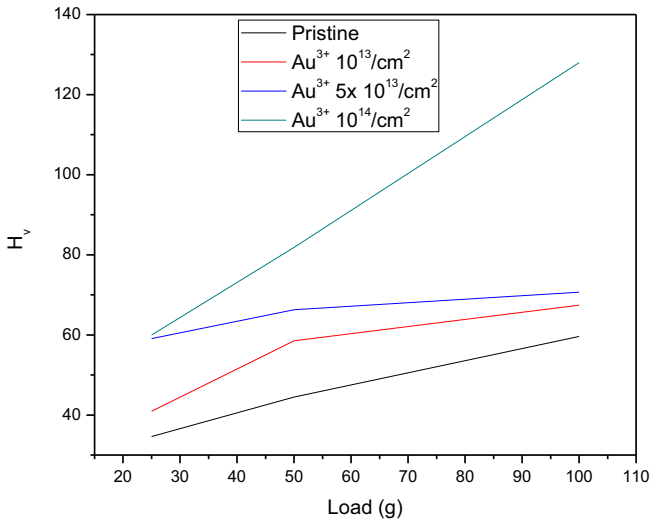

Fig. 4.15 Vicker's microhardness of pristine and Au^{3+} ion irradiated crystal of 2-amino-5-nitropyridinium chloride (2A5NPCl) NLO single crystal.

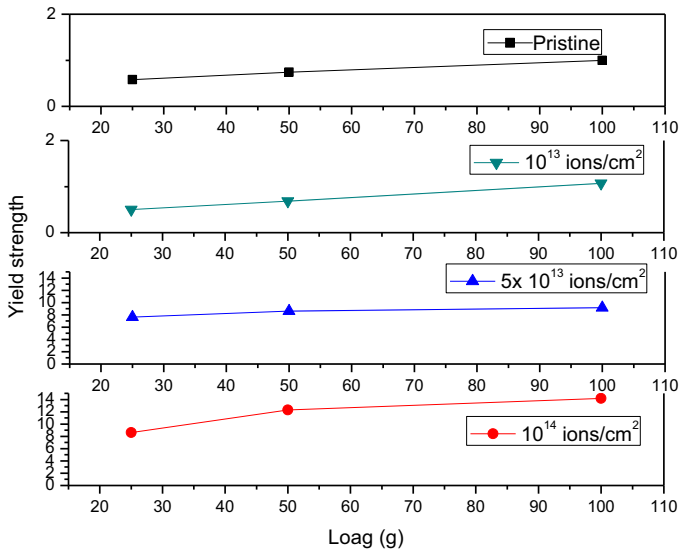

Fig. 4.16 Yield strength of pristine and Au^{3+}ion irradiated 2-amino-5-nitropyridinium chloride (2A5NPCl) NLO single crystal

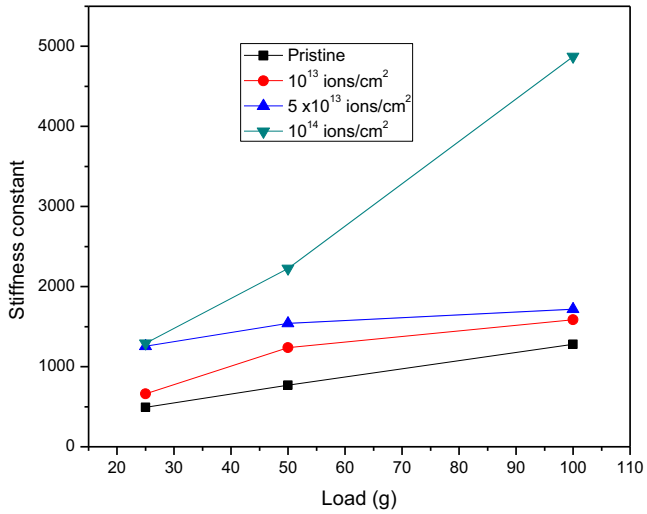

Fig. 4.17 Stiffness of pristine and Au^{3+}ion irradiated 2-amino-5-nitropyridinium chloride (2A5NPCl) NLO single crystal

Wooster's emprical formula (Wooster 1953) and it is given by $C_{11}= H_v^{(7/4)}$. Yield strength was calculated using $\sigma_y= (H_v/3)\ (0.1)^{(n-2)}$. Fig. 4.16 and 4.17 show yield strength and stiffness of pristine and irradiated 2-amino-5-nitropyridinium chloride (2A5NPCl) NLO single crystal. It is noticed from the stiffness and yield strength graph that stiffness and yield strength increase with increase of applied load. Both stiffness and yield strength show linear behaviour with applied load. It is also obsorved from the graph that stiffness and yield strength of pristine samples are lesser than the irradiated crystals. Increase of plastic deformation and stiffness in irradiated crystals are due to the formation rich defects which tighten the bonding between two ionic molecules. Crystalline nature of semiorganic crystal is changed slowly into amorphous in nature due to these rich defects.

4.4.6 Dielectric study

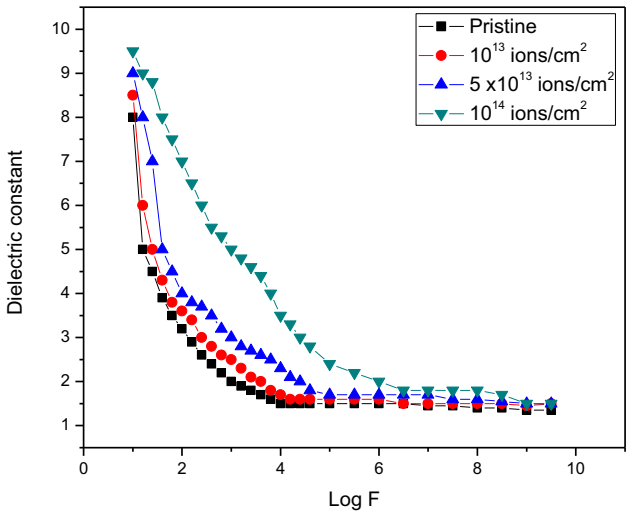

Fig. 4.18 Dielectric constant of pristine and Au^{3+}ion irradiated 2-amino-5-nitropyridinium chloride (2A5NPCl) NLO single crystal

Fig. 4.18 shows dielectric properties of monoclinic system of pristine and irradiated samples. Fabrication of opto-electronic devices depends on the dielectric properties of the crystals (Boomadevi et al 2004). Suitably cut and polished NLO single crystal of 2-amino-5-nitropyridinium chloride (2A5NPCl) was used to study the dielectric studies. The dielectric constant was calculated using the equation $\varepsilon_r = Cd/\varepsilon_0 A$

where, A is the area of the sample and d is the thickness of the sample. It is revealed from the graph that dielectric constant decreases with increase of applied frequency of both pristine and irradiated crystals. It is also noticed that dielectric constant of pristine is lesser than the irradiated samples. Increase of dielectric constant in irradiation crystal with three different ion fluences is due the interaction of swift heavy ion with solid which creates region of disorderness with defects in the crystal lattice. Further, increase of ion fluence creates amorphous containing region of defects and also isolate the amorphous region from each other. At higher fluence more ions are activated with lattice disorderness which increases more activation of interaction between the ions (Horiuchi et al 2002, and Wooster 1953). Capacitance increases due to this interaction of ions hence dielectric constant increases as we increase the ion fluence from 10^{13} ions/cm^2 to 10^{14}ions/cm^2.

4.4.7 Fluorescence

The luminescence emission was measured for pristine and irradiated crystal of 2-amino-5-nitropyridinium chloride (2A5NPCl) at room temperature. Fig. 4.19 shows fluorescence spectra of pristine and irradiated crystals. For a pristine sample the intensity peak displays a remarkable high intensity band around 529 nm may be attributed to π-π^* transitions due to interaction between the ligand molecules and swift heavy ion. It is also evident from the spectra that, the intensity peak of irradiated

crystals decreases compared with pristine sample. The decrease in intensity peak and shifting of high intensity peak may be lattice deformation produced due to the displacement of cations. Lattice damage on the surface of the sample is due to high energetic ion irradiation. Intensity decreases due to loss of luminescence property of the material. Au^{3+} ion on 2-amino-5-nitropyridinium chloride could act as a non-radiactive recombination centre.

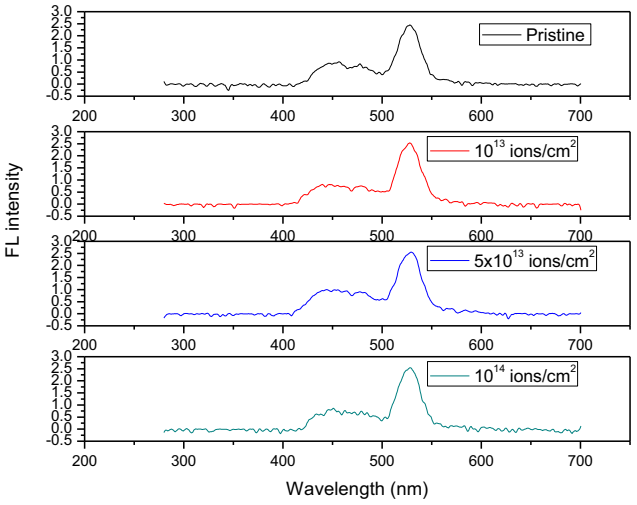

Fig. 4.19 Fluorescence of pristine and Au^{3+} ion irradiated crystal of 2-amino-5-nitropyridinium chloride (2A5NPCl) NLO single crystal

4.4.8 Scanning Electron Microscope (SEM)

Surface morphology of pristine and irradiated crystal was analysed using scanning electron microscope (SEM). Fig. 4.20 (a, b, c & d) shows SEM image of pristine and irradiated crystals. SEM image shows like hillock on the surface of irradiated crystal. This is due to swift heavy ion which displaced the lattice on the surface of the crystal. It is also noticed that there is some morphological changes due to high energetic ions. On the surface of irradiated crystal, Pores and cracks were

formed along with roughness when a semiorganic 2-amino-5-nitropyridinium chloride (2A5NPCl) was irradiated with high fluence.

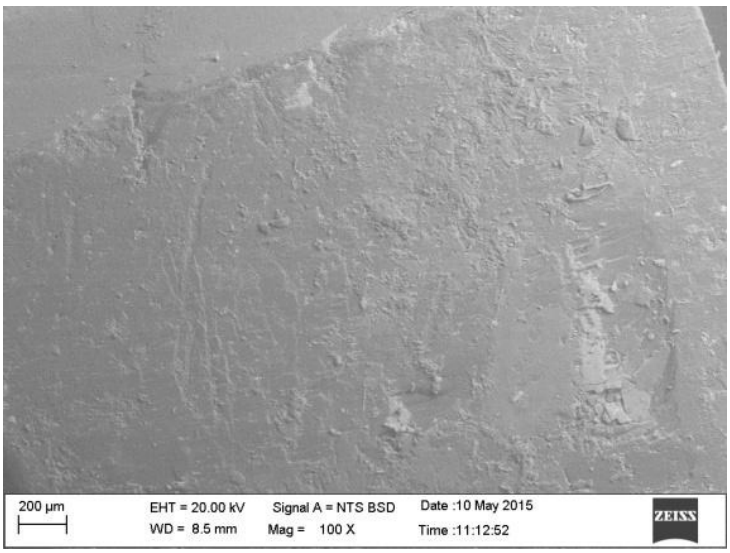

Fig.4.20 a) SEM image of 2-amino-5-nitropyridinium chloride (2A5NPCl) NLO single crystal

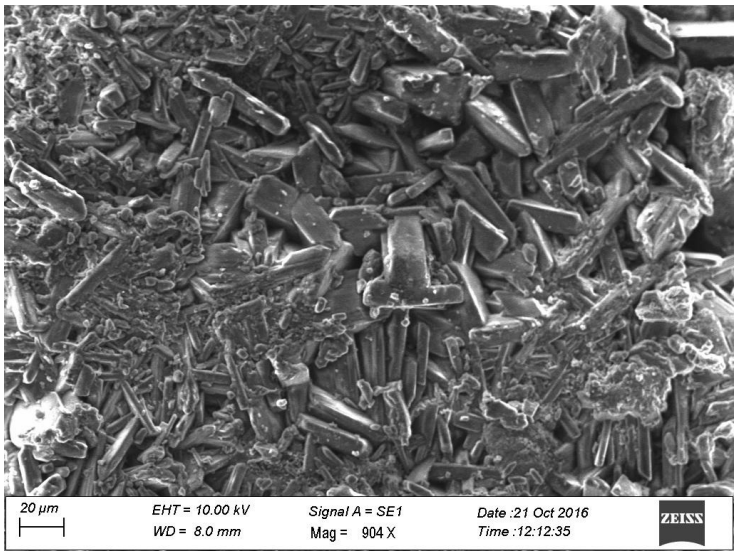

Fig.4.20 b) SEM image of Au^{3+} ion irradiated (10^{13} ions/cm^2) 2-amino-5-nitropyridinium chloride (2A5NPCl) NLO single crystal

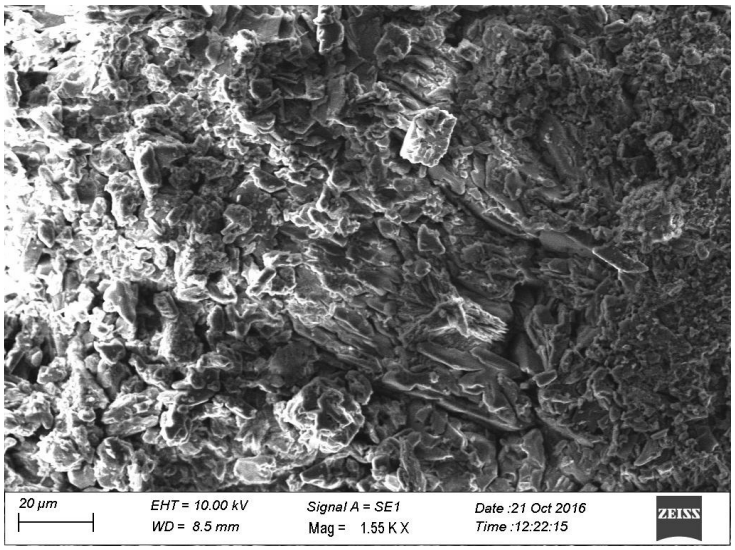

Fig.4.20 c) SEM image of Au^{3+} ion irradiated (5x 10^{13} ions/cm^2)

2-amino-5-nitropyridinium chloride (2A5NPCl) NLO single crystal

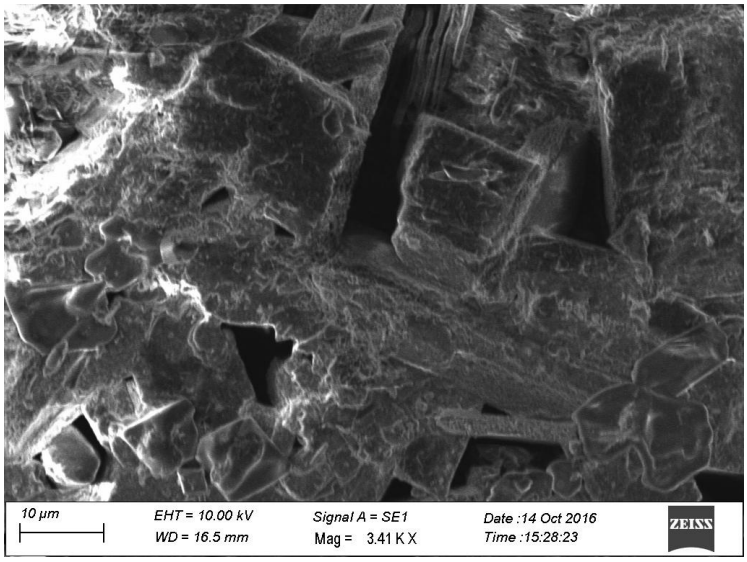

d)

Fig.4.20 d) SEM image of Au^{3+} ion irradiated (10^{14} ions/cm^2)

2-amino-5-nitropyridinium chloride (2A5NPCl) NLO single crystal

4.4.9 NLO Test

Kurtz powder technique was used to measure nonlinear optical (NLO) property. Out put was measured by the emission of green laser light. 2-amino-5-nitropyridinium chloride (2A5NPCl) output intensity was 164 mV whereas that of KDP was 55 mV. 2-amino-5-nitropyridinium chloride (2A5NPCl) is suitable for short wavelength generation. This efficiency is due to the high density of chromophores, which one of the highest is observed among the herringbone structure built with the 2-amino-5-nitropyridinium entity. 2-amino-5-nitropyridinium chloride (2A5NPCl) is a potential candidate for frequency doubling and an optical parametric oscillator. By comparing 2A5NPCl with other crystals of p- nitroaniloine family, it is found that 2A5NPCl is advantageous for the generation of the short wavelength until 400 nm, and its output intensity is superior to that of the 2-amino-5-nitropyridinium dihydrogen phosphate (2A5NPDP) (145 mV) (Ambrose Rajkumar et al 2016), and 2-amino-5-nitropyridinium sulfamate (2A5NPS) (138 mV) (Ambrose Rajkumar et al 2016(a). The inorganic part and its arrangement are important factors that modify the hyperpolarizabilities (β_{ij}) of the $2A5NP^{+}$ action (Horiuchi et al 2002). Nonlinear property, irradiated crystals were measured using Kurtz powder technique how as we measured pristine sample. Outputs of irradiated samples were measured by the emission of green laser light. The output intensity of irradiated samples are 125 mV, 118 mV, and 63 mV for ion fluence 10^{13} ions/cm^2, 5x 10^{13} ions/cm^2 and 10^{14} ions/cm^2 respectively. It is noticed from the output value that there is decrease of nonlinear property than the pristine but it is not less than reference material KDP. It is understood from the comparison with pristine that noncentro symmetric system is not highly affected in 2-amino-5-nitropyridinium chloride (2A5NPCl) than the other derivatives of 2-amino-5-nitropyridinium family of crystals.

4.4.10 Thermal Analysis

TG and DTA of grown crystal of 2-amino-5-nitropyridinium chloride (2A5NPCl) are shown in fig. 4.21a. The TG and DTA graph reveals that there are three stages of decompositions. In DTA curve there is an endothermic peak at 188° C. An endothermic peak at which there is no weight loss observed in TG curve. In first stage there is no weight loss up to 188°C from room temperature. The material starts to decompose at 188°C in the second the stage, which is known as melting point of the material. In DTA there is an exothermic peak at 288° C. In third stage the molecular network started to dissociate above 288° C. Fig. 4.19. (b, c & d) shows TG an DTA of Au^{3+} ion irradiated crystals.

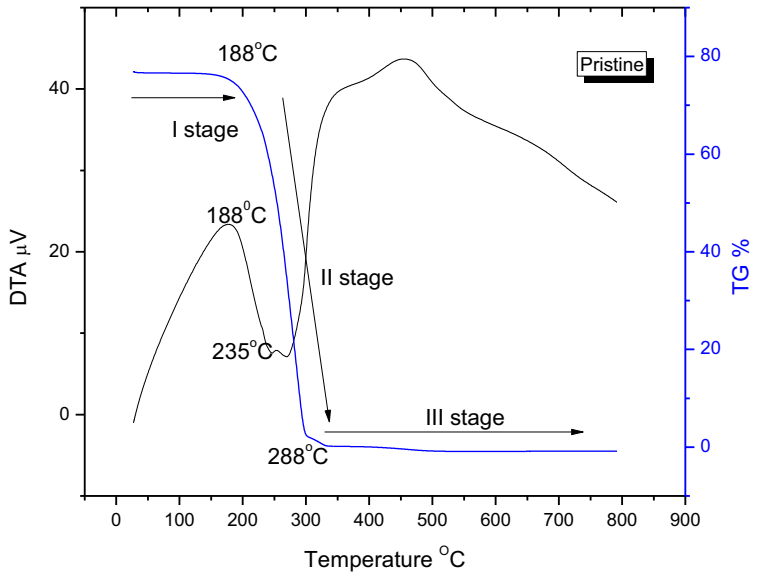

Fig.4.21 a) Thermal analysis of 2-amino-5-nitropyridinium chloride (2A5NPCl) NLO single crystal

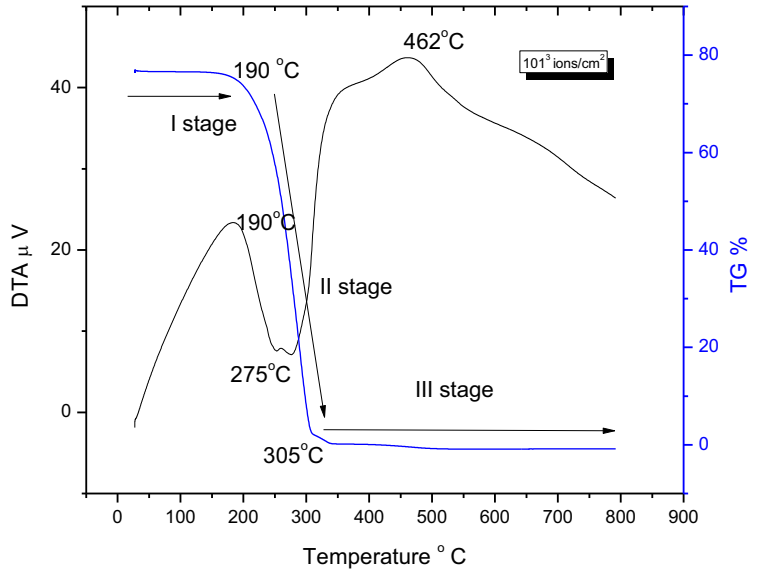

Fig.4.21 b) Thermal analysis of Au^{3+} ion irradiated (10^{13} ions/cm^2)

2-amino-5-nitropyridinium chloride (2A5NPCl) NLO single crystal

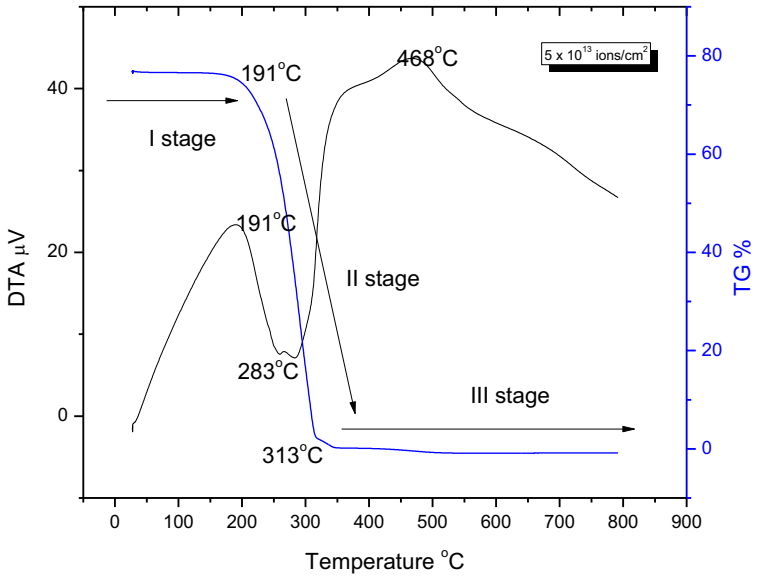

Fig.4.21 c) Thermal analysis of Au^{3+} ion irradiated (5x 10^{13} ions/cm2)

2-amino-5-nitropyridinium chloride (2A5NPCl) NLO single crystal

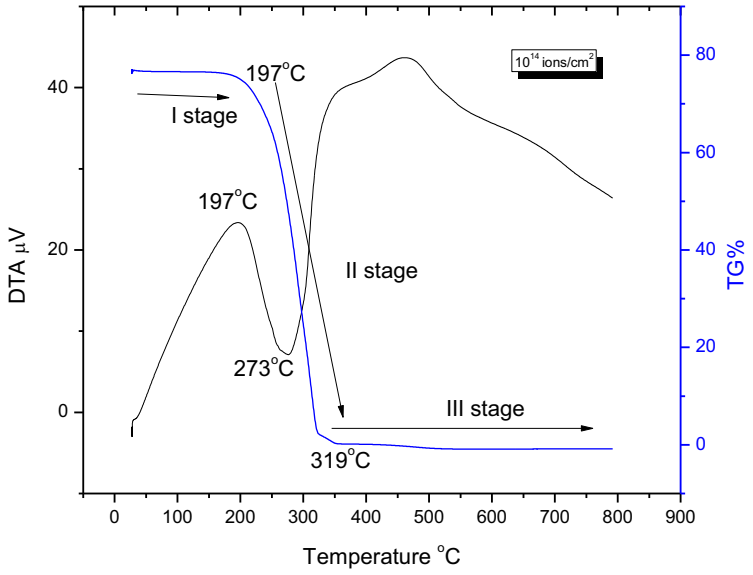

Fig.4.21 d) Thermal analysis of Au^{3+} ion irradiated (10^{14} ions/cm^2)

2-amino-5-nitropyridinium chloride (2A5NPCl) NLO single crystal

It is observed from these graph that melting point of the irradiated crystal increases with increase of ion fluence from 10^{13} ions/cm^2 to 10^{14} ions/cm^2 and melting points are 190°C, 191°C, and 197°C for three different fluence (10^{13} ions/cm^2, 5x 10^{13} ions/cm^2 and 10^{14} ions/cm^2) respectively. The increase of thermal stability and sharpness in the decomposition after melting point is due to disorderness of the crystals after irradiation. It is understood that degree of crystallinity decreases after irradiation.

4.4.11 Impedance Analysis

Electrical impedance gives a measure of opposition to alternating current and it extends the concept of resistance to Ac circuits, describing not only the relative amplitude of the voltage and current but also the relative phases. The frequency

dependent properties of a materials are often represented as complex impedance Z* and which is related as

$$Z^*(\omega) = Z' - j\,Z''$$

where Z' and Z'' real and imaginary components of impedance. Fig. 4.22 and 4.23 show real and imaginary part of impedance of pristine and irradiated NLO single crystals. It is noticed from the graph that real and imaginary part of impedance decreases with increase of frequency in pristine as well as irradiated crystals. It is the indication of large polarization due to space charge polarization. It is also noticed that the impedance of irradiated crystal is large than the pristine sample. It is also observed broad peak in real and imaginary part of impedance. This is due to relaxation processes in the samples. It is also observed that broadening and shifting of the peak is due to creation rich defects at higher fluence. The results in real and imaginary part of impedance provide an indication of deceasing impedance with increase of frequency is increasing the conduction with frequency. Fig. 4.24 shows Nyquist's plot of pristine and Au^{3+} ion irradiated 2-amino-5-nitropyridinium chloride (2A5NPCl) NLO single crystal. A semicircle is seen in pristine and as well as Au^{3+} ion irradiated crystal due to bulk effect of the sample. A combination of capacitor and resistor creates bulk effect in the samples. It is also noticed from the Nyquist's plot that bulk resistance of irradiated crystal was increased more than the pristine crystal. It is also revealed from the graph that bulk resistance increases with increase of ion fluences from 10^{13} ions/cm^2 to 10^{14} ions/cm^2. The bulk resistance and grain boundary resistance were calculated from the intercept of the semicircle arc on the real axis and peak of the semi circle respectively. Tab. 4.3 shows bulk resistance and grain boundary resistance of pristine and irradiated crystal.

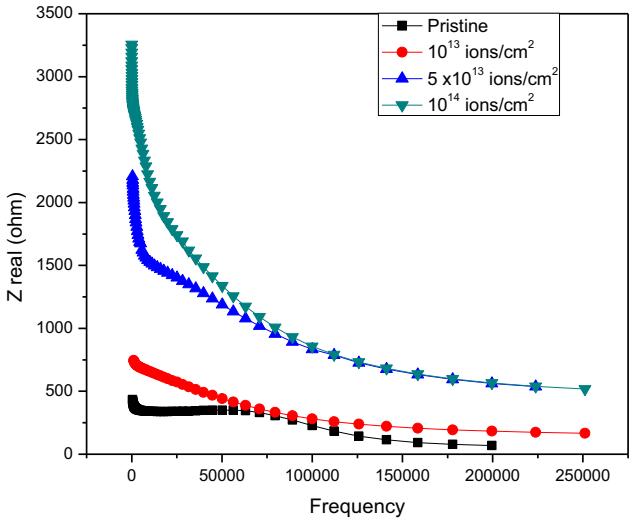

Fig. 4.22 Real part of impedance of pristine and Au^{3+} ion irradiated 2-amino-5-nitropyridinium chloride (2A5NPCl) NLO single crystal

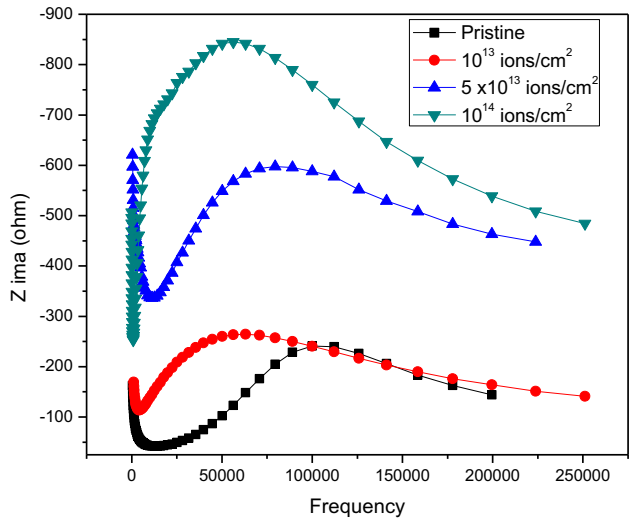

Fig. 4.23 Imaginary part of pristine and Au^{3+} ion irradiated 2-amino-5-nitropyridinium chloride (2A5NPCl) NLO single crystal

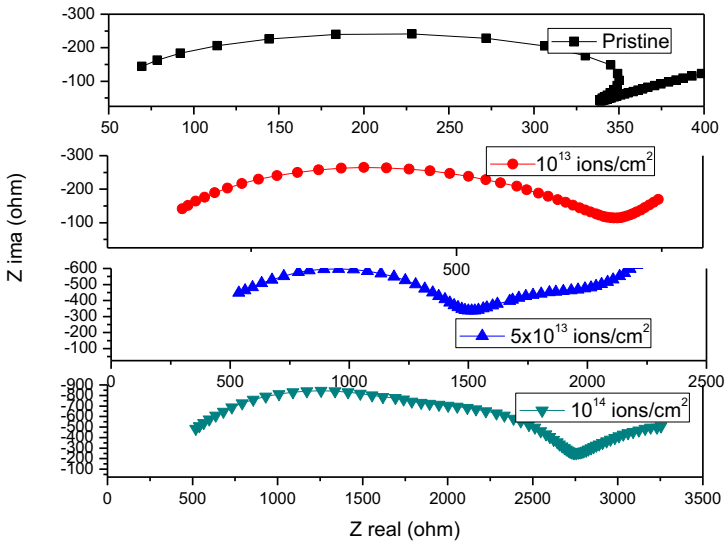

Fig. 4.24 Nyquist's plot of pristine and Au^{3+} ion irradiated 2-amino-5-nitropyridinium chloride (2A5NPCl) NLO single crystal

S.No	Ion fluence	Bulk resistance (Ohm)	Grain boundary resistance (Ohm)
1	Pristine	230	339
2	10^{13} ions/cm^2	420	680
3	5 x 10^{13} ions/cm^2	1075	1500
4	10^{14} ions/cm^2	1680	2750

Tab. 4.3 Bulk resistance and grain boundary resistance of pristine and Au^{3+} ion irradiated 2-amino-5-nitropyridinium chloride (2A5NPCl) NLO single crystal.

4.5 Conclusion

2-amino-5-nitropyridinum chloride (2A5NPCl) was grown from slow evaporation and Assembled Temperature Reduction (ATR) method. The grown crystal is a monoclinic with a space group $P2_1$ and lattice parameters are a = 9.957Å, b = 7.384 Å, c= 4.821Å, β= 95.85^0 and Z= 2. Semiorganic crystal of 2-amino-5-nitropyrodinium chloride (2A5NPCl) was irradiated with swift heavy ion of Au^{3+} with varied fluences (1x 10^{13} ions/cm^2, 5x 10^{13} ions/cm^2 and 1x 10^{14} ions/cm^2. It was subjected to the single crystal X-ray diffraction to study crystalline quality of the irradiated crystal. Crystalline quality decreased with increase of ion fluence because of the formation of defects produced after irradiation. It was also observed that crystal surface was not completely affected by swift heavy ion of 10.8 MeV. Functional group of irradiated crystal was measured. From the absorption spectra, it was noticed that absorption increased with increase of ion fluence due to capture of existing ion vacancies and there was no additional peak observed. It was due to the energy transferred by SHI was not enough to move atoms from lattice to substitution position. Hardness of the irradiated crystal increased with increase of ion fluence was due to the internal stress produced on the surface that increased the microhardnes of the irradiated samples. Luminescence reveals that intensity decreased due to the loss of luminescence property of the material, which caused by swift heavy ion (SHI). Formation of intermediate energy levels which converted the photon into phonon affected the radiative transition. Hence, peak shifted and intensity of peak decreased. At higher fluence more ions were activated with lattice disorderness which increased more activation of interaction between the ions. Capacitance increased due to this interaction of ions hence dielectric constant increased as increased the ion fluence from 10^{13} ions/cm^2 to 10^{14} ions/cm^2. Pores and cracks were seen clearly in SEM along

CHAPTER V

STUDIES ON Au^{3+} SWIFT HEAVY ION IRRADIATED 2-AMINO-5-NITROPYRIDINIUM DIHYDROGEN PHOSPHATE (2A5NPDP) NONLINEAR OPTICAL (NLO) SINGLE CRYSTAL

5.1 Introduction

Recent decades, swift heavy ion (SHI) has been used to irradiate solids. Using irradiation process one can modify the structural, mechanical, optical, thermal and electrical properties of the materials. Ion irradiation plays a vital role in modification of engineering materials. Ion beam interaction has wide application such as industrial, technological and medical application for the compound formation, nanostrucrute, thin film, biological diagnosis etc. Swift heavy ion irradiation methods provide a highly controllable set of tool which can be used for investigation systematically at the atomic level. When an energetic ion beam interacts with solid or crystal, energy is transferred from ion to solid. Penetration of ion beam in the material involves charge exchange between the projectile ion and target (Jain & Garima Agarwal 2011). This energy transfer induces lattice deformation and defects in the crystal that changes the properties of the crystal (Nagarau et al 2001). Energy, fluence and ion beam current are key parameters in determining the efforts of ion irradiation (sreeramana et al 1997; and Bhat et al 2000). Semiorganic crystals are new kind of materials which has interesting nonlinear optical properties (Jang & Fang 1999; Angeli Mary & Dhanuskodi 2001). These hybrid materials combining the advantages of organic and inorganic crystals are built up by the anchorage of organic molecules into inorganic matrices through strong hydrogen bonds. Semiorganic crystals exhibit wide transparency range and bulk crystals morphologies. Donor –acceptor conjugated NLO materials, high molecular polarizability and acentric structure materials are used to

build efficient NLO materials. The donor and acceptor groups are linked through conjugated rings, such as benzene or pyridine that are more used. Among various organic molecules, 2–amino-5-nitropyridine allow for the growth of numerous slats (Pal et al 2003). 2–amino-5-nitropyridine is a potential nonlinear optical candidate. 2–amino-5-nitropyridine has an interesting molecular structure which has a nitro group as an electron donor and amino group as an electron acceptor. Further, the pyridine ring acts as a cationic bonding site, the nitro group as hydrogen acceptor and amino group as a hydrogen donor. Because of these special molecular building blocks of nonlinear optical materials, these have been the subjects of very intensive studies in the last few years for their potential applicability in image processing and optical communications. It has also been used within hydrogen- bonded organic anionic networks, or as counterions in organic- inorganic salts. Using organic molecule of 2–amino-5-nitropyridine, a numerous salts were grown like 2–amino-5-nitropyridinium sulfamate (2A5NPS), 2–amino-5-nitropyridinium chloride (2A5NPCl), 2–amino-5-nitro pyridinium hydrogen oxalate (2A5NPHO), 2–amino-5-nitropyridinium bromide (2A5NPBr), 2-amino-5-nitropyridinium trifluoroacetate, 2-amino-5-nitropyridinium phenolsulfonate, 2–amino-5-nitropyridinium dihydrogen arsenate (2A5NDA), 2-amino-5-nitropyridinium dihydrogen monophosphate (2A5NPDP), 2-amino-5-nitropyridinium- L-monohydrogentartrate, 2-amino-5-nitropyridinium halides (Cl^-, Br^-), 2-amino-5-nitropyridine adsorbed on roughened polycrystalline silver electrodes, 2-amino-5-nitropyridinium acetophosphonate, 2-amino-5-nitropyridine adsorbed on silver sols, 2-amino-5-nitropyridinium dihydrogen phosphate, 2-amino-5-nitropyridine and n- chloroacetic acid assemblies, 2-amino-5-nitropyridine-L-(+)-Tartrate, 2-amino-5-

nitropyridinium chloride, two 5-nitro-2-aminopyridinium cuprates: $(5\text{-NAP})_2\ CuCl_4$ and the quantum magnetic ladder $(5\text{-NAP})_2\ CuBr_4 \bullet H_2O$, 2-amino-5-nitropyridine with benzenesulfonic acids, 2-amino-5-nitropyridinium tetrafluoroborate, 2-amino-pyridinium p-nitro-benzoate, 2-amino-5-nitropyridinium l-tartrate, 2-amino-5-chloropyridinium hydrogen selenate, 2-amino-5-nitropyridinium toluenesulfonate, 2-amino-5-nitropyridinium hydrogen selenate, 2-amino-5-nitropyridinium tetraoxidorhenate (VII) monohydrate, quantum chemical studies on structure of 2-amino-5-nitropyrimidine, 5-amino-2-pyridine, 2-amino-5-nitro pyridinium nitrate (2A5NPN), were grown and structure solved and their properties were reported (Masse et al 1991; Horiuchi et al 1995; Anna Puig et al 1998; Morela et al 2002; Pricilla Jeyakumari et al 2007; Zyss et al 1993; Osamu Watanabe et al 1993; Oussaid et al 1996; Pecaut et al 1993; Foresti et al 1994; Pecaut and Masse 1994; Maurizio Muniz et al 1995; Yvette Le Fur et al 1996; Oussaid et al 1996; Horiuchi et al 1997; Ibanez et al 1997; Dhanuskodi et al 2004; Horiuchi et al 2004; Zaccaro et al 1998; Turnbull et al 2002; Hideko et al 2004; Manivannan et al 2005; Jebas and Balasubramanian 2006; Manikandan and Dhanuskodi 2007; Lorenc et al 2008; Akriche et al 2009; Anandha Babu et al 2009; Rodrigues et al 2009; Arivazhagana and Subhasinib 2012; Lin Chen et al 2013; Sivasubramani et al 2015; and Sivasubramani et at 2016; Ambrose Rajkumar et al 2015; Horiuchi et al 1999, Kotler et al 1992; Ambrose Rajkumar et al 2014; Dhanuskodi et al 2005; Jovita et al 2013; Anandha babu et al 2011; Feve et al 1999; Bagieu-Beucher et al 1991; and Ambrose Rajkumar et al 2016). 2–amino-5-nitropyridinium hydrogen oxalate (2A5NPHO) was grown and structure also solved. Using Sankaranarayanan- Ramasamy (SR) method, 2–amino-5-nitropyridinium dihydrogen phosphate (2A5NPDP) was grown and properties were reported (Ambrose Rajkumar et al 2016). Mechanical, electrical and

photoconductivity of 2–amino-5-nitropyridinium hydrogen oxalate (2A5NPHO), 2–amino-5-nitropyridinium dihydrogen phosphate (2A5NPDP) and 2–amino-5-nitropyridinium nitrate (2A5NPN) were also reported (Ambrose Rajkumar et al 2014; Ambrose Rajkumar et al 2014a; Ambrose Rajkumar et al 2014b; Ambrose Rajkumar et al 2014c; Ambrose Rajkumar et al 2014d; Ambrose Rajkumar et al 2015; Ambrose Rajkumar et al 2016; and Ambrose Rajkumar et al 2016a). 2–amino-5-nitropyridinium chloride (2A5NPCl) was grown using Assembled Temperature Reduction method (ATR) and characterizations were reported (Ambrose Rajkumar et al 2017). In this chapter, modifications in morphology, mechanical, optical, electrical, and thermal and NLO properties of Au^{3+} swift heavy ion irradiated 2–amino-5-nitropyridinium dihydrogen phosphate (2A5NPDP) is investigated.

5.2 Experimental procedure

5.2.1 Crystal growth

The commercially available 2-amino-5-nitropyridine (Sigma– Aldrich, purity > 97%) is a weak bronested base and can acquire a proton in strong acidic aqueous medium (pH < 2).This induces the dissolution of this molecule in an aqueous acidic medium by forming $2A5NP^{+}$cation and leads to the synthesis of hydrogen bonded salts with the conjugated bases of strong or medium acids. The organic– inorganic 2-amino-5-nitropyridinium dihydrogen phosphate (2A5NPDP) is obtained by dissolving the 2-amino-5-nitropyridine in orthophosphoric acid at 50°C in millipore water of resistivity 18.6 ohm cm. Single crystals of 2-amino-5-nitropyridinium dihydrogen Phosphate (2A5NPDP) were grown from aqueous solution using slow solvent evaporation technique. The solvent of the supersaturated solution was allowed to evaporate through the perforated lid of the container. The reaction scheme and chemical structures are illustrated in Fig. 5.1. Numerous tiny crystals were formed at

the bottom of the container due to spontaneous nucleation. Fig. 5. 2 shows NLO single crystals of 2-amino-5-nitropyridinium dihydrogen phosphate (2A5NPDP) from slow evaporation.

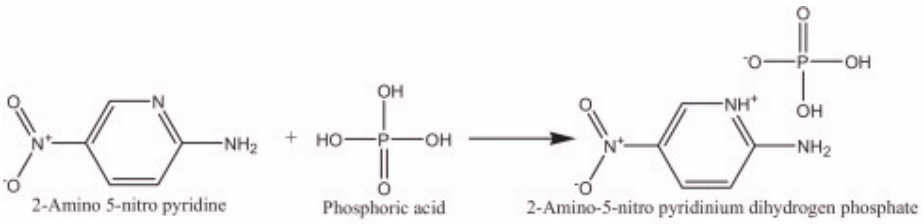

Fig. 5.1 Reaction scheme of 2-amino-5-nitropyridinium dihydrogen phosphate (2A5NPDP)

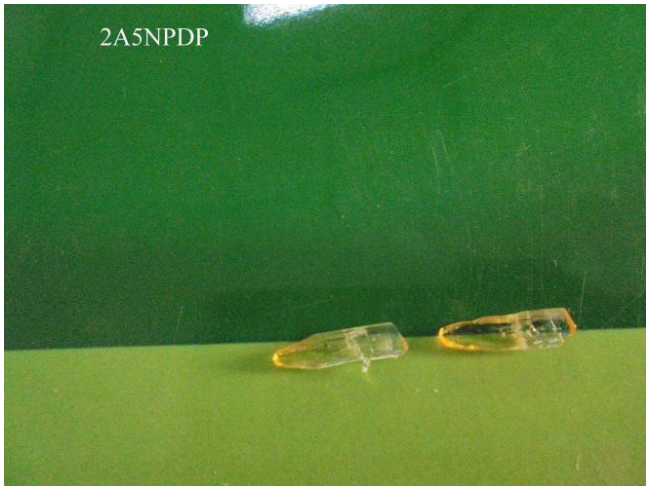

Fig.5.2 As grown 2-amino-5-nitropyridinium dihydrogen phosphate (2A5NPDP)NLO single crystal from slow evaporation method.

5.2.2 Solubility of 2-amino-5-nitropyridinium dihydrogen phosphate (2A5NPDP)

The synthesized salt was used to measure the solubility of 2-amino-5-nitropyridinium dihydrogen phosphate (2A5NPDP) in distilled water. A 250 ml glass beaker filled with 100 ml of distilled water was placed inside a constant temperature bath whose temperature was fixed at 30°C. An acrylic sheet with a circular hole at the

middle through which a spindle from an electronic motor placed over a sheet was introduced into the solution. A Teflon paddle was attached at the end of the rod for stirring the solution.2-amino-5-nitropyridinium dihydrogen phosphate (2A5NPDP) salt was added in small amounts. The addition of the salt and stirring were continued till the formation of precipitate which confirmed the saturation of the solution. The solubility study of 2-amino-5-nitropyridinium dihydrogen Phosphate (2A5NPDP) was carried out by increasing the amount of 2-amino-5-nitropyridinium dihydrogen phosphate (2A5NPDP) salt that dissolved in water at 30^{o}, 35°, 40^{o}, 45^{o}, and 50°C. Fig. 5.3 shows the solubility of 2-amino-5-nitropyridinium dihydrogen phosphate (2A5NPDP) in 100 ml of double distilled water at different temperatures. It is seen from the solubility curve that the solubility increases with temperature. The solubility of 2-amino-5-nitropyridinium dihydrogen phosphate (2A5NPDP) at room temperature was found to be moderate (17 g/100 ml of water).

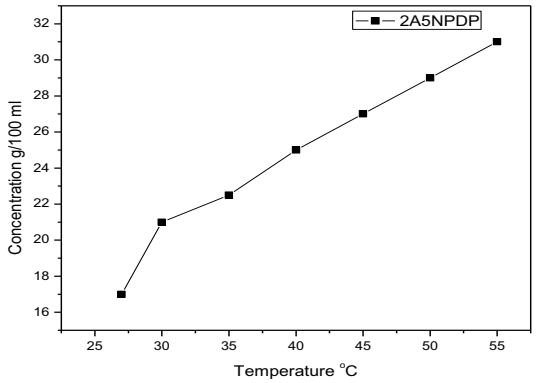

Fig. 5.3 Solubility of 2-amino-5-nitropyridinium dihydrogen phosphate (2A5NPDP)

5.2.3 Crystal growth from Sankaranarayanan– Ramasamy (SR) method

The saturated solution of 2-amino-5-nitropyridinium dihydrogen phosphate (2A5NPDP) was prepared in accordance with the solubility data. Among them transparent and defect free crystals were chosen as seed for growing bulk crystals

Fig. 5.4 Sankaranarayanan-Ramasamy (SR) method apparatus

using modified Sankaranarayanan– Ramasamy (SR) method. Experimental setup of Sankaranarayanan– Ramasamy (SR) method is shown in Fig. 5.4. Using this crystal growth apparatus good optical quality crystal with dimensions 43 mm × 10 mm × 8 mm was harvested after a period of 60–80 days. The temperature gradient was adjusted according to the requirement by varying the ring heaters. The seed-fitted ampoule was filled with saturated solution of the synthesized salt, prepared at 35˚C. The temperature at the top of the ampoule was maintained at 45˚C using temperature controller setup for the evaporation of the saturated solution. A constant temperature of 35˚C using a controlling unit was maintained in the outer surface of the growth setup. The temperature gradient makes the concentration gradient maximum at the bottom and top of the ampoule for avoiding spurious nucleation along the length of the ampoule. The growth rate of the crystal was found to be 1 mm per day. The grown crystal (110) from SR method is shown in Fig.5.5. The polished single crystal which was irradiated using Au^{3+} ion is shown in Fig. 5.6 (a, b).

Fig. 5.5 As grown 2-amino-5-nitropyridinium dihydrogen phosphate (2A5NPDP)NLO single crystal from Sankaranarayanan-Ramasamy (SR) method

Fig.5.6 (a) Polished NLO single crystal of 2-amino-5-nitropyridinium dihydrogen phosphate (2A5NPDP)

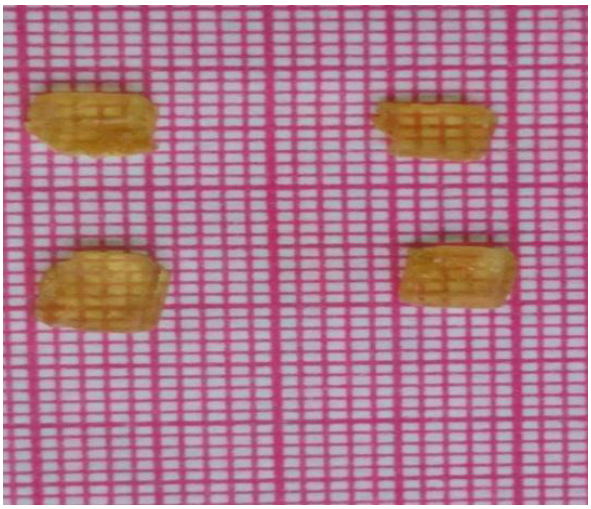

Fig.5.6 (b) Polished NLO single crystal of 2-amino-5-nitropyridinium dihydrogen phosphate (2A5NPDP)

5.3 Crystal structure of 2-amino-5-nitropyridinium dihydrogen phosphate (2A5NPDP)

The crystal structure was solved using SHELXS97 (Sheldrick, 2008) and was refined. Molecular graphics was drawn using ORTEP-3 software for Windows (Farrugia, 2012) and Mercury (Macrae et al 2008). The solved crystal structure was similar with reported by Masse and Zyss. The 2-amino-5-nitropyridinium dihydrogen phosphate (2A5NPDP) crystal structure established by Masse and Zyss **(**Masse,and Zyss 1991**)** consists of a herringbone arrangement of $2A5NP^{+}$cations in between planar layers of $H_2PO_4^-$ parallel to (1 0 0) plane. The $2A5NP^{+}$cations form three hydrogen bonds to the phosphate groups. The $2A5NP^{+}$cation has a polarizability due to the para position of the donor and acceptor substituent group of the aromatic ring; the charge transfer direction (C1= >C4) makes an angle of 36.70 with the crystal two fold axis (c-direction) (Pecaut et al 1993) and its orientation in the structure imparts sizable d-coefficients of 2-amino-5-nitropyridinium dihydrogen phosphate crystal. The 2-amino-5-nitropyridinium dihydrogen phosphate (2A5NPD) is believed to

prevent crystallization in a centro symmetric space group and also to provide mechanical and thermal stability (Puig-Molina et al 1998). The molecular structure using ORTEP, crystal packing and unit cell packing of 2-amino-5-nitropyridinium dihydrogen phosphate (2A5PDP) are shown in Fig. 5.7, 5.8 and 5.9 respectively. Bond length and bond angles of 2-amino-5-nitropyridinium dihydrogen phosphate are shown in Tab.5.1 and 5.2 respectively.

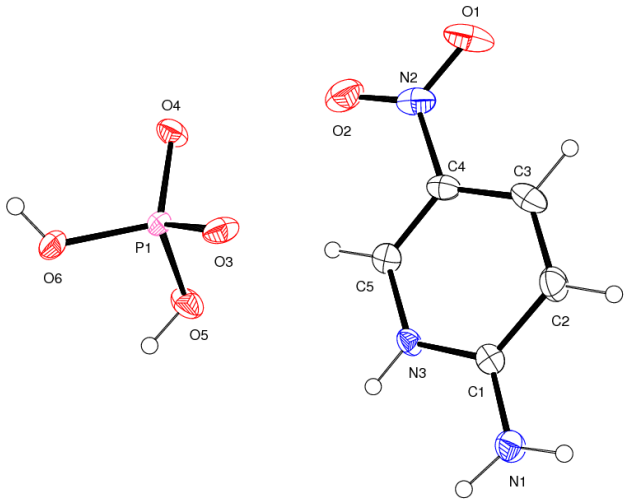

Fig. 5.7 View of the molecular structure of 2-amino-5-nitropyridinium dihydrogen phosphate (2A5NPDP) NLO single crystal using ORTEP-3 software.

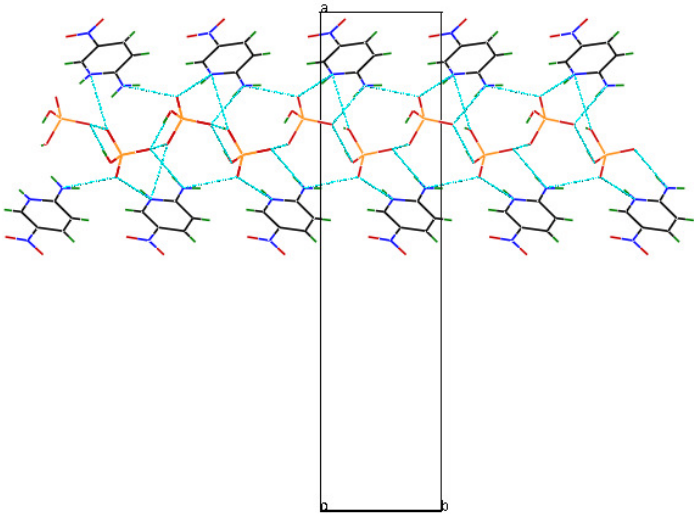

Fig.5.8 Crystal packing of 2-amino-5-nitropyridinium dihydrogen phosphate (2A5NPDP) NLO single crystal

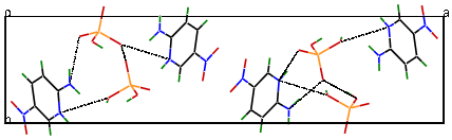

Fig. 5.9 Packing of unit cell of 2-amino-5-nitropyridinium dihydrogen phosphate (2A5NPDP) NLO single crystal

Tab.5.1 Bond lengths [Å] 2-amino-5-nitropyridinium dihydrogen phosphate (2A5NPDP) NLO single crystal

C(1)-N(1)	1.317(4)
C(1)-N(3)	1.351(3)
C(1)-C(2)	1.416(4)
C(2)-C(3)	1.360(4)
C(2)-H(2)	0.9300
C(3)-C(4)	1.390(4)
C(3)-H(3)	0.9300
C(4)-C(5)	1.352(4)
C(4)-N(2)	1.447(4)
C(5)-N(3)	1.342(3)
C(5)-H(5)	0.9300
N(1)-H(1A)	0.90(3)
N(1)-H(1B)	0.90(3)
N(2)-O(2)	1.218(3)
N(2)-O(1)	1.230(3)
N(3)-H(6)	0.8600
O(3)-P(1)	1.5085(16)
O(4)-P(1)	1.4971(17)
O(5)-P(1)	1.566(2)
O(5)-H(5A)	0.82(5)
O(6)-P(1)	1.540(2)
O(6)-H(6A)	0.74(4)

Tab.5.2 Bond angles [deg] of 2-amino-5-nitropyridinium dihydrogen phosphate (2A5NPDP) NLO single crystal

N(1)-C(1)-N(3)	119.6(2)
N(1)-C(1)-C(2)	121.8(3)
N(3)-C(1)-C(2)	118.5(2)
C(3)-C(2)-C(1)	119.9(2)
C(3)-C(2)-H(2)	120.1
C(1)-C(2)-H(2)	120.1
C(2)-C(3)-C(4)	118.7(2)
C(2)-C(3)-H(3)	120.6
C(4)-C(3)-H(3)	120.6
C(5)-C(4)-C(3)	120.9(2)
C(5)-C(4)-N(2)	118.4(3)
C(3)-C(4)-N(2)	120.7(2)
N(3)-C(5)-C(4)	120.1(2)
N(3)-C(5)-H(5)	119.9
C(4)-C(5)-H(5)	119.9
C(1)-N(1)-H(1A)	117.0(17)
C(1)-N(1)-H(1B)	115(2)
H(1A)-N(1)-H(1B)	125(3)
O(2)-N(2)-O(1)	123.7(3)
O(2)-N(2)-C(4)	119.3(3)
O(1)-N(2)-C(4)	117.0(3)
C(5)-N(3)-C(1)	121.8(2)
C(5)-N(3)-H(6)	119.1
C(1)-N(3)-H(6)	119.1
P(1)-O(5)-H(5A)	110(3)
P(1)-O(6)-H(6A)	121(3)
O(4)-P(1)-O(3)	112.44(10)
O(4)-P(1)-O(6)	113.66(11)
O(3)-P(1)-O(6)	108.66(12)
O(4)-P(1)-O(5)	107.82(11)
O(3)-P(1)-O(5)	109.45(12)
O(6)-P(1)-O(5)	104.46(12)

5.4 Au^{3+} ion irradiation

In order to understand the reaction between solid and ion, grown crystals were irradiated. A cut and polished single crystal was used for irradiation. 2-amino-5-nitropyridinium dihydrogen phosphate (2A5NPDP) was irradiated using 3MV Pelletron Tandam accelerator in National Centre for Accelerator based Research (NCAR), Department of Pure and Applied Physics, Guru Ghasidas Vishwavidyalaya (a central university), at Bilaspur, Chhattisgarh. A metallic ion and source of negative ions by cesium sputtering (SNICS) of Au^{3+} was selected for irradiation. Using copper paste, the as grown crystals were kept on the stainless steel sample holder. The as grown crystal was irradiated with three ion fluences such as 1 x 10^{13} ions/ cm^2, 5 x 10^{13} ions/ cm^2, and 1 x 10^{14} ions/ cm^2 with beam current of 1.55 A, 1.35 A, and 8 p nA respectively. Ion beam was scanned over a sample normal to its face for uniform irradiation at room temperature. A dosimeter was given to measure the radiation around the lab which was almost zero.

5.5 Results and discussion

5.5.1 Stopping and range of ions in matter (SRIM)

2-amino-5-nitropyridinium dihydrogen phosphate (2A5NPDP) was irradiated by using Au^{3+} swift heavy ion. When swift heavy ion (SHI) interacted with solid, it lost its energy continuously and changed its direction by colliding with solid. Fig.5.10 shows electronic and nuclear energy losses in 2-amino -5-nitropyridinium dihydrogen phosphate (2A5NPDP) NLO single crystal. It was noticed from the graph that, the electronic loss increases with increase of ion energy and nuclear loss decreased with increase of energy. Using SRIM software, maximum electronic loss was calculated and was found to be 1.361x 10^1 eV/Å at 11 MeV. The mean projectile range (R) and

projected straggling also calculated and presented in the Tab.5.3. Fig.5.11. shows penetration depth of Au^{3+} ion as a function of energy.

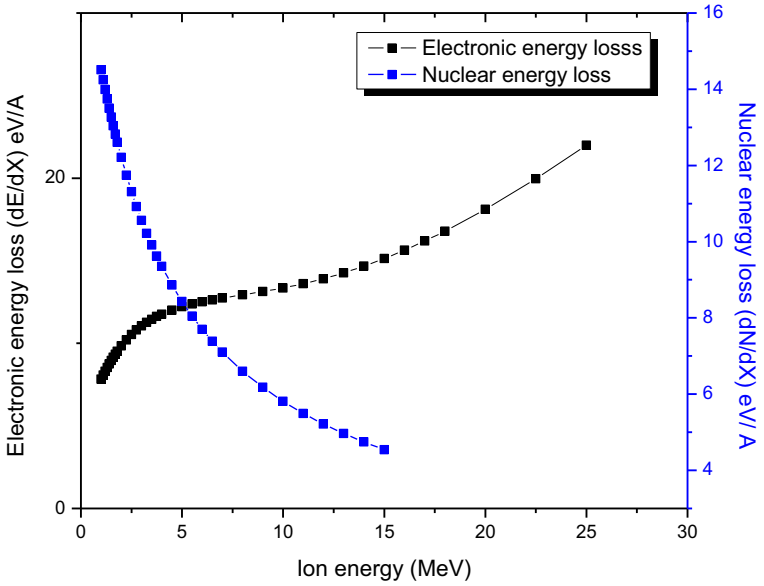

Fig.5.10 Electronic and nuclear energy losses of Au^{3+} ion energies in 2-amino-5-nitropyridinium dihydrogen Phosphate (2A5NPDP) NLO single crystal.

Ion Energy (MeV)	dE/dx (Elec.)	dN/dx (Nuclear)	Projected Range (µm)	Longitudinal Straggling (Å)	Lateral Straggling (Å)
10.00	1.335E+01	5.812E+00	2.69	1837	1881
11.00	1.361E+01	5.494E+00	2.98	1980	2043

Tab.5.3 Mean projectile range (R) and projected straggling of 2-amino-5-nitropyridinium dihydrogen Phosphate (2A5NPDP) NLO single crystal.

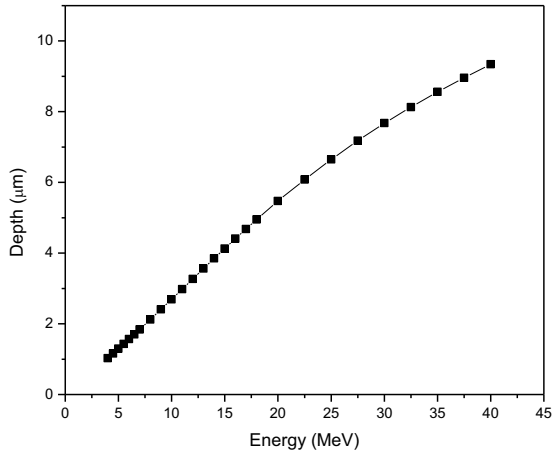

Fig.5.11 penetration depth of Au^{3+} swift heavy ion in 2-amino-5-nitropyridinium dihydrogen phosphate (2A5NPDP) NLO single crystals as a function of energy.

5.5.2 Single crystal X-ray diffraction

The single crystal X-ray diffraction was measured by Brucker Kappa Apex11 CCD diffractometer with Mo K_α radiation and λ = 1.5406 Å was employed to collect the single crystal X-ray data of 2-amino-5-nitropyridinium dihydrogen phosphate (2A5NPDP) single crystal. It is observed that 2-amino-5-nitropyridinium dihydrogen phosphate (2A5NPDP single crystal belongs to orthorhombic crystal system with the space group Pna21 and the unit cell dimensions are a = 25.6090 Å, b = 6.2140 Å and c = 5.6600 Å and $\alpha = \beta = \gamma = 90^o$. The volume of the unit cell is 900.70$Å^3$ and Z is 4. Crystal data and structure refinement of 2-amino-5-nitropyridinium dihydrogen phosphate (2A5NPDP) is given in Tab 5.4. Fig.5.12 shows X- diffraction pattern of pristine and Au^{3+} ion irradiated 2-amino-5-nitropyridinium dihydrogen phosphate (2A5NPDP) single crystals. Single crystal data (Caculated) and reported (Masse and Zyss 1991) single crystal data is reported in Tab.5.5. It was clear from the X- ray diffraction patterns that, interaction of solid- ion, librated thermal energy that produced defects along the path of the ion. It is noticed from the X- ray diffraction

pattern that intensity of irradiated crystal decreases with increase of ion fluencies. At fluencies of Au^{3+} (5 x 10^{13} ions/cm^2) almost all the peaks were vanished and intensity of (111), (211), (022), (122), (222) planes increased due to reordering and cross linkage of bands taking place. It was also observed from the X- ray diffraction pattern that, defects were formed and lattice was deformed. Lattice deformation was not in the entire crystal surface because deformation was taken place only in al small area that was around the ion paths. Peaks were observed at higher fluencies due to the unaffected planes in the irradiated crystal.

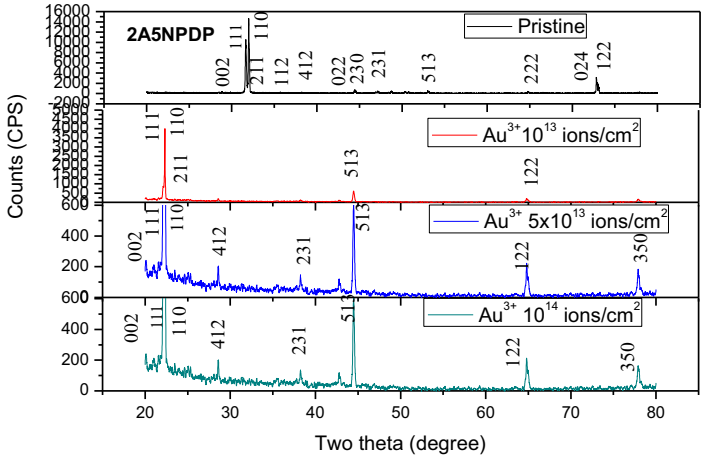

Fig.5.12 single crystal X-ray diffraction pattern of pristine and Au^{3+} ion irradiated 2-amino-5-nitropyridinium dihydrogen phosphate (2A5NPDP) NLO single crystals

Tab.5.4 Crystal data and structure refinement for 2-amino-5-nitropyridinium dihydrogen phosphate (2A5NPDP) NLO single crystal

Identification code	Shelxl
Empirical formula	$C_5 H_8 N_3 O_6 P$
Formula weight	237.11
Temperature	293(2) K
Wavelength	0.71073 Å
Crystal system, space group	Orthorhombic, Pna21
Unit cell dimensions	a = 25.6090(7) Å alpha = 90°
	b = 6.2140(2) Å beta = 90°.
	c = 5.6600(2) Å gamma = 90°.
Volume	900.70(5) A^3
Z, Calculated density	4, 1.749 Mg/m^3
Absorption coefficient	0.323 mm^{-1}
F(000)	488
Crystal size	0.30 x 0.20 x 0.20 mm
Theta range for data collection	3.18 to 25.98 deg.
Limiting indices	-31<=h<=31, -7<=k<=5, -6<=l<=6
Reflections collected / unique	11569 / 1761 [R(int) = 0.0266]
Completeness to theta = 25.98	99.9 %
Absorption correction	Semi-empirical from equivalents
Max. and min. transmission	0.9393 and 0.9024
Refinement method	Full-matrix least-squares onF^2
Data / restraints / parameters	1761 / 1 / 152
Goodness-of-fit on F^2	1.143
Final R indices [I>2sigma(I)]	R1 = 0.0306, wR2 = 0.0699
R indices (all data)	R1 = 0.0319, wR2 = 0.0705
Absolute structure parameter	0.10(12)
Largest diff. peak and hole	0.172 and -0.282 $e.A^{-3}$

Tab.5.5 Single crystal X-ray diffraction values of 2-amino-5-nitropyridinium dihydrogen phosphate (2A5NPDP) NLO single crystal

	Calculated	Reported
Volume	900.70(5)	900.70(5)
Space group	P n a 21	Pna21
Hall group	P 2c -2n	?
Moiety formula	C_5 H_6 N_3 O_2, H_2 O_4 P	C_5 H_6 N_3 O_2, H_2 O_4 P
Sum formula	C_5 H_8 N_3 O_6 P	C_5 H_8 N_3 O_6 P
Mr	237.11	237.11
Dx,g cm-3	1.749	1.749
Z	4	4
Mu (mm-1)	0.323	0.323
F000	488.0	488.0
F000’	488.70	
h,k,l max	31,7,6	31,7,6
N ref	1760[974]	1761
T min,T max	0.925,0.937	0.902,0.939
Tmin’	0.908	

5.5.3 FTIR spectrum analysis

Functional group of pristine and Au^{3+} ion irradiated 2-amino-5-nitropyridinium dihydrogen phosphate (2A5NPDP) single crystals were analyzed using FTIR analyzer. Fig.5.13 and Fig.5.14 show FTIR spectrum of pristine and irradiated crystals. Observed vibrational frequencies are listed in Tab.5.6 There are twelve vibrations originate from pyridine ring. Among twelve, five are in stretching modes, four in-plane and three out-of plane bending modes. Nine modes are present in

stretching and bending motions of C-N and C-C. Two pyridine hydrogen atoms describe the C-H bonds [two stretching (CH), two in-plane bending (CH) and two out-of-plane bending (CH)]. In the same way, C-NO_2 group participates in six vibrations, i.e. three stretching [(CN), (NO_2) and (NO_2)] and three bending [two (CNO) and one (NO_2)] modes. Vibrations at 3490, 3263 and 3174 cm^{-1} is assigned to the vibrations corresponding to the overtone modes of the double N-H, H-N system, respectively.

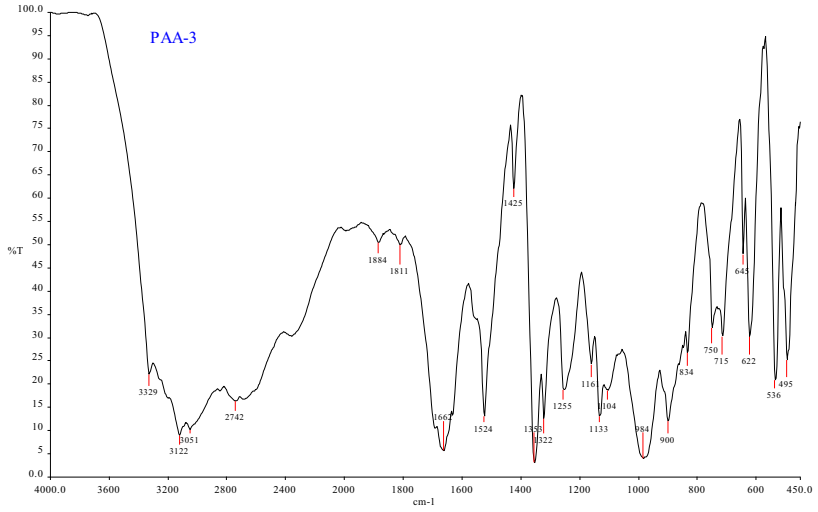

Fig.5.13 FTIR spectra of 2-amino-5-nitropyridinium dihydrogen phosphate (2A5NPDP) NLO single crystal

The strong and broad –OH stretching bands observed at 3600-3000 cm^{-1} from which salt compounds are attributed (Partal Urena et al 2003). The vibration at 1662 cm^{-1} (C=N stretching band) originates from the pyridine ring. The N–O stretching at 1524 cm^{-1}, 1355 cm^{-1} clearly confirm the presence of nitro group and consecutively, the bending N-H group appears at range of the 1407 cm^{-1} (Partal Urena et al 2003). C–H vibrations of pyridine are assigned at 1321 cm^{-1}. The coupled in-plane bending

(C-H) vibrations and pyridine (C-C) stretching mode are appeared in the following regions: 1221 (1223) cm^{-1}. Similarly1130 cm^{-1} is attributed to P–O in plane of phosphate group. Out-of plane bending (C-H) modes lie in typical range, two bands are observed at 857 cm^{-1}. Wagging and rocking modes of the nitro group are observed at 756 (755), 531 (514) cm^{-1}. In irradiated crystal with three different fluencies (1 $x10^{13}$ ions/$cm^{2,}$ 5 x 10^{13} ions/ cm^2 , and 1 $x10^{14}$ ions/ cm^2) the ring stretching vibration (C-H) bands are observed at 3098 and 3084 cm^{-1} from pyridine ring of the molecule (Köse et al 2012). The 1250 cm^{-1} are assigned to C–H vibrations of pyridine. Other vibrations of the pyridine ring are observed at about 463 (457 and 428) cm^{-1}. Below 300 cm^{-1} region very complex vibrations of the whole skeleton is observed. They form concerted movements in which almost all fragments of the cluster built by several molecules joined by hydrogen bonds take part.

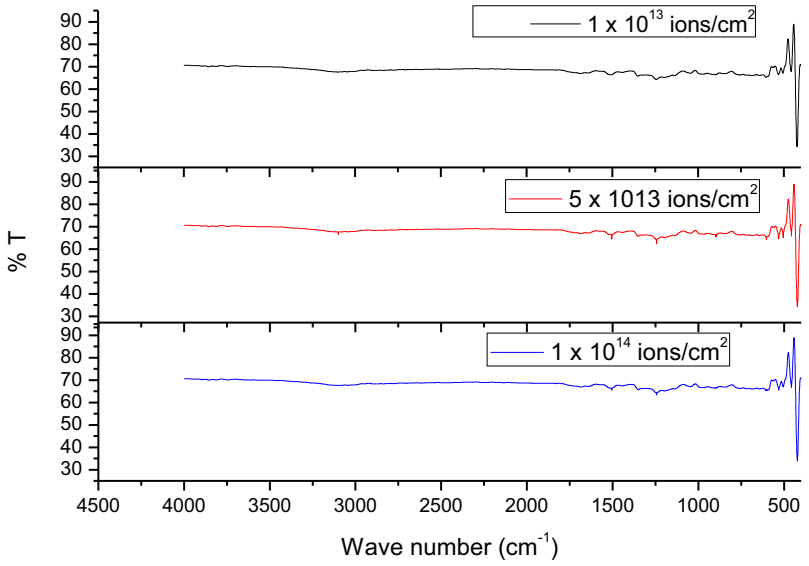

Fig. 5.14 FTIR spectra of Au^{3+} ion irradiated 2-amino-5-nitropyridinium dihydrogen phosphate (2A5NPDP) NLO single crystal

Tab.5.6 Vibrational assignments of 2-amino-5-nitropyridinium dihydrogen phosphate 2A5NPDP NLO single crystal.

Observed frequency in cm^{-1}	Assignment
3329	γ_s (N H. . .O)
3122	γ_s (N H. . .O)
1662	γ_s (C N)
1524	γ_s (N O)
1353	γ_s (N O)
1322	C-H in plane
1161	C- H in plane
984	γ_s (P -O- H)
834	γ_s (P- O -H)
645	δ (O -P- O)
536	δ (O- P -O)

5.5.4 Optical properties

Optical properties of 2-amino-5-nitropyridinium dihydrogen phosphate (2A5NPDP) were subjected to Perklin Elmer lamda 35 Uv- vis NIR spectrometer. Fig.5.15 shows absorption spectra of pristine and irradiated semiorgaic crystal of 2-amino-5-nitropyridinium dihydrogen phosphate (2A5NPDP). Lower cut off wavelength of pristine is 364 nm. It is revealed from the Uv-vis spectra that absorption of irradiated crystal increases with increase of ion fluencies. Maximum absorption are 356.1 nm, 357 nm and 357.7 nm for ion fluences 1 $x10^{13}$ ions/$cm^{2,}$ 5 x 10^{13} ions/ cm^2 and 1 $x10^{14}$ ions/ cm^2 respectively. Both pristine and irradiated

crystal have wide transparency window which is one of the additional key requirements for

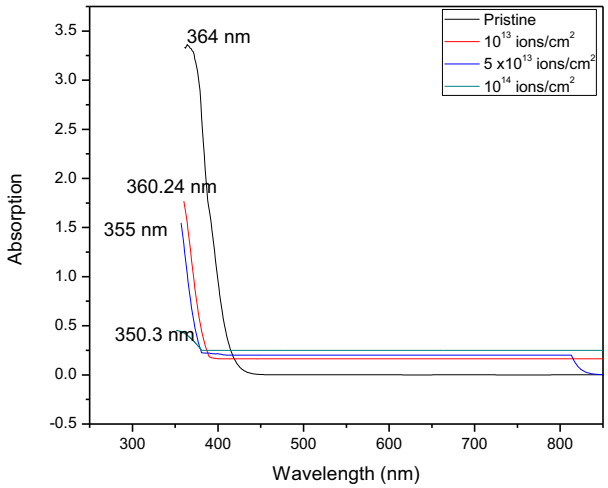

Fig.5.15 Absorption spectra of pristine and Au^{3+} ion irradiated 2-amino-5-nitropyridinium dihydrogen phosphate (2A5NPDP) NLO single crystal.

having efficient NLO character. The increase of absorption is due to excited electrons which are formed by vacancies and formation of additional defects centers. It is also noticed that there is no additional peak in the visible region. Due to insufficient energy that is observed by electrons from swift heavy ion (SHI) to move lattice to substitution. Transmittance of irradiated crystal decreases as ion fluencies increase. The decrease of transmittance of irradiated crystals is due to creation of defects. It is noticed from the spectra that the absorption spectra shifted towards shorter wavelength (blue shift) with increase of ion fluences. The change in the absorption may also be the creation of some intermediate energy levels due to structural rearrangements. Fig.5.16 shows Tauc's plot of pristine and irradiated NLO single crystal of 2-amino-5-nitropyridinium dihydrogen phosphate (2A5NPDP). It is

calculated from the graph that photon (hν) of pristine is 3.14 eV which is equal to the band gap of the crystal (E_g= hν). Band gap of irradiated samples with varied fluences are 3.07 eV, 3.08 eV, and 3.09 eV. It is revealed from the graph that there is a change

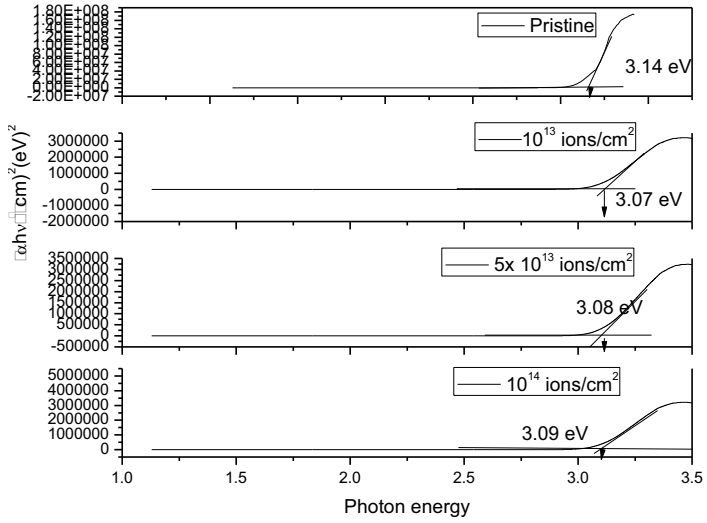

Fig.5.16 Tauc's plot of pristine and Au^{3+} ion irradiated 2-amino-5-nitropyridinium dihydrogen phosphate (2A5NPDP) NLO single crystal.

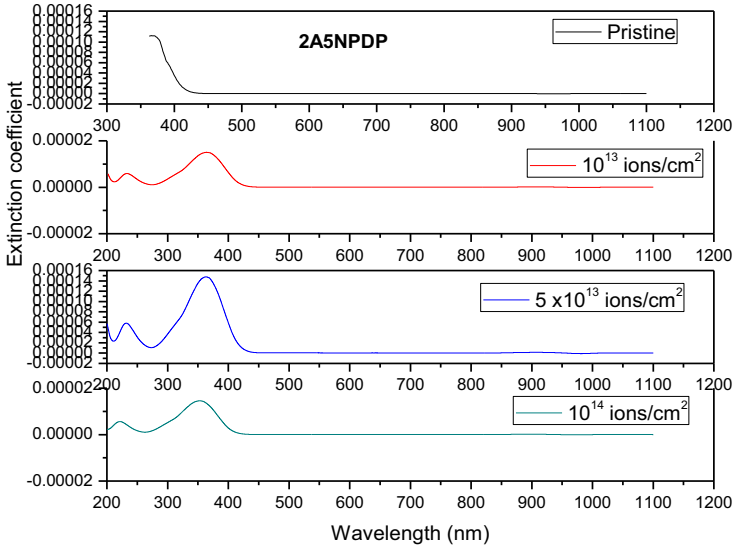

Fig. 5.17 Extinction coefficient of pristine and Au^{3+} ion irradiated 2-amino-5-nitropyridinium dihydrogen phosphate (2A5NPDP) NLO single crystal

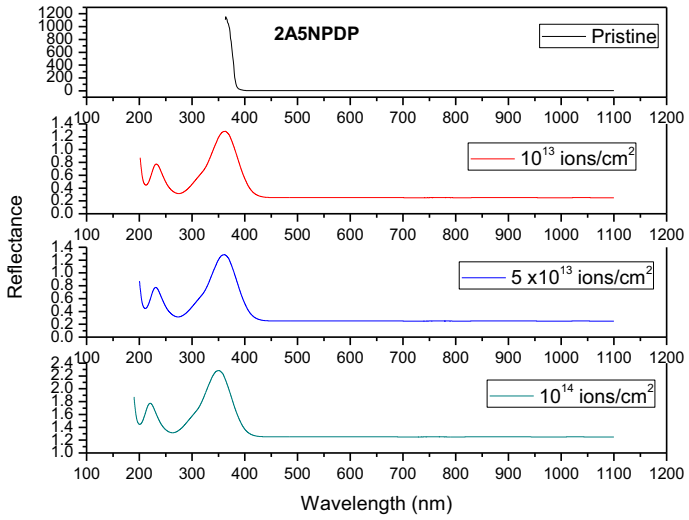

Fig. 5.18 Reflectance spectra of pristine and Au^{3+} ion irradiated 2-amino-5-nitropyridinium dihydrogen phosphate (2A5NPDP) NLO single crystals.

in the energy band gap. Swift heavy ion (SHI) irradiation produces point defects such as vacancies, anti-site defects and interstitial causing lattice damage. The change in the band gap may be understood through the creation of some intermediate energy levels. Fig. 5.17 shows extinction coefficient of pristine and irradiated crystals. Fig.5.18 shows reflectance of pristine and irradiated crystals. It is noticed from these graph that the scattering and absorption of electromagnetic light per unit thickness of both (pristine and irradiated) crystal is very small. Swift heavy ion (SHI) does not make any notable change in the absorption and scattering (Extinction coefficient). This small value of extinction coefficient in the visible region exhibit by 2-amino-5-nitropyridinium dihydrogen phosphate (2A5NPDP) (both pristine and irradiated) crystal has suitable property for anti reflecting coating of solar thermal devices. It is observed from the reflectance graph of both (pristine and irradiated) crystals, reflectance of electromagnetic light is very low in the visible region. It is also

revealed from the graph that reflectance increases slightly with increase of ion fluencies. It is understood from the graph that optical properties of 2-amino-5-nitropyridinium dihydrogen phosphate (2A5NPDP) does not altered considerably by swift heavy ion (SHI).

5.5.5 Microhardness

Vicker's hardness (H_v) test was carried out for pristine and irradiated 2-amino-5-nitropyridinium dihydrogen phosphate (2A5NPDP) crystal with varied fluencies at room temperature. Load was applied on the selected plane range from 25 g to 100 g. Fig.5.19 shows microhardness of pristine and irradiated semiorganic crystal of 2-amino-5-nitropyridinium dihydrogen phosphate (2A5NPDP). It is noticed from the graph that hardness of pristine and irradiated crystal increases with applied load. It is

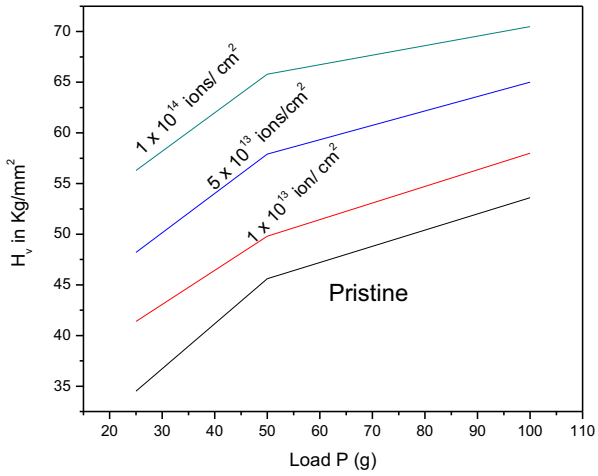

Fig. 5.19 Microhardness graph of pristine and Au^{3+} ion irradiated 2-amino-5-nitropyridinium dihydrogen phosphate (2A5NPDP) NLO single crystal

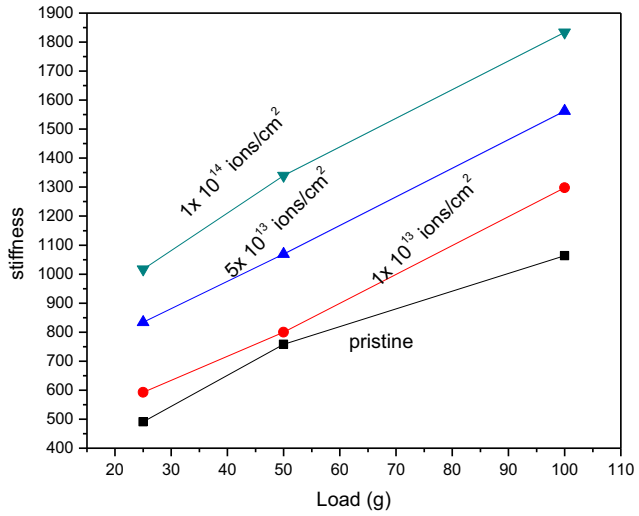

Fig.5.20 Stiffness of pristine and Au^{3+} ion irradiated 2-amino-5-nitropyrdinium dihydrogen phosphate (2A5NPDP) NLO single crystal

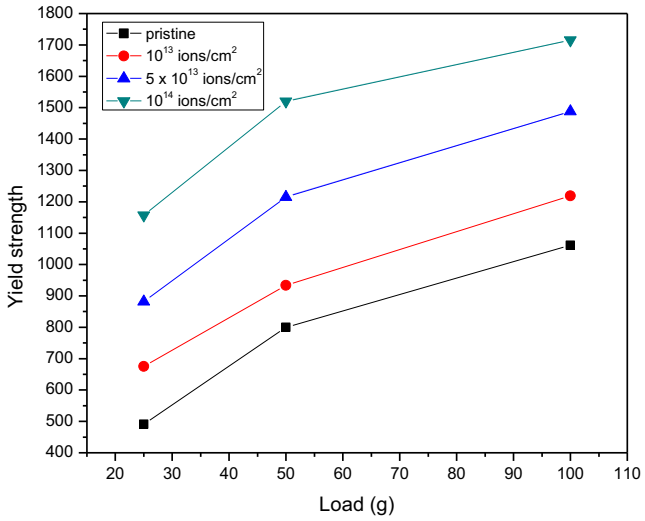

Fig. 5.21 Yield strength of pristine and Au^{3+} ion irradiated 2-amino-5-nitropyrdinium dihydrogen phosphate (2A5NPDP) NLO single crystal

also observed that hardness of pristine is lesser than the irradiated crystal. Hardness of irradiated crystal increases with increase of ion fluencies. Increases of hardness are due to increase in density of lattice defects caused by the passage of implanted ions through 2-amino-5-nitropyridinium dihydrogen phosphate (2A5NPDP) lattices. In an irradiated crystal a residual surface compression stress is produced in the irradiated surface layer because of increased density of lattice defects. Fig.5.20 and Fig.5.21 show stiffness and yield strength of pristine and irradiated crystals. It is noticed from the graph that yield strength increases with increase of applied load. Yield strength and stiffness of 2-amino-5-nitropyridinium dihydrogen phosphate (2A5NPDP) crystal increases with increase of ion fluences, the mechanical strength of irradiated crystal is relatively high.

5.5.6 Dielectric study

Electrical properties of dielectric constant of pristine and irradiated crystals of 2-amino-5-nitropyrdinium dihydrogen phosphate (2A5NPDP) were studied. Fig.5.22 shows dielectric constant of pristine and Au^{3+} ion irradiated NLO single crystal. It is observed from the graph that, dielectric constant increases at lower applied frequencies. High value of dielectric constant at lower frequencies is due to the contribution of space, electronic, ionic, and dipolar polarizations. Among these polarizations, Space charge polarization plays a vital role to get high dielectric constant at low frequency. The value of dielectric constant decreases with increase of applied frequency. This is because, after certain frequency the charge carriers cannot follow the alternation of AC electric field. It is also noticed from the graph that at low frequency, the dielectric constant of pristine crystal is lesser than the Au^{3+} irradiated crystals. The higher dielectric constant than the pristine could be attributed that, when solid is irradiated using swift heavy ion (SHI), ions are attached into a target material

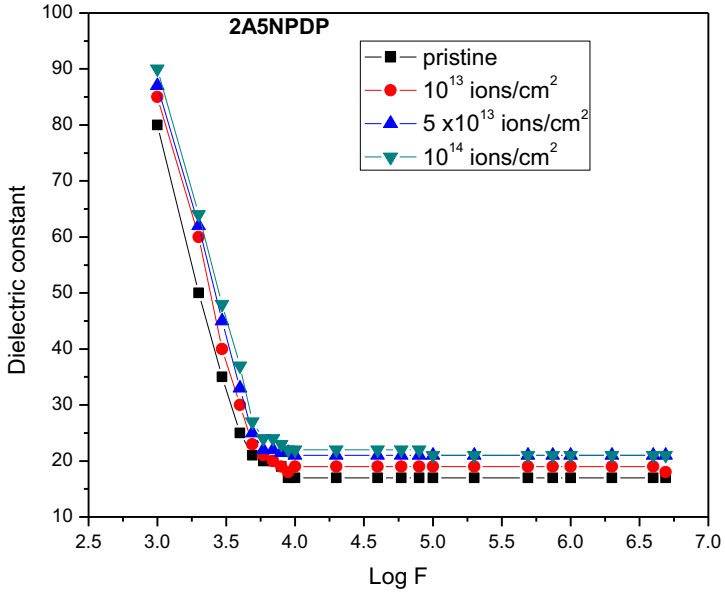

Fig. 5.22 Dielectric constant of pristine and Au^{3+} ion irradiated 2-amino-5-nitropyrdinium dihydrogen phosphate (2A5NPDP) NLO single crystal

and they transfer energy to the target material until it loses energy completely. This transfer of energy from ion to solid results defects formation and disordering of the crystal structure. Defects are created along the ion tracks. This formation of defects increases the dielectric constant. It is elucidated from the graph that, dielectric constant increases with increase of ion fluencies. This might be explained that damage was created along the surface of the sample, when high fluence ion beam was irradiated. Damage created by swift heavy ion (SHI) was isolated from each other. It increased charge carriers which in turn increased the space charge polarization at low frequency.

5.5.7 Fluorescence study

Fluoroscence study was carried out for as grown pristine and Au^{3+} ion irradiated 2-amino-5-nitropyridinium dihydrogen phosphate (2A5NPDP) NLO single

crystal. Fig.5.23 shows fluorescence spectra of pristine and irradiated NLO single crystal, which was carried out at room temperature. It is observed from the spectrum that, as grown pristine sample shows high luminescence intensity at 528 nm. Energy band gap was calculated using conversion, wavelength to energy relation $E_g = 1.24/\lambda$ eV. The energy band of pristine was calculated and it is 2.34 eV from the wavelength 528 nm. This emission of (528 nm) green light is due to π- π^* transitions. 2-amino-5-nitropyridinium dihydrogen phosphate (2A5NPDP) NLO single crystal emits green radiation which is an excellent candidate for nonlinear applications and device fabrications

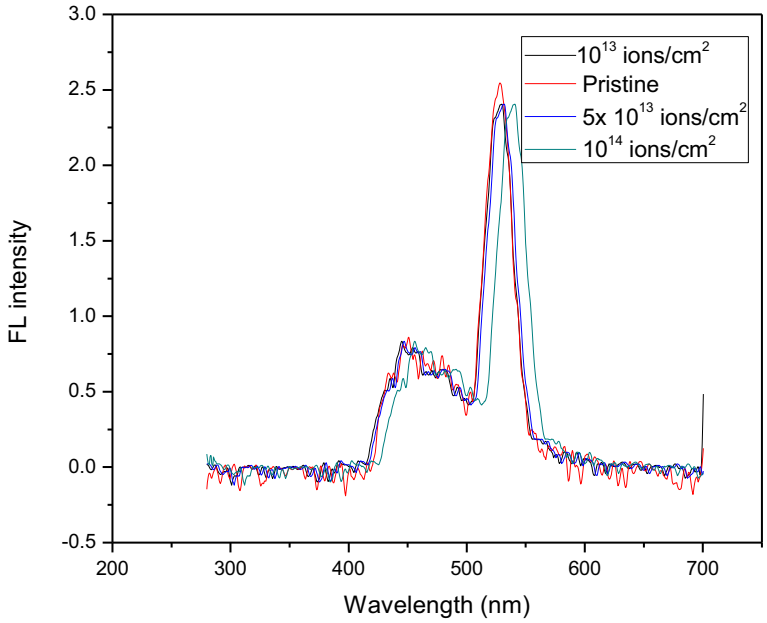

.

Fig. 5.23 Fluroscence spectra of pristine and Au^{3+} ion irradiated 2-amino-5-nitropyridinium dihydrogen phosphate (2A5NPDP) NLO single crystal.

It is also observed from the luminescence spectra that, intensity peak of ion irradiated NLO single crystal decreases with increase of ion fluences. It is also revealed from

the spectra that, intensity of irradiated crystals is less than that of unirradiated crystal. It is noticed from the spectra that there is a change in the peak position, when ion fluences are increased from 10^{13} ions/cm^2 to 10^{14} ions/cm^2. The decrease of intensity than the unirradiated sample is due to the effect of ion irradiation in the crystal lattice. Swift heavy Ion (SHI) irradiation creates defects in the crystal and which is rich at high ion fluence. Rich defects are due to high ion fluence that affect the radiative transitions in which crystal losses its luminescence property. It is also absorbed from the fluorescence spectra that intensity of peak decreases and shifting of peak with increase of ion fluence. This is due to exchange of electron between F and F^+ centers, which were released from the conduction band. The decrease of intensity peak is due to the formation of new defects by swift heavy ion (SHI) irradiation.

5.5.8 Scanning electron microscope (SEM)

Scanning electron microscope used to study on morphology, crystal orientation and etc. Fig.5.24 (a, b, c,& d) shows SEM image of pristine and irradiated NLO single crystal of 2- amino -5-nitropyridinium dihydrogen phosphate (2A5NPDP) for 1 x10^{13} ions/cm^{2,} 5 x 10^{13} ions/ cm^2 , and 1 x10^{14} ions/ cm^2 respectively. It is noticed from the pristine SEM image that, the semiorganic crystal has leniently distributed grains. It looks like a smooth surface. In irradiated crystals, the roughness of the surface increases with increase of ion fluences from 1 x 10^{13} ions/ cm^2 to 10^{14} ions/cm^2. Craters were formed in the irradiated crystals. This is due to shock waves produced in the solid. When swift heavy ion (SHI) was bombarded with solid, Shock waves were produced which created crater in the crystalline surface (Bagieu- Beucher 1991). It is also observed from the SEM image that, some changes or modifications in the crystal orientation were due to swift heavy ion (SHI). At 5 x 10^{13} ions/cm^2 fluence, bud like produced along with roughness of the surface. It is also found at

higher fluence cracks were produced on the surface of crystal sample and also valley like structures were formed at ion fluence 10^{14} ions/cm^2. Surface of crystal was heavily damaged and degree of crystallinity decreases when ion fluences increase.

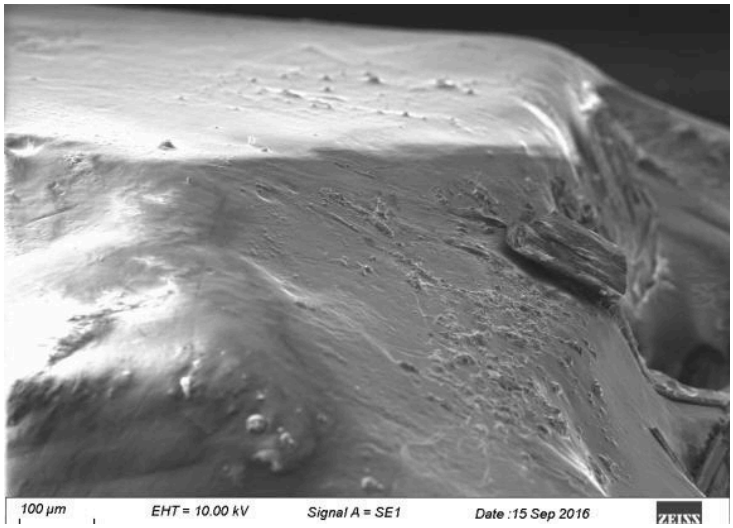

Fig. 5.24 a) SEM image of 2-amino-5-nitropyridinium dihydrogen phosphate (2A5NPDP) NLO single crystal.

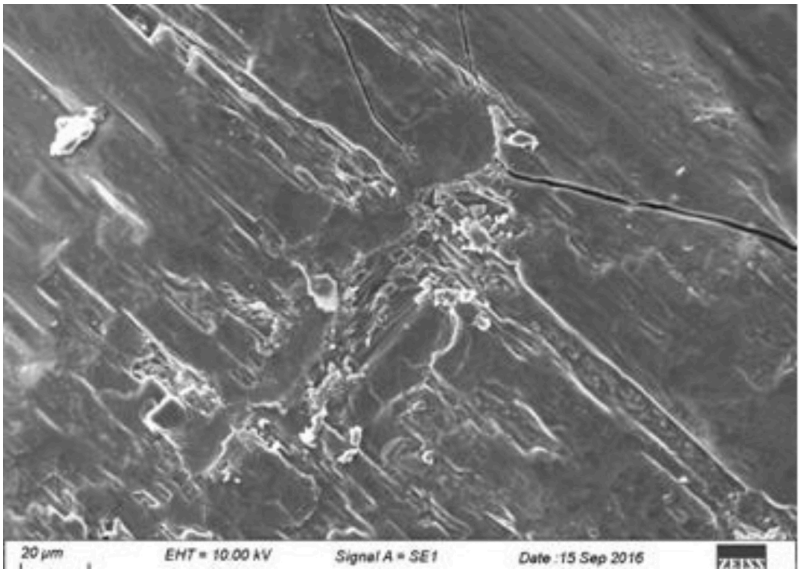

Fig. 5.24 b) SEM image of Au^{3+} ion irradiated (10^{13} ions/cm^2) 2-amino-5-nitropyridinium dihydrogen phosphate (2A5NPDP) NLO single crystal.

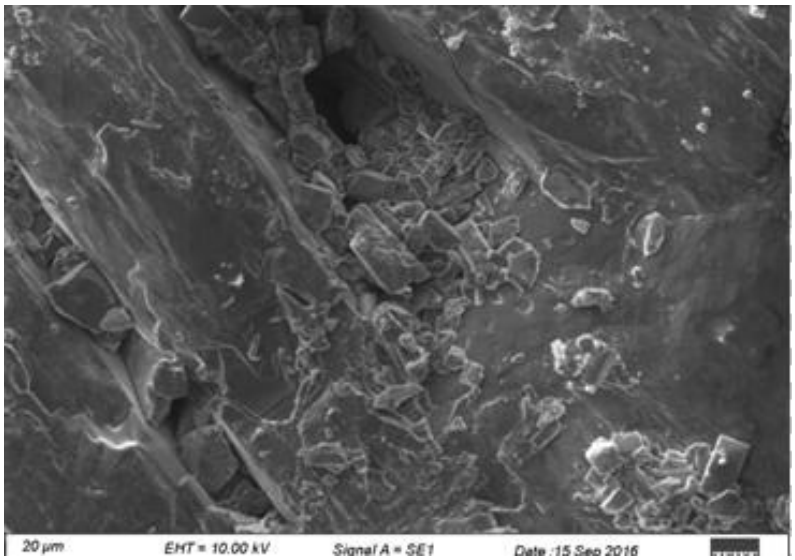

Fig. 5.24 c) SEM image of Au^{3+} ion irradiated (5x 10^{13} ions/cm^2) 2-amino-5-nitropyridinium dihydrogen phosphate (2A5NPDP) NLO single crystal.

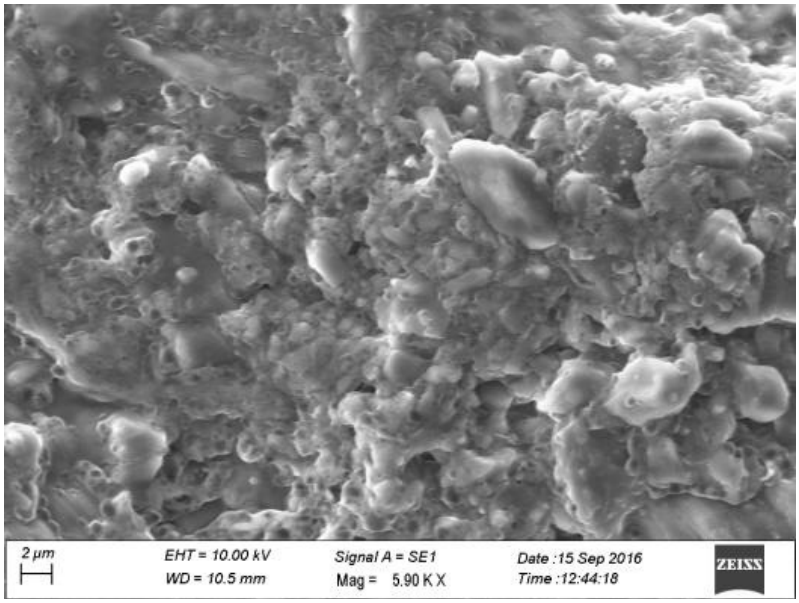

Fig.5.24 d) SEM image of Au^{3+} ion irradiated (10^{14} ions/cm^2) 2-amino-5-nitropyridinium dihydrogen phosphate (2A5NPDP) NLO single crystals.

5.5.9 NLO test

A semiorganic single crystal of 2-amino-5-nitropyridinium dihydrogen phosphate (2A5NPDP) of pristine and irradiated samples was subjected to second harmonic generation (SHG). Kurtz powder technique was used to measure second harmonic generation (SHG). A Q- switched Nd-YAG laser of 1064 nm was used as a primary source with an input power of 1.2 mJ/ pulse with repetition rate of 10HZ and pulse width of 10 ns. A convex lens of 20 cm focal length was used to collimate laser rays on the sample. Pristine and irradiated samples were powdered and filled in a microcapillary tubes. Photomultiplier tube was used to detect the green light and second harmonic generation (SHG) output of green laser (532 nm) light was seen on digital oscilloscope. SHG results revealed that, output of pristine was 45 mV and irradiated samples with varied fluencies (1 $x10^{13}$ ions/$cm^{2,}$ 5 x 10^{13} ions/ cm^2 , and 1 $x10^{14}$ ions/ cm^2) were 5 mV, 1 mV and 1 mV respectively whereas that of KDP was 22 mV. It is observed from the result that, when the samples are subjected to laser thermal diffusion comes to play and damage the crystal further. Spreading of thermal energy increases along the swift heavy ion (SHI) path, defects in the crystal surface also increases and second harmonic generation (SHG) efficiency decreases. The decrease of second harmonic generation (SHG) is due to higher ion fluence, which almost affected the noncentro symmetric packing of the molecular crystal. Swift heavy ion (SHI) irradiated crystals too contain many defects.

5.5.10 Thermal analysis

Thermogravimetric (TG) and differential thermal analysis (DTA) gives information about phase transition, water of crystallization and different stages of decomposition. TG and DTA were carried out for pristine and irradiated of orthorhombic NLO single crystal of 2-amino-5-nitropyridinium dihydrogen phosphate

(2A5NPDP). A pristine sample was started to decompose at 179^0 C. Au $^{3+}$ ion irradiated single crystal with different fluences (1 x10^{13} ions/cm^2, 5 x 10^{13} ions/ cm^2, and 1 x10^{14} ions/ cm^2) were decomposed with weight loss was little more than the pristine at 183^0 C, 185.5^0 C and 186^0 C respectively. There was no endothermic peak observed before decomposition which is the melting point of crystal system. Increase of thermal stability was due to the decrease of degree of crystallinity. It was also noted that thermal stability increased with increase of ion fluences. This was due to increase of defects with increase of ion fluencies. Fig. 5.23 (a, b, c, & d) shows thermogravimetric (TG) and differential thermal analysis (DTA) which gives information about phase transition, water of crystallization and different stages of decomposition of both pristine and irradiated crystals.

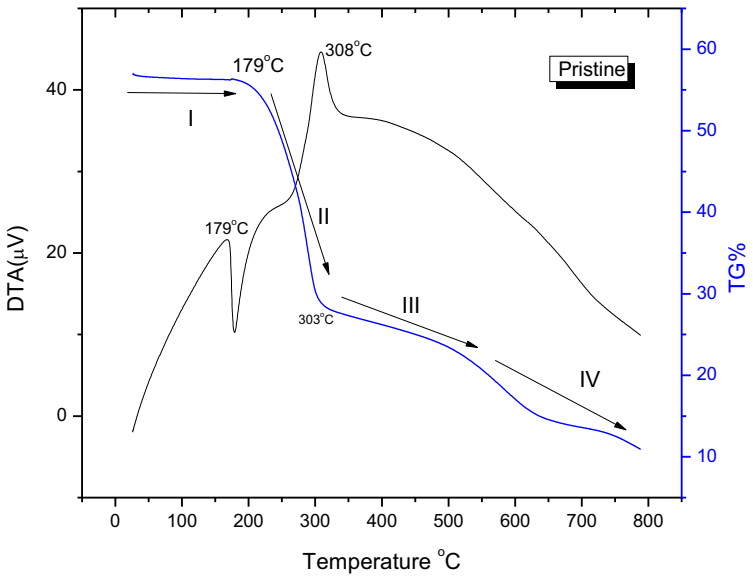

Fig.5.25 a) Thermal analysis of 2-amino-5-nitropyridinium dihydrogen phosphate (2A5NPDP) NLO single crystal.

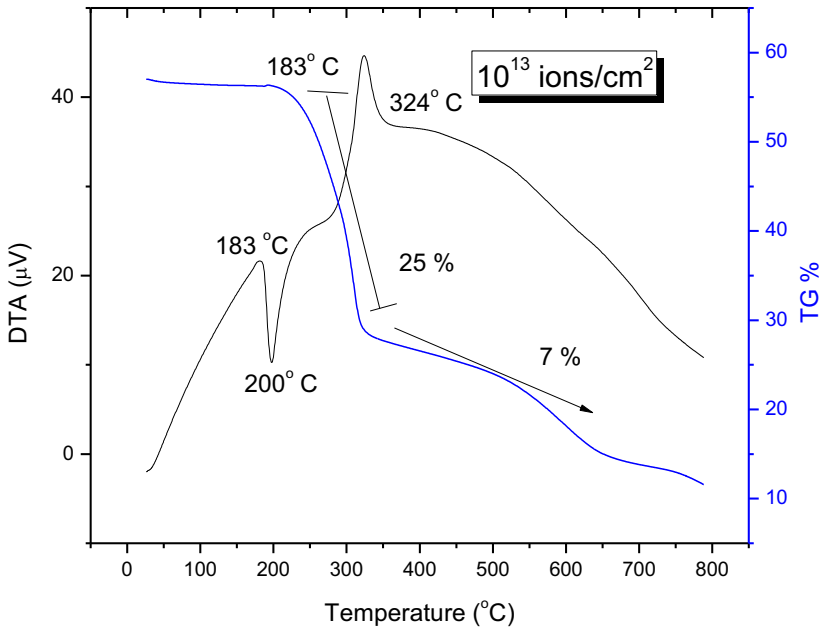

Fig.5.25 b) Thermal analysis of Au^{3+} ion irradiated (10^{13}ions/cm^2) 2-amino-5-nitropyridinium dihydrogen phosphate (2A5NPDP) NLO single crystal.

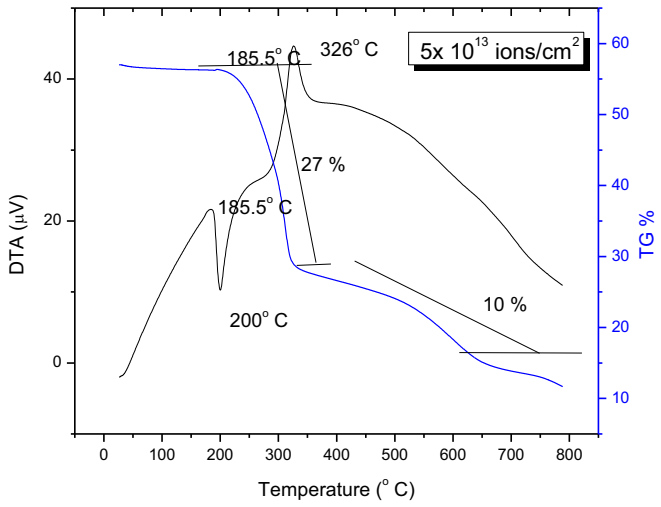

Fig.5.25 c) Thermal analysis of Au^{3+} ion irradiated (5x 10^{13}ions/cm^2) 2-amino-5-nitropyridinium dihydrogen phosphate (2A5NPDP) NLO single crystal.

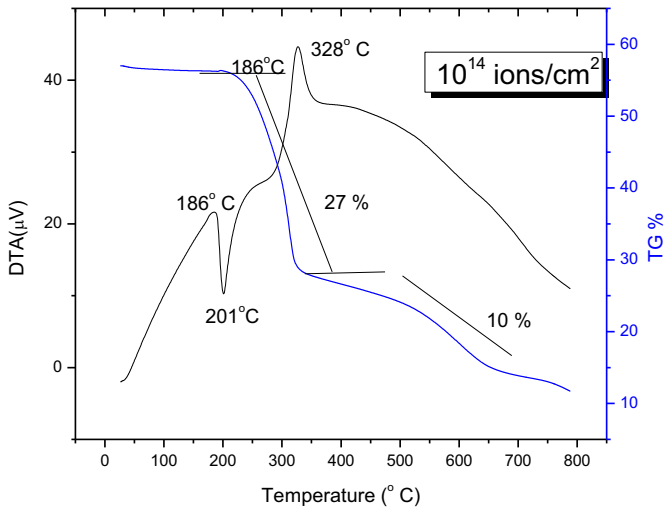

Fig.5.25 d) Thermal analysis of Au^{3+} ion irradiated (10^{14} ions/cm^2) 2-amino-5-nitropyridinium dihydrogen phosphate (2A5NPDP) NLO single crystal.

5.5.11 Impedance Analysis

Electrical properties of impedance of semiorganic crystal of 2-amino-5-nitropyridinium dihydrogen phosphate (2A5NPDP) NLO single crystal of pristine and Au^{3+} ion irradiated studied using complex impedance spectroscopy. Complex impedance was analyzed at room temperature. The frequency dependent properties of materials is represented as a complex impedance Z^*, which is $Z^* = Z' - j\,Z''$, where Z' and Z'' are real and imaginary components of impedance respectively. Fig. 5.25 and fig.5.27 Show a frequency response of real (Z') and imaginary (Z'') parts of impedance. It is observed from the graph that impedance decreases with increase of applied frequency. High value of impedance at low frequency indicates that polarization is more due to space charge. In real part impedance decreases with increase of applied frequency up to certain frequency value afterwards it is independent. It is also revealed from the graph that the value of impedance increases with Au^{3+} ion fluences. It is noticed from the graph that the impedance of irradiated

crystal is greater than the pristine sample. This is due to the formation defects which were created by Au^{3+} ion with fluence of 10^{13} ions/cm^2, 5 x 10^{13} ions/cm^2 and 10^{14} ions/cm^2. Fig.5.28 shows Nyquist's plot of pristine and Au^{3+} ion irradiated 2-amino-5-nitropyridinium dihydrogen phosphate (2A5NPDP) NLO single crystal. A semicircle is seen in pristine and as well as Au^{3+} ion irradiated crystal due to bulk effect of the sample. A combination of capacitor and resistor create bulk effect in the samples. It is also noticed from the Nyquist's plot that bulk resistance of irradiated crystal increased more than the pristine crystal. It is also revealed from the graph that bulk resistance increases with increase of ion fluences from 10^{13} ions/cm^2 to 10^{14} ions/cm^2. The bulk resistance and grain boundary resistance were calculated from the intercept of the semicircle arc on the real axis and peak of the semi circle respectively. Tab.5.7 shows bulk resistance and grain boundary resistance of pristine and irradiated crystal.

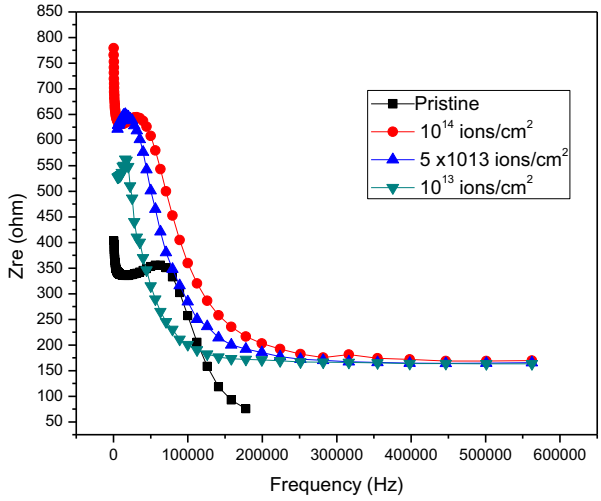

Fig. 5.26 Plots of real part of impedance with frequency for pristiine and Au^{3+} ion irradiated 2-amino-5-nitropyridinium dihydrogen phosphate (2A5NPDP) NLO single crystal.

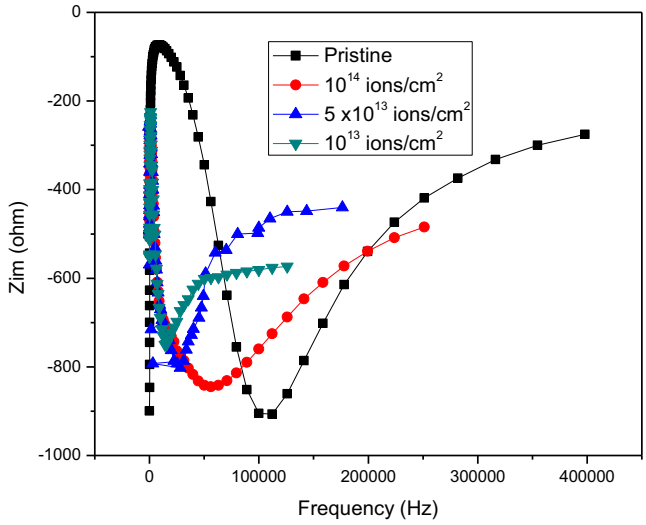

Fig. 5.27 Plots of imaginary part of impedance with frequency for pristine and Au^{3+} ion irradiated 2-amino-5-nitropyridinium dihydrogen phosphate (2A5NPDP) NLO single crystal.

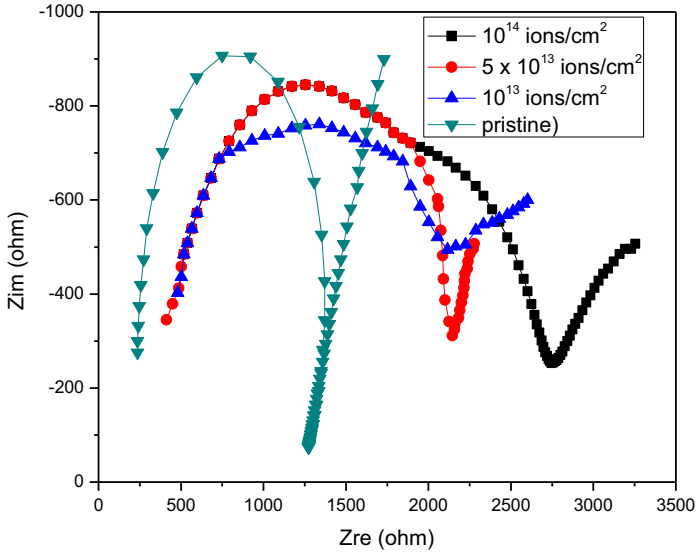

Fig. 5.28 Nyquist's plots for pristine and Au^{3+} ion irradiated 2-amino-5-nitropyridinium dihydrogen phosphate (2A5NPDP) NLO single crystal.

S.No	Ion fluence	Bulk resistance (Ohm)	Grain boundary resistance (Ohm)
1	Pristine	1200	848
2	10^{13} ions/cm^2	1750	1250
3	5 x 10^{13} ions/cm^2	2000	1250
4	10^{14} ions/cm^2	2750	1289

Tab. 5.7 Value of bulk and grain boundary resistance of both pristine and Au^{3+} ion irradiated 2-amino-5-nitropyridinium dihydrogen phosphate (2A5NPDP) NLO single crystal

5.6 Conclusion

2-amino-5-nitropyridinium dihydrogen phosphate (2A5NPDP) was irradiated by using Au^{3+} ion. Swift heavy ion (SHI) interacts with solid; it loses its energy continuously and changes its direction by collision with solid. It is observed from the X- ray diffraction pattern that, defects were formed and lattice was deformed. Lattice deformation was not in the entire crystal surface because deformation was taken place only in a small area that was around the ion paths. It is revealed from the Uv-vis spectra that absorption of irradiated crystal decreased with increase of ion fluencies. The change in the absorption may also be the creation of some intermediate energy levels due to structural rearrangements. Optical energy band gap of both the samples were calculated and it was found to be 3.14 eV, 3.07 eV, 3.08 eV and 3.09 eV for pristine and irradiated crystal respectively. Hardness of irradiated crystal increased with increases of ion fluencies. Increase of hardness was due to increase in density of lattice defects caused by the passage of implanted ions through 2-amino-5-nitropyridinium dihydrogen phosphate (2A5NPDP) lattices. It is elucidated from the

CHAPTER VII

Summary

Nonlinear optical (NLO) single crystal of 2-amino-5-nitropyridinium sulfamate (2A5NPS) was grown by using slow evaporation method and structure was solved. Bulk crystal of 2-amino-5-nitropyridinium sulfamate (2A5NPS) was grown using Assembled Temperature Reduction (ATR) method. The new crystal was subjected to single crystal X-ray diffraction. It was revealed from the single crystal X-ray diffraction that 2-amino-5-nitropyridinium sulfamate (2A5NPS) belongs to orthorhombic crystal system with the space group of Pbcn.

2-amino-5-nitropyridinum chloride (2A5NPCl) was grown from slow evaporation and Assembled Temperature Reduction (ATR) method. The grown crystal is a monoclinic with a space group P21 and lattice parameters are a= 9.957Å, b= 7.384 Å, c= 4.821Å, β= 95.85° and Z= 2.

2-amino-5-nitropyridinium dihydrogen phosphate (2A5NPDP single crystal belongs to orthorhombic crystal system with the space group Pna21 and the unit cell dimensions are a= 25.6090 Å, b= 6.2140 Å and c= 5.6600 Å and α= β= γ= 90°. The volume of the unit cell is 900.70Å^3 and Z is 4.

Organic-inorganic NLO single crystal of 2-amino-5-nitropyridinium hydrogen oxalate (2A5NPHO) was grown using slow evaporation and bulk crystal was grown from assembled temperature reduction (ATR) method. A proton transfer from the carboxyl group of oxalic acid to atom N1 of 2-amino-5-nitropyridinine resulted in the formation of a salt. The crystal structure was solved and it belongs to triclinic crystal system with the space group of P$\bar{1}$. 2-amino-5-nitropyridinium hydrogen oxalate (2A5NPHO) NLO single crystal is a colourless crystal with volume of 459.74 (Å)^3 and number of atom present in the crystal cell is Z= 2. The cell parameter of as the

grown crystal are a= 5.5609(2) Å, b= 9.2012 (4) Å, c= 6.2305(4) Å, α= 90.245°, β= 98.500°, and γ= 100.038°.

Grown crystals were irradiated using Au^{3+} ion with three different flunces such as 10^{13} ions/cm^2, 5x 10^{13} ions/cm^2 and 10^{14} ions/cm^2 using 3 MV Pelletron Tandem Accelerator having high current beams (Typically 100-300 μ A from the ion source and post acceleration currents ~ 50 μ A) at National Centre for Accelerator based Research (NCAR), Bilaspur, Chhattisgarh, India.

Pristine and Au^{3+} Irradiated crystals were subjected to single crystal X-ray diffraction. It revealed that defects were formed and lattice was deformed. Lattice deformation was not in the entire crystal surface because deformation was taken place only in all small area that was round the ion paths. Intensity of peak decreased with increase of ion fluencies from 10^{13} ions/cm^2 to 10^{14} ions/cm^2. This was due to amorphization created by swift heavy ion (SHI). Intensity of peaks decreased at lower fluence but at higher fluence (10^{14} ion/cm^2) some of the peaks were vanished and quality of the crystalline nature was decreased.

It is revealed from the UV-Vis spectra that absorption of irradiated crystal decreased with increase of ion fluencies. The change in the absorption may also be the creation of some intermediate and additional energy levels due to structural rearrangements. It was also noticed that there was no additional peak in the visible region. This was due to lack of energy that electrons observed from swift heavy ion (SHI) to move lattice to substitution position and it was difficult to form ion vacancies. It also was noticed that energy band gap of irradiated crystals increased with increase of ion fluence in 2-amino-5-nitropyridinium sulfamate (2A5NPS), 2-amino-5-nitropyridinum chloride (2A5NPCl), and 2-amino-5-nitropyridinum hydrogen oxalate (2A5NPHO) but in 2-amino-5-nitropyridinum dihydrogen

phosphate (2A5NPDP) energy band gap decreases with increase of ion fluences. This was due to the creation of intermediate energy levels below the conduction band. The small value of extinction coefficient in the visible region exhibited by 2-amino-5-nitropyridinium hydrogen oxalate (2A5NPHO) (both pristine and irradiated) crystal has suitable property for anti reflecting coating of solar thermal devices.

Hardness of Au^{3+} irradiated crystal increased with increases of ion fluencies. Increase of hardness was due to increase in density of lattice defects caused by the passage of implanted ions. High dense lattice defects produced residual surface compression stress which increased the hardness of the irradiated crystals.

It is elucidated from the dielectric studies that, dielectric constant increased with increase of ion fluencies. This was due to damage created along the surface of the sample, when high fluence ion beam was irradiated. Damage created by swift heavy ion (SHI) was isolated from each other, which increased charge carriers.

SEM reveals that the surface of irradiated crystal was heavily damaged and degree of crystallinity decreased when ion fluencies increases. Defects due to high ion fluence affected the radiative transitions in which crystal lost its luminescence property. Decrease of intensity peak was due to transition of excited electron to intermediated energy levels from excited state that converted into vibrational energy of lattice atoms (phonon). Then phonon was converted into thermal energy. So, large number of defects are formed which affect the radiative transitions.

Second harmonic generation (SHG) of pristine and irradiated samples was also studied. Second harmonic generation (SHG) efficiency of irradiated crystal decreased. The decrease of second harmonic generation (SHG) was due to higher ion fluence, which almost affected the noncentro symmetric packing of the molecular crystal.

Second harmonic generation (SHG) of pristine and Au^{3+} irradiated 2-amino-5-nitropyridine (2A5NP) family NLO crystalline derivatives are given below.

fluences/ samples	2A5NPS	2A5NPCl	2A5NPDP	2A5NPHO
Pristine	24 mV	164 mV	45 mV	98 mV
10^{13}ions/cm^2	4 mV	125 mV	5 mV	10 mV
5x 10^{13}ions/cm^2	1 mV	118 mV	1 mV	4 mV
10^{14} ions/cm^2	1 mV	63mV	1 mV	1mV
KDP	22 mV	55 mV	22 mV	120 mV

It is noticed from the thermal studies that, thermal stability increased with increase of ion fluencies. This was due to increase of defects with increase of ion fluences. This was due to disorderness produced in the crystalline surface by swift heavy ion irradiation which created amorphization in the surface. Decrease of degree of crystallinity increased the thermal stability in the Au^{3+} ion irradiated crystals. Increase of impedance of irradiated crystal than the pristine was due to the formation defects which were created by Au^{3+} ion. It is also revealed that bulk resistance increases with increase of ion fluences.

Suggestions for the future work

- Swift heavy ion of Au^{3+} was irradiated to enhance the structural, optical, thermal, and electrical properties of the newer variety of organic 2-amino-5-nitropyridine (2A5NP) family NLO crystalline derivatives. Attempts were made to increase the Second Harmonic Generation (SHG) of 2-amino-5-nitropyridine (2A5NP) family NLO crystalline derivatives but SHI affected the noncentro symmetric molecules in the irradiated crystals. In order to increase the Second Harmonic Generation (SHG) of 2-amino-5-nitropyridine (2A5NP) family NLO

REFERENCES

1. Ahlam, M. A, Ravishankar, Vijayan, N, Govindaraj, Siddaramaiah, G, & Gnana Prakash, A. P, 2012, 'Investigation of gamma radiation effect on chemical properties and surface morphology of some nonlinear optical (NLO) single crystals', Nucl. Instr. and Meth. B, Vol.278, PP. 26-33.
2. Akkermann. A, Levinson, J, Ilberg. D, & Lifshitz. Y, Editor - R. Baragiola, Ionisation of Solids , 1992, Heavy Particles, NATO Advanced Study Institutes Series 306, Plenum Press, New York, P. 431
3. Akriche, Sham Toumi & Rzaigui. M, 2009, '2-amino-5-nitropyridinium hydrogen selenate', Acta Cryst. E65, PP. 3009-3010.
4. Ambrose Rajkumar M, Stanly John Xavier. X, Anbarasu. S, & Prem Anand. D, 2014(a),' Photoconductivity, Microhardness and dielectric studies of 2-amino-5- nitropyridinium hydrogen oxalate (2A5NPHO) single crystal', International Journal of Emerging Trends in Science and Technology Vol.1, issue.10, PP. 1579- 1585.
5. Ambrose Rajkumar. M, Stanly John Xavier. X, Anbarasu.S, & Prem Anand. D, 2016(a), 'Growth and characterization studies of an efficient semiorganic NLO single crystal: 2-amino-5-nitropyridinium sulfamate (2A5NPS) by assembled temperature reduction (ATR) method', Optical Materials, Vol. 55, PP.153–159.
6. Ambrose Rajkumar. M, Stanly John Xavier. X, Anbarasu.S, & Prem Anand. D, 2014, '2-amino-5-nitropyridinium hydrogen oxalate', Acta Cryst. E70,PP. o473–o474,
7. Ambrose Rajkumar. M, Stanly John Xavier. X, Anbarasu.S, & Prem Anand. D, 2014(b), 'Microhardness, dielectric and photoconductivity, studies of 2-amino-5- nitropyridinium dihydrogen phosphate (2A5NPDP) nlo single crystal', International Journal of Emerging Trends in Science and Technology Vol.1, issue.10, PP.1610-1615.
8. Ambrose Rajkumar. M, Stanly John Xavier. X, Anbarasu.S, & Prem Anand. D, 2014(c), 'A Convenient Route to Synthesize and Grow 2-amino-5-nitropyridinium nitrate crystals for laser generation 'Sciencia Acta Xaveriana, Vol.4, 2, PP.73-78.

9. Ambrose Rajkumar. M, Stanly John Xavier. X, Anbarasu.S, & Prem Anand. D, 2014(d), 'Microhardness, Dielectric and photoconductivity, studies of 2-amino-5- nitropyridinium nitrate (2A5NPN) NLO single crystal', Res. J. Physical Sci, Vol. 2(1), PP.1-4.
10. Ambrose Rajkumar. M, Stanly John Xavier. X, Anbarasu.S, & Prem Anand. D, 2015, 'Crystal structure of 2-amino-5-nitropyridinium sulfamate,'Acta Cryst. E71.
11. Ambrose Rajkumar. M, Stanly John Xavier. X, Anbarasu.S, & Prem Anand, D,2016, ' Growth and characterization studies of an efficient semiorganic NLO single crystal: 2-amino-5-nitropyridinium dihydrogen phosphate (2A5NPDP) by Sankaranarayanan- Ramasamy method', Optik Vol.127, PP. 2187-2192.
12. Ambrose Rajkumar. M, Stanly John Xavier. X, Anbarasu.S, & Prem Anand,D, 2017, 'Crystal growth and characterizations of an efficient semiorganic nonlinear optical (NLO) single crystal: 2-amino-5-nitropyridinium chloride (2A5NPCl) by assembled temperature reduction apparatus (ATR) method', Materials research innovations,.
13. Anandha Babu. G, Ramasamy. P, Vijayan.N, kanjilal. D,& Asokan. K, 2008,' Effect of 50 MeV Li^{3+} ion irradiation on electrical, optical and mechanical properties of 4,4′-dimethylbenzophenone' , Nucl. Instr. and Meth. B, Vol. 266, 23, PP.5032- 5036.
14. Anandha Babu. G, Perumal Ramasamy. R, Ramasamy. P & Krishna Kumar. V, 2009, ' Synthesis, Crystal Growth, and Characterization of an Organic Nonlinear Optical Donor-π-Acceptor Single Crystal: 2-amino-5-nitropyridinium-toluenesulfonate', Cryst. Growth Des, Vol.9, 7, PP. 3333–3337.
15. Anandha babu. G, Ramasamy. P, & Chandramohan. A, 2011, 'Studies on the synthesis, structure, growth and physical properties of an organic NLO crystal: 2-amino-5-nitropyridinium Phenolsulfonate', Materials Research Bulletin, Vol. 46, PP. 2247-2251.
16. Anderson, F. P., Gallagher, J. F., Kenny, P. T. M. & Lough, A, 2005, 'Redetermination of para-aminopyridine (fampridine, EL-970) at 150 K', J. Acta Cryst. E61, PP.1350–1353.

17. Angeli Mary. P.A, & Dhanuskodi. S, 2001, 'EPR and optical absorption studies of VO^{2+} doped L- arginine Phosphate Monohydrate single crystals spectrochemica Acta A, Vol. 57, PP. 2345, 2001.

18. Anna Puig-Molina, Angel Alvarez-Larena, Juan. F. Piniella, Sean. T. Howard & François Baert, 1998, 'The Electron Distribution in the Nonlinear Optical Material 2-Amino-5-Nitropyridinium Dihydrogen Phosphate, Structural Chemistry, Vol. 9, No. 6, PP. 395–402.

19. Arivazhagana. M & Subhasinib. V.P, 2012, 'Quantum chemical studies on structure of 2-amino-5-nitropyrimidine', Spectrochimica Acta Part A 91, PP. 402– 410.

20. Arun kumar. R, & Dhanasekaran, 2012, 'Effect of 120 MeV Ag^{9+} ion irradiation of YCOB single crystals', Nucl. Instr. and Meth. B, 287, PP 109-112.

21. Avasthi. D.K, 2002,' some interesting aspects of swift heavy ions in materials science', Current Science, 78, 11, PP. 1297-1306.

22. Avasthi. D.K, 2005, 'Nanostructuring by Energetic Ion Beams', Hyperfine Interact. 160, PP. 95-106.

23. Babu, K. S. S, Peramaiyan, G, NizamMohideen, M. & Mohan, R, 2014, '2-Amino-6-methylpyridinium 2, 2, 2-trichloroacetate' Acta Cryst. E70, PP.391–392.

24. Bagieu-Beucher, M, Masse, R, & Ban qui, T, 1991, 'Structural Investigations of two 2-amino-5-nitropyridinium Salts: $C_5H_6N_3O_2^+$ NO_3^- and $(C_6H_5N_3O_2^+)_2$ $CUCI_4^{2-}$ 'Z. anorg. allg. Chem. Vol.606, PP. 59–71.

25. Balamurugan. S, Mehta. B. R, Avasthi. D. K, Singh. F, Akhilesh. Arora. K, Rajalakshmi. M, Raghavan. G, Tyagi. A. K & Shivaprasad S. M, 2002, 'Modifying the nanocrystalline characteristics- structure, size, and surface states of copper oxide thin films by high-energy heavy-ion irradiation', J. Appl. Phys. Vol.92, 6, PP. 3304-3310.

26. Banarji Behera, Nayaka, P, & Choudhary, R.N.P, 2007, 'Impedance spectroscopy study of $NaBa_2$ V_5O_{15} ceramic' J. Alloys and compounds, Vol. 436, 226, 2007.

27. Bangaru .S, 2011'Luminescence, optical and laser Raman scattering studies on γ -irradiated terbium-doped potassium iodide crystals', Radiation Effects & Defects in Solids, 166, 2, PP. 114-123.

28. Barzoukas. M, Blanchard-Desce. M, Josse. D, Lehn. J.M, & Zyss. J, 1989. J, Chem. Phys. Vol. 133, PP. 323–329.
29. Benyagoub, A, Couvreur. F, Bouffard. S, Levesque. F, Dufour. C & Paumier. E, 2001, 'Phase transformation induced in pure zirconia by high energy heavy ion irradiation', Nucl. Instrum. Methods. Phys. Res. B, Vol.175-177, PP. 417-421.
30. Bernstein, J, Davis, R. E., Shimoni, L. & Chang, N.-LAngew,1995, 'Patterns in hydrogen bonding- functionality and graph- set analysis in crystals' Angew. Chem. Int. Ed. Engl. Vol. 34, PP. 1555–1573.
31. Bhat. A. P, Aithal. P.S, Mohan Rao. P, & Avasthi. D. K, 2000, 'Effects of swift heavy ions on the dielectric properties of doped and undoped ammonium dihydrogen phosphate crystals', Nucl. Instr. and Meth. B, 166-167, PP 964-967.
32. Bhat. A.P, Aithal. P.S, Rao. P.M, Avasti. D. K, 1996,' Mater. Sci. forum, Vol.213, PP. 223-224,
33. Bierlein. J.D, vanherzeele. H, 1989. J. Opt. Soc. Am. B Vol.4 (6), PP. 622–633.
34. Boomadevi. S, Mittal. H.P, & Dhanasekaran. R, 2004 'Synthesis, crystal growth and characterization of 3-methyl 4-nitropyridine 1-oxide (POM) single crystals' J. Cryst. Growth, 261, PP.55-62.
35. Bright. K.C, & Freeda. T.H, 2010 'Growth and characterization of organometallic L-alanine cadmium chloride single crystal by slow evaporation technique', Physica B: Condensed Matter, Vol. 405, 18, PP. 3857–3861.
36. Bruker (2004). APEX2, SAINT, XPREP and SADABS. Bruker AXSInc., Madison, Wisconsin, USA.
37. Buchal. C.H, Withrow. S.P, White. C.W, & Poker. D.B, 1994, 'Ion Implantation of Optical Materials', Rev. Mater. Sci, Vol. 24, PP.125-157.
38. Busby. C.C, J. & Creighton, A, 1982, 'Factors influencing the enhancement of raman spectral intensity from a roughened silver surface: The adsorption and surface Raman scattering of 2-amino-5-nitro pyridine', Journal of Electroanalytical Chemistry and Interfacial Electrochemistry, Vol. 133, 1, PP. 183-193.
39. Chaikin & Lubensky, 1995, Principles of Condensed Matter Physics, Cambridge University Press

40. Chemla. D.S, & Zyss. J, 1987, Nonlinear Optical Properties of Organic Molecules and Crystals Academic Press. Inc, Vol. 23–191.

41. Chernov A.A, 1984, Modern Crystallography III, Crystal Growth, Springer Series in Solid-State Sciences,

42. Christer B. Aakeroy, Alicia M. Beatty, Mark Nieuwenhuyzen, & Min Zou,1998 'A structural study of 2-amino-5-nitropyridine and 2-amino-3-nitropyridine: intermolecular forces and polymorphism', J. Mater. Chem. Vol. 8, PP.1385– 389.

43. Chun. M. K, Goldberg. L & Weller. J. F, 1988. 'Second-harmonic generation at 421 nm using injection-locked GaAlAs laser array and $KNbO_3$', Appl. Phys. Lett. Vol. 53, PP. 1170.

44. Deepthy, K.S.R. Rao, H.L. Bhat, Ravikumar, & Asokan, K, 2001, 'Gray track formation in $KTiOPO_4$ by swift ion irradiation', J. Appl. Phy, Vol.89, PP.6560-6562.

45. Derissen, J. L. & Smith, P. H., 1974.'Refinement of crystal structures on Anhydrous α and β Oxalic acids', Acta Cryst. B30, PP 2240–2242.

46. Dhanuskodi. S, & Manikandan. S, 2004, 'Single Crystal EPR Study on g-irradiated NLO Material (2-amino-5-nitropyridinium chloride)' Radiation Effects & Defects in Solids, Vol. 159, PP. 173– 180.

47. Dhanuskodi. S, Pricilla Jeyakumari. A, & Manivannan. S, 'Semiorganic NLO Material for Short Wavelength Generation: 2-amino-5-nitro Pyridinium Bromide', Journal of crystal growth, Vol.282, PP.72-78, 2005.

48. Dixit. V.K, Rodrigues. B.V, Bhat. H.L, Ravi Kumar, Venkataraghavan. & R, Chandrasekaran, 1993 'Synthesis, crystal structure and non-linear optical properties of 2-amino-5-nitropyridine-L-(+)- tartrate, a new second- harmonic generation crystal'Journal of material chemistry , 3(10), PP. 1053-1057.

49. Dufour. C, Audouard. A, Beuneu. F, Dural. J, Girard. J. P, Hairie. A, Levalois. M, Paumier. E, & Toulemonde. M, 1993,' A high-resistivity phase induced by swift heavy-ion irradiation of Bi: a probe for thermal spike damage?', J. Phys.: Condens. Matter 5, PP. 4573- 4584.

50. Fan. T.Y, Huang. C.E, Hu. B.Q, Eckard. R.C, Fan. Y.X, Byer. R.l, & Feigelson. R.S, 1987, 'Second harmonic generation and accurate index of refraction measurements in flux-grown $KTiOPO_4$', Appl. Opt. Vol. 26, PP.2390–2394.

51. Farrugia, L. J. (2012). J. Appl. Cryst. 45, 849–854.

52. Feng Chen, Xue-Lin Wang, & Ke-Ming Wang, 2007 'Development of ion-implanted optical waveguides in optical materials: A review', Optical Materials, Vol.29, PP. 1523–1542.

53. Feve. J.P, Boulanger. B, Rousseau. I, Marnier. G, Zaccaro. J& Ibanez, 1999'Optical studies of laser-induced gray-tracking in KTP', IEEE journal of quantum electronics, Vol.35, (1), PP. 281-286.

54. Fleisher. R. L, Price. P. B, & Walker. R. M, Nuclear Tracks in Solids, University of California Press, 1975

55. Foresti. M.L, Funtikov. A.M, Guidelli. R, & Muniz-Miranda. M, 1994, 'Relation between surface enhanced Raman intensity and surface concentration for 2-amino 5-nitro pyridine adsorbed on roughened polycrystalline silver electrodes' Journal of Electroanalytical Chemistry, Vol.367, 1–2, , PP 223-237.

56. Franken. P. A, A.E. Hill, C.W. Peters and G. Weinreich, 1961,' Generation of Optical Harmonics', Phys. Rev.Lett, Vol.7, PP. 18-120

57. Fu, D.W, Zhang, W, Cai, H.-L, Ge, J.-Z, Zhang, Y. & Xiong. R.-G, 2011, 'Diisopropylammonium chloride: a ferroelectric organic salt with a high phase transition temperature and practical utilization level of spontaneous polarization', Adv. Mater. Vol.23, PP.5658–5662.

58. Fur. Y, Beucher. M, Masse. R, Nicoud. J, & Levy, 1996, J,' Crystal Engineering of Noncentrosymmetric Structures Based on 2-Amino-5-nitropyridine and n-Chloroacetic Acid Assemblies', Chem. Mater. Vol. 8, PP. 68–75.

59. Gilbert- Mougel. C, Couvreur. F, Costantini. J. M, Bouffard. S, Levesque. F, Hemon. S, Paumier. E & Dufour. C, 2001, 'Phase transformation of polycrystalline zirconia induced by swift heavy ion irradiation', J. Nucl. Mater, Vol.295, PP 121-125.

60. Haja Hameed A S, Rohain S, Yu W C, Tai C Y & Lan C W, J. 2006, 'Surface defects and mechanical hardness of rapidly grown DAST crystals', Cryst. Growth, Vol. 297, PP. 146-151.

61. Hideko Koshima , Hironori Miyamoto , Ichizo Yagi & Kohei Uosaki, 2004' Cocrystals of 2-amino-5-Nitropyridine with Benzenesulfonic Acids for

Second-Order Nonlinear Optical Materials', Journal Molecular Crystals and Liquid Crystals, Vol. 420, 1, 2004.

62. Hohenberg. P. C. & Halperin. B. I, 1977, 'Theory of dynamic critical phenomena' Rev. Mod. Phys. 49, PP.435- 479 .

63. Horiuchi. N, Kodaira. T, Watanabe. A, & Matsuda, M, 1997, ' Protonation and solvent-interaction effects on the first hyperpolarizability of 2-amino-5-nitropyridine', Chem. Phys. Lett. Vol. 276, PP. 92–96.

64. Horiuchi. N, Lefaucheux. F, Ibanez. A, Jose. D, & Zyss. J, 1999' An organic–inorganic crystal for blue SHG: crystal growth and quadratic optical effect of 2-amino-5-nitropyridinium chloride, 'Optical materials, Vol.12, PP. 351-356.

65. Horiuchi. N, Lefaucheux. F, Ibanez. A, Josse. D, & Zyss. J, 2002, 'Quadratic nonlinear optical coefficients of organic–inorganic crystal: 2-amino-5-nitropyridinium chloride', J. Opt. Soc. Am. B, Vol. 19, 8, PP.1830-1838.

66. Horiuchi. N, Lefaucheux. F, Ibanez. A, Lorut. F, & Baruchel. J, 2004, ' X-ray characterization of an organic- inorganic solution grown crystal: case of 2-amino-5-nitropyridinium chloride', Journal of crystal growth, Vol. 262, PP. 594-601.

67. Horiuchi. N, Lefaucheux. F, Robert. M.C, Jose. D, Khodja. S, & Zyss. J, 1995,' Gel growth of 2-amino-5nitropyridinium dihydrogen phosphate organomineral crystals: X-ray and nonlinear optics characterization', Journal of crystal growth 147, PP. 361-368.

68. Huq, C. A. M. A., Fouzia, S. & NizamMohideen, M, 2013,' 5-Acetyl-4-(3-hydroxyphenyl)-6-methyl-1,2,3,4-tetrahydropyrimidin-2-one–tris(hydroxymethyl)ammonium chloride (2/1)' , Acta Cryst. E69, PP. 1766–1767.

69. Ibanez. A, Levy. J.P, Mouget. C, Proeur. E, J. 1997,'Crystal growth of a promising nonlinear optical material: 2-amino-5-nitropyridinium chloride', Solid State Chem. Vol. 129, PP. 22–29.

70. Ingram. D. C, & Mc Cormick. A. W, 1988, 'The effect of MeV ion irradiation on the hydrogen content and resistivity of direct ion beam deposited diamondlike carbon', Nucl. Instrum. Methods. Phys. Res. B, Vol. 34, PP. 68-73.

71. Ishwar Bhat. S, Mohan Rao P, Ganesh Bhat. A.P, & Avathi. D.K, 2002, 'Irradiation effects on the optical properties of a new NLO mixed borate crystal S, urface and coating Technology, Vol.158, PP.725-728.

72. Iyanar. M, Muthamizhchelvan. C, Ponnusamy. S, & Thomas Joseph Prakash, 2010 'Synthesis, growth and characterization of semi-organic nonlinear optical crystal: glycine zinc chloride', J. Recent Research in Science and Technology, Vol.2, 1, PP. 97-100.

73. Iyanar. M, Thomas Joseph Prakash. J, Muthamizhchelvan. C, & Ponnusamy. S, 2009,' Growth, and Characterization Studies of a Semiorganic Nonlinear Optical Single Crystal of Gamma Glycine', Journal of Physical Sciences, Vol. 13, PP. 235-244.

74. Jain.I.P, & Garima Agarwal, 2011, 'Ion beam induced surface and interface engineering,'Surface Science Reports', Vol. 66, Issues 3–4, PP. 77–172.

75. Jang. Min- hua, & Fang. Q, 1999 'Organic and Semiorganic Nonlinear Optical Materials', Adv. Mater, Vol.11(13), PP. 1147.

76. Jebas. S. R. & Balasubramanian. T, 2006; 'Hydrogen-bonding patterns of 2-aminopyridinium p-nitrobenzoate', Acta Cryst. E62, PP. 2209-2211.

77. Josephine Viavulamary Jovita J, Sathya S, Usha G, Vasanthi R, & Ezhilarasi KS, 2013, '2-amino-5-nitropyridinium trifluoroacetate', Acta Cryst. E 69, PP. 841-842.

78. Justin Raj. C.& Jerome Das. S, 2008,' Bulk Growth and Characterization of Semiorganic Nonlinear Optical l-Alanine Cadmium Chloride Single Crystal by Modified Sankaranarayanan−Ramasamy Method', Cryst. Growth Des,Vol. 8, 8, PP.2729–2732.

79. Kamboj, Maninder Singh, Kaur. G, Thangaraj. R & Avasthi. D. K, 2002, 'Effect of heavy ion irradiation on the electrical and optical properties of amorphous chalcogenide thin films', J. Phys. D; Appl. Phys. 35, PP 477-479.

80. Kamitsos. E, 2003,' Infrared studies of borate glasses', Physics and Chemistry of Glasses, vol. 44(2), PP. 79–87.

81. Kanagasekaran. T, Mythili. P, Bhagavannarayana. G, Kanjilal, & D, Gopalakrishnan. R, 2009, 'Investigations of structural, dielectric and optical properties on silicon ion irradiated glycine monophosphate single crystals', Nucl. Instr. Methods Phys. Res. B 267, PP 2495-2502.

82. Kanagasekaran.T, Mythili.P , Binay Kumar, & Gopalakrishnan. R, 2010'Effect of ion irradiation on the M-Nitroaniline single crystals', Nucl. Instrum.Methods Phys. Res.B, Vol.268, PP. 36-41.

83. Kanagasekaran.T, Gunasekaran. M, Srinivasan. P, Jayaraman. D, Gopalakrishnan. R. & Ramasamy. P, 2005, 'Studies on growth, induction period, interfacial energy and metastable zonewidth of m-nitroaniline', Crystal Research and Technology, Vol.40, PP.1128-1133.

84. Kanjilal. D, 2001, 'Swift heavy ion-induced modification and track formation in materials' Curr.sci, Vol. 80, PP.1560.

85. Karle, I, Gilardi, R. D, Chandrashekhar Rao, C, Muraleedharan, K. M.& Ranganathan, S. 2003, 'Unique assemblies of alternating positively and negatively charged layers, directed by hydrogen bonds, ionic interactions, and pi-stacking in the crystal structures of complexes between mellitic acid (benzene hexa carboxylic acid) and five planar aromatic bases' J. Chem. Crystallogr. Vol.33, PP.727–749.

86. Katz. R, Loh. K.S, Daling. L, & Huang. G.R, 1990 'An analytic representation of the radial distribution of dose from energetic heavy ions in water, Si, LiF, NaI, and SiO2', Rad. Effects and Defects in Solids, Vol.114, PP.15-20.

87. Kiritani. M, 1998, 'The need for improved temperature control during reactor irradiation' J. Nucl.Mater, Vol.160, PP. 135.

88. Knaster. J, Moeslang. A, & Muroga. T, 2016 'Materials research for fusion'Nature Physics, Vol.12, PP. 424–434.

89. Köse. DA, Beckett. MA, & Çolak. N, 2012, 'Synthesis, spectroscopic and thermal characterization of non-metal cation (NMC) pentaborates salts containing cations derived from histidine and arginine' J. Biol. & Chem., Vol. 40 (3), PP. 219– 224.

90. Koter. Z, Hierli. R, josses. D, Zyss. J, & Masse. R, 1992, 'Quadratic nonlinear-optical properties of a new transparent and highly efficient organic–inorganic crystal: 2-amino-5-nitropyridinium-dihydrogen phosphate (2A5NPDP)' J. Opt.Soc. Am. B, Vol.9, PP. 534-547.

91. Kraft. S, Schattat. B, & Bolse. W, 2002, 'Ion beam mixing of ZnO/SiO_2 and Sb/Ni/Si interfaces under swift heavy ion irradiation', J. Appl. Phys 91, PP. 1129-1134.

92. Kramer. M, 1995, 'Calculation of heavy-ion track structure', Nucl. Instr. and Meth. B 105, PP. 14-20.

93. Krishnakumar. V, Avasthi D.K, Fouran Singh, Kulriya. P.K., Nagalakshmi. R, 2007, 'Study of the damage produced in $K[CS(NH_2)_2]_4Br$ – A non-linear optical single crystal by swift heavy ion irradiation' Nucl.Instrum. methods. phys. Res. B: Beam Interactions with Materials and Atoms, Vol. 256, 2, PP. 675-682.

94. Kucheyev. S. O, Williams J.S, Zou. J, Jagadish. C & Li. G, 2001, 'The effects of ion mass, energy, dose, flux and irradiation temperature on implantation disorder in GaN', Nucl. Instrum. Methods B, Vol.178, PP. 209-213.

95. Kucheyev. S. O, Williams. J. S, Jagadish. C, Zou. J, Evans. C, Nelson. A. J,& Hamza. A. V, 2003, Ion-beam-produced structural defects in ZnO' Phys. Rev. B 67, PP. 94115-94126.

96. Kucheyeva. S.O, Williams. J.S, Zou. J, Jagadisha. C, & Lic. G, 2001. Nucl.Instrum. methods. phys. Res. B: Beam Interactions with Materials and Atoms, Vol. 175–177, PP. 214–218,

97. Kumaresan. p, Moorthy babu. S, & Anbarasan. P.M, 2008, 'Effect of irradiation of swift heavy ions on dyes-doped KDP crystals for laser applications', Journal crystal growth, 310, PP. 1999-2004.

98. Kurtz. S.K, & Perry. T.T, 1968 'A Powder Technique for the Evaluation of Nonlinear Optical Materials', J. Appl. Phys. Vol.39, PP. 3798-3813.

99. Lesuer. O & Dunlop. A,1993, 'Damage creation via electronic excitations in metallic targets part I: Experimental results', Radi. eff. defect in solids, Vol. 126, PP. 123-128.

100. Levalois. M & Marie. P, 1999, 'Damage induced in semiconductors by swift heavy ion irradiation', Nucl. Instr. and Meth. B 156, PP. 64-71.

101. Levine. B.F & Bethea. C.G, 1975, 'Second and third order hyperpolarizabilities of organic molecules', J. Chem. Phys. Vol. 63, 6, PP. 2666–2682.

102. Levine. B.F, & Bethea. C.G, 1974,'Molecular hyperpolarizabilities determined from conjugated and nonconjugated organic liquids', Appl. Phys. Lett.Vol.24, 9, PP. 445–447.

103. Li Fucin, Luping, Himaru Manbuies, Kurt E. Sicafus, & Philos, 2000, 'Effect of heavy ion irradiation on near-surface microstructure in single crystals of rutile TiO_2', Mag.B, Vol. 80, PP.1947-1954.

104. Lian Zhang, Peng Liu, Tao Liu, Yu- Fan Zhou, Jian- Rong Sun, Zhi- Guang Wang,& Xue- Lin Wang, 2013,'Optical properties of planar waveguide in Nd:YVO_4 crystal formed by swift Kr^{8+} ion irradiation', Nucl. Instr. and Meth. B, 307, PP. 459-462.

105. Lin Chen, Yang Cao, Tiantian Fang, Wei Yue, Jing Wang, Xin Zhang, & Fengchun Yang, 2013, 'Synthesis and characterization of degradable polyimides from p-phenylenedioxybis(5-amino-2-pyridine)', Polymer Degradation and Stability, Vol. 98, PP. 839- 843.

106. Long. N.J, 1995, 'Organometallic Compounds for Nonlinear Optics—The Search for En-light-enment!', Angew. Chem. Int.Ed. Engl. Vol.34, PP. 21–38.

107. Lorenc. J, Bryndal, M. Marchewka, E. Kucharska, T. Lis & Hanuza, J 2008, 'Crystal and molecular structure of 2-amino-5-chloropyridinium hydrogen selenate – its IR and Raman spectra, DFT calculations and physicochemical properties', Journal of raman spectroscopy, Vol.39, PP. 863–872.

108. Lorenc. v, Bryndal, Marchewka. M, Kucharska. E, Lis. T & Hanuza. J, 2008,' Crystal and molecular structure of 2-amino-5-chloropyridinium hydrogen selenate—its IR and Raman spectra, DFT calculations and physicochemical properties', Journal of raman spectroscopy, 39, PP. 863–872.

109. Macrae, C. F., Bruno, I. J., Chisholm, J. A., Edgington, P. R., McCabe,P., Pidcock, E., Rodriguez-Monge, L., Taylor, R., van de Streek, J. &Wood, P. A. (2008). J. Appl. Cryst. 41, 466–470.

110. Manikandan. S, Dhanuskodi. S, 2007, ' EPR of- irradiated single crystals of 2-amino-5-nitropyridinium l-tartrate: A NLO material', Spectrochimica Acta Part A, Vol.67, PP.160–165.

111. Manivannan. S, Dhanuskodi. S, Kirschbaum. K, & Tiwari. S. K, 2005, 'Design of an Efficient Solution Grown Semiorganic NLO Crystal for Short Wavelength Generation: 2-Amino-5-nitropyridinium Tetrafluoroborate', Crystal Growth & Design, Vol.5, 4, PP. 1463–1468.

112. Masse,R & Zyss,J, 1991,'A new approach in the design of polar crystals for quadratic nonlinear optics exemplified by the synthesis and crystal structure of 2-amino-5-nitropyridinium dihydrogen monophosphate (2A5NPDP), Molecular Engineering, Vol. 1, 2, PP. 141–152.

113. Masse. R, & Zyss. J,1991, 'A new approach in the design of polar crystals for quadratic nonlinear optics exemplified by the synthesis and crystal structure of 2-amino-5-nitropyridinium dihydrogen monophosphate (2A5NPDP)', Mol. Eng.Vol.1, 2, PP. 141–152.

114. Masse. R, 1995, Nonlinear Opt. Vol.9, PP.113,.

115. Masse. R, Bagien- Beucher. M, Pecaut. J, Levy. J.P, Zyss. J, 1993. J. Nonlinear Opt.Vol.5, PP.413–423.

116. Masse. R, Grenier. J.C, 1971, Bull. Soc. Fr. Mineral. Cristallogr. Vol.94, PP. 437–439,.

117. Maurizio Muniz- Miranda, Natale Neto and Giuseppe Sbrane, 1995, 'Halide anion effect on surface enhanced raman scattering of 2-amino-5-nitropyridine adsorbed on silver sols' Journal of molecular structure, Vol. 348, PP 261-264.

118. Meng. F.Q, Lu. M.K, Yang. Z.H, & Zeng. H, 1998, ' Thermal and crystallographic properties of a new NLO material, urea-(d) tartaric acid single crystal', J. Mater. Lett. Vol.33, 5-6, PP. 265–268.

119. Morela. Y, Zaccarob. J, Ibanezb. A, & Baldecka. P.L, 2002, 'Nonlinear absorption and optical limiting properties of the 2-amino-5-nitropyridinium dihydrogenophosphate hybrid crystal', Optics Communications, Vol. 201,PP. 457–464.

120. Mythili. P, Kanagasekaran. T, Khan. K. A, Kulriya. P. K, Kanjilal. D, & Gopalakrishnan. R, 2008, ' Irradiation effects on sodium sulphanilate dihydrate single crystals', Nucl. Instr. and Meth. B, 266, 8, PP 1754-1758.

121. Nagabhushana. H, Prashantha. S.C, Nagabhushana. B.M, Lakshminarasappa. B.N, & Fouran Singh, 2008, ' Damage creation in swift heavy ion-irradiated calcite single crystals: Raman and Infrared study', Spectrochimica Acta Part A , Vol.71,3, PP.1070–1073,.

122. Nagabhushana. H, Prashantha. S.C, Nagabhushana. B.M, Lakshminarasappa. B.N, Fouran Singh, & Chakradhar. R.P.S,2008a 'Ion beam-induced luminescence and photoluminescence of 100 MeV Si^{8+} ion irradiated kyanite single crystals', Solid Status Commun. 147, 9-10, PP. 377-380.

123. Nagarau. H . S, Neumann. T, & Mohan Rao. P, 2001, ' Ion-induced craters on the surface of benzoyl glycine single-crystals studied by scanning force microscopy', Nucl. Instrum. Method B, Vol. 185, 1-4, PP. 66-70.

124. Nakao. S, Saitosh. K, Ikeyama. M, Niwa. H, Tanemura. S, Miyagawa. Y & Miyagawa. S, 1996, 'Microstructure of germanium films crystallized by high energy ion irradiation', Thin Solid Films 281, PP. 10-13.

125. Nalwa, and Miyata, 1996, Nonlinear Optics of Organic Molecules and Polymers, by CRC Press,

126. Nicoud, J. F, & R. J. Twieg, 1987, Nonlinear Optical Properties of Organic Molecules and Crystals, Eds. D. S. Chemla and J. Academic Press, London, pp 227-296.

127. Ning Yu, Michael Nastasi, Kurtz E. Sickafus, Kazuhiro Yasadu, & Joseph R. Tesmer, 1997, ' In situ study of ion-beam induced lattice damage in calcium fluoride crystals', Nucl. Inst.Meth.Phy. Res.B Vol. 127/128, PP. 591-595.

128. Ohara, Makoto & Robert C. Reid , 1973, Modeling crystal growth rates from solution, Prentice-Hall,

129. Olivares.J, García-Navarro. A, García. G, Agulló-López. F, Agulló-Rueda. F, García-Cabañes. A & Carrascosa. M, 2007, ' Nonlinear optical waveguides generated in lithium niobate by swift-ion irradiation at ultralow fluences ', Optics letters,Vol.32, 17, PP. 2587-2589.

130. Olivares.J, García. G, García-Navarro. A, Agulló-López. F, Caballero. O & García-Cabañes. A, 2005, 'Generation of high-confinement step-like optical waveguides in $LiNbO_3$ by swift heavy ion-beam irradiation', Appl. Phys. Lett. Vol.86, PP. 183501-183501.

131. Onitsch. E.M., 1947, Mikroskopie Vol.2, 131-151,.

132. Osamu Watanabe, Tatsuo Noritake, Yoshiharu Hirose, Akane Okada & Toshio Kurauchi,1993 ' Synthesis, crystal structure and non-linear optical properties of 2- Amino 5-nitropyridine –L-(+)- tartrate', Journal of material chemistry , 3(10), 1053-1057.

133. Oudar. J.L, 1977, ' Optical nonlinearities of conjugated molecules. Stilbene derivatives and highly polar aromatic compounds', J. Chem. Phys. Vol. 67, PP. 446–457.

134. Oudar. J.L, Le Person. V, 1975, ' Second-order polarizabilities of some aromatic molecules', Opt. Comm.Vol. 15, 2, PP. 258–262.

135. Oussaid. M, kemich. M, becker. P, Carabatos-Nedelec. C, & Watanab,1996, ' Raman Scattering in 2-Amino-5-Nitropyridine-L-(+)-Tartrate Single Crystals', Phys. stat. sol. (b) 196,PP. 487.

136. Pamplin Brian, R, 1980, Crystal Growth, International Series on the Science of the Solid State.

137. Partal Urena. F, Fernandez Gomez. M, Lopez Gonzales. J.J, & Martinez Torres. E,2003, 'A new insight into the vibrational analysis of pyridine', Spectrochim. Acta A, Vol.59 PP. 2815-2839.

138. Pecaut. J, & Masse. R, 1993, 'Structure of bis(2-amino-5-nitropyridinium) dichromate as a step towards the design of efficient organic-inorganic non-linear optical crystals', Acta Crystallogr. B Vol.49 ,PP. 277–282.

139. Pecaut. J, & Masse. R, J, 1994, '2-amino-5-nitropyridinium acetophosphonate: a deliberately engineered non-linear optical crystal', Mater. Chem. Vol.4 , PP.1851–1854.

140. Pecaut. J, Levy. J. P, & Masse. R, 1993 'Structural evidence in 2-amino-5-nitropyridinium halides (Cl^-, Br^-) of Herringbone motifs favourable to efficient quadratic non-linear optical properties', Journal of material chemistry, Vol. 3, 10, PP.999-1003.

141. Pecaut. J. and Masse. R, 1994, '2- Amino -5- nitropyridinium Acetophosphonate : A Deliberately Engineering non linear optical crystal', Journal of material chemistry, 4(12), PP. 1851-1854.

142. Prabha. K, Ramesh babu. M, Prabukanthan. P, Chen. H, Chen. X.L, & Sagayaraj. P, 2012, 'Irradiation effects on ammonium penta borate (APB) single crystals', Materials Science and Engineering , 73, PP 12043-12047.

Prabukanthan. P, Asokan. K, , Kanjilal. D, & Dhanasekaran. R,2008, 'Effect of swift heavy ion Ag9+ irradiation on the surface morphology, structure and optical properties of AgGaS2 single crystals', Semicond. Sci. Tehnol. 23, PP. 125042- 125047.

143. Prasad. P.N. and William. D.J, 1991, Wiley, Newyork,.

144. Pricilla Jeyakumari. A, Manivannan. S, & Dhanuskodi. S, 2007, 'Spectral and optical studies of 2-amino-5-nitropyridinium dihydrogen phosphate: A semiorganic nonlinear optical material', Spectrochimica Acta Part A, Vol. 67, PP.83– 86.

145. Ramesh kumar. G, Gokul Raj. S, V. Mathhivanan. V, Kovendhan. M, Mohan. R, Thenneti Raghavalu, Kanjilal. D, Asokan. K, Tripathi. A,Sulania. I, & Pawan K Kulriya, 2007, 'Swift ion irradiation effects on L-threonine amino acid single crystals', J. Phy. condens. Matter, Vol. 19, PP 466108- 466118.

146. Rao. K.V, & Smakula. A, 1965, 'Dielectric Properties of Cobalt Oxide, Nickel Oxide, and Their Mixed Crystals', J. Appl. Phy Vol.36, PP. 2031- 2038.

147. Ravi. S, & Subramanian. P, 2007, EPR study of Cu^{2+} in glycine zinc sulphate single crystal'Solid State Communications, Vol. 143, 6–7, PP. 277-279.

148. Ravishankar. M. N, Chandramani. R, & Gnanaprakash. A.P, 2011, 'Optical and mechanical characterization of solution grown semi organic NLO crystals', RJCABP, Vol.4, No.1, PP. 86-90.

149. Rodrigues. V. H, Costa. M. M. R. R, Dekola. T & de Matos Gomes. E, 2009, '2-Amino-5-nitropyridinium tetraoxidorhenate(VII) monohydrate', Acta Cryst. E65, 2009.

150. Rout. B, Kamila. J, Ghose. S.K, Mahapatra. D.P, & Dev. B.N, 2001,'Characterization of microstructures formed on MeV ion-irradiated silver films on Si(1 1 1) surfaces' Nucl. Instr. and Meth. B, 181, 1-4, PP 268-273.

151. Sagawa. M, Kagawa. H, Kakuta. A, Kaji. M, Saeki. M & Namba. Y, 1995, 'Blue light emission from a laser diode pumped ring resonator with an organic second-harmonic generation crystal of 8-(4'-acetylphenyl)-1,4-dioxa-8-azaspirol[4.5]decane', Appl. Phys. Lett. Vol. 66, PP. 547-549.

152. Samah Toumi Akriche, Mohamed Rzaigui, Noura Al-Hokbany & Refaat Mohamedahfouz, 2010 '2-Amino-3-nitropyridinium perchlorate', Acta Crystallographica Section E, E 66, PP. 300-304.

153. Samuel. I. D. W, Villacampa. B, Josse. D, Khodja. S, & Zyss. J, 1995, 'Efficient optical parametric generation in an organomineral crystal', Appl. Phys. Lett. Vol.66.PP. 2019-2021.

154. Sangeetha. K, Ramesh babu.R, Ramamurthi. K, Jai Prakash, & Khan. S.A, 2011,'Spectral studies on Ag^{8+} ions irradiated $LAHCl.H_2O$ and $LAHBr.H_2O$ single crystal', spectrochimica Acta part A, 79, PP. 884-888.

155. Sankar.R, Raghavan. C. M, Mohan Kumar. R, & Jayavel. R, J.2007, 'Growth and Characterization of a new semiorganic nonlinear optical Thiosemicarbazide Cadmium Chloride Monohydrate (Cd ($NH_2NHCSNH_2$) $Cl_2.H_2O$) single crystals', Cryst. Growth Vol. 305, PP. 156–161.

156. Sankaranarayanan & Ramasamy, 2006, 'Growth of benzophenone single crystals from solution: A novel approach with 100% solute-crystal conversion efficiency', Crys.Res. Technol, 41, 3, PP 225-230.

157. Sarkar. A, Mukherjee. P, & Barat. P, 2008, 'Effect of heavy ion irradiation on microstructure of zirconium alloy characterised by X-ray diffraction', Journal of Nuclear Materials, Vol. 372, 2–3, PP. 285–292.

158. Sathyavathi. P, Chavan. S. T, Kanjilal. D, & Bhoraskar. V. N, 1999, 'Heavy ion induced damage in crystalline silicon and diodes', Nucl. Instrum. Methods. Phys. Res. B 156, 1-4, PP 72-77.

159. Schattat. B. and Bolse. W, 2004, 'Fast heavy ion induced interface mixing in thin-film systems', Nucl. Instrum. Methods. Phys. Res. B 225, PP. 105-110.

160. Schiwietz. G, Luderee. E, Xiao. G, & Grande. P. L, 2001,' Energy dissipation of fast heavy ions in matter', Nucl. Instrum. Methods B 175, PP. 1-11.

161. Seager. C.H, Fleming. R.M, Lang. D.V, Cooper. P.J, Bielejec. E, & Campbell. J.M, 2007, 'Effects of defect clustering in neutron irradiated silicon', Physica B: Condensed Matter, Vol. 401–402, PP. 491–494.

162. Seitz. F, Koehler. J. S, Solid State Phys. 2 (1956) 305

163. Sethuram, M, Bhargavi, G, Dhandapani, M, Amirthaganesan, G. & NizamMohideen, M. 2013a, 'N^2-(4-Methoxysalicylidene)arginine hemihydrates', Acta Cryst. E69, PP.1301–1302.

164. Sethuram, M., Rajasekharan, M. V., Dhandapani, M., Amirthaganesan, G. & NizamMohideen, M, 2013b,' l-Histidinium dipicrate dihydrate' Acta Cryst. E69, PP. 957–958, 2013b.

165. Sethuraman. K, Ramesh Babu. R, Gopalakrishnan. R & Ramasamy. P, 2008, 'Synthesis, Growth, and Characterization of a New Semiorganic Nonlinear Optical Crystal: l-Alanine Sodium Nitrate (LASN)', Cryst. Growth Des, 8 (6), PP. 1863–1869.

166. Shah. P, Kumar. S, Gupta. A & Avasthi. D. K, 1999, 'Thermal properties of swift heavy ion irradiated CuO', Nucl. Instrum. Methods. Phys. Res. B 156, 1-4, PP. 222-226.

167. Sharada Prabhu. G, Mohan Rao. P, Avasthi. D.K, Shiuli, & Guptha, 2001, 'Effect of swift heavy ion (SHI) irradiation on dielectric properties of acetoacetanilide crystals', Nucl.Instrum. Methods Phys. Res.B Vol.174, PP. PP. 159-162.

168. Sheldrick, G. M. (2008). Acta Cryst. A64, 112–122.

169. Shihabuddeen Syed, A., Rajarajan, K. & NizamMohideen, M. 2013, '(Thiocyanato-κS)tris(thiourea-κS)mercury(II) chloride', Acta Cryst. E69, 33-38, 2013.

170. Showrilu, K, Rajarajan, K. & NizamMohideen, M, 2013, 'Diammonium tetra kis(isothiocyanato)zincate–1,4,10,13,16-hexaoxacyclooctadecane–water (1/2/1)', Acta Cryst. E69, PP. m469– m470.

171. Singh. J.P, Singh. R, Gosh. S, Tripathi. A, Kabiraj. D, Gupta. S, Som. T, Ravikumar, Arora. S.K, Asokan. K, Avasthi. D.K, Kanjilal. D, Mishra. N.C, & Metha. G.K, 1999, 'Swift heavy ion-based materials science research at NSC', Nucl. Instr. and Meth. B, 156, 1-4 PP 206-211.

172. Sivasubramani. V, Senthil Pandian. M, & Ramasamy. P, 2015, 'Studies on 2-amino 5- nitropyridinium nitrate (2A5NPN) a semi- organic third order nonlinear optical single crystal' AIP conference, 150, PP 765-771, 2015

173. Sivasubramani. V, Senthilpandian. M, Boopathi. k,& Ramasamy. P, 2016, ' Crystal growth, structural, optical, thermal and dielectric studies of non-linear optical 2-amino-5-nitropyridinium nitrate (2A5NPN) single crystals' Materials Research Innovations, PP 1-9.

174. Sreekumar. R, Jayakrishnan. R, Sudha Kartha. C, Vijayakumar. K.P, Khan. S. A, & Avasthi. D. K, 2008, 'Enhancement of band gap and photoconductivity in gamma indium selenide due to swift heavy ion irradiation', J. Appl. Phys. 103, PP 23709- 23718.

175. Sreeramana Aithal. P, Nagaraja. H.S, Mohan Rao. P, Avasthi. D.K, & Asati Sarma, 1997 'Effect of high energy ion irradiation on electrical and optical properties of para-hydroxy acetophenone', J. Appl. Phys. 81, PP 7526-7528.

176. Srivastava. P.C, Pandey. S.P, Avasthi. D.K & Asokan. K, 1997, 'PdSi device characteristics on 100 MeV gold ions irradiation', Vacuum, 48, 12, PP 975-1034.

177. Sun. Y., Zhang. C, Zhu. Z, Wang. Z, Jin. Y, Liu. J & Wang. Y, 2006, 'Evolution of radiation-induced carbon–oxygen-related defects in silicon upon annealing: LVM studies',Nuclear Instruments and Methodsin Physics Research Section B: Beam Interactions with Materials and Atoms, Vol. 245, PP. 210-213.

178. Suriya kumar. K, Gokulraj. S, Ramesh kumar. G & Mohan. R, 2009, '50 MeV Li^{3+} Irradiation Effects on Structural, Optical and Surface Properties of L-Alanine Single Crystals ', Science of advanced materials, Vol.1, 3, PP. 286-291.

179. Tao1. X. T, Yuan. D. R, Zhang. N, Jiang. M. H & Shao. Z. S, 1992, ' Novel organic molecular second harmonic generation crystal: 3-methoxy-4-hydroxy-benzaldehyde', Applied Physics Letters, Vol. 60, PP.1415-1417.

180. Thomas. P.C, Aruna. S, Packiam Julius. J, Joseph Arul Pragasam. A & Sagayaraj. P, 2006, 'Growth and characterization of semiorganic NLO crystals of LAHClBr ', Crystal Research Technology, Vol.41, PP. 1231- 1235.

181. Tie-Jun Wang, Yu-Fan Zhou, Xiao-Fei Yu, Tao Liu, Lian Zhang, Hong-Lian Song, Mei Qiao & Xue-Lin Wang, 2015, Optical waveguide properties of $Ca0._4Ba0.6Nb_2O_6$ crystal formed by oxygen ion irradiation', Nuclear Instruments and Methodsin Physics Research SectionB: Beam Interac tions with Materials and Atoms, Vol.354, PP. 187-191.

182. Tordjman.I, Masse. R & Guitel. J.C, 1974, 'Structure cristalline du monophosphate $KTiPO_5$', Zeitschrift für Kristallographie- Crystalline Materials, Vol.139, PP. 103–115.

183. Townsend. P.D, Chandler. P.J, & Zhang. L, 1994, Optical effects of ion implantation, Cambridge University Press - Cambridge studies in modern optics, Cambridge.

184. Trautmann. C, Roulemonde. M, Schwartz. K, Costantini. J.M & Muller. A, 2000, 'Damage structure in the ionic crystal LiF irradiated with swift heavy ions', Nuclear Instruments and Methods in Physics Research Section B: Beam Interactions with Materials and Atoms, Vol. 164-165, PP. 365-376.

185. Turnbull. Mark M, Galeriu. Calin, Giantsidis. John & Christopher P. Landee, 2002, ' Synthesis, Structure and Magnetic Susceptibility of two 5-Nitro-2-Aminopyridinium Cuprates: $(5\text{-NAP})_2$ $CuCl_4$ and the Quantum Magnetic

Ladder (5-NAP)$_2$ CuBr$_4$ ·H$_2$O', Journal Molecular Crystals and Liquid Crystals, Vol.376, 1, PP. 469-476.

186. Ulrich, D., Brockbank, W., & Yeung, A, 1989, 'Beyond belief: A benchmark for human resources', Human Resource Management, 28, PP 311-335.

187. Uma Devi. T, Lawrence. N, Rameshbabu. R, Selvanayagam. S , Helen Stoeckli-Evans , Bhagavannarayana. G & Ramamurthi. K, 2010,' Synthesis, Crystal Growth, Structural, Optical, Thermal and Mechanical Properties of Semiorganic Nonlinear Optical Material: L-Cystine Dihydrochloride', Journal of Minerals & Materials Characterization & Engineering, Vol. 9,5, PP.495-507.

188. Von Hundelshausen, U, 1971, 'Electrooptic effect and dielectric properties of cadmium-mercury-thiocyanate crystals', Physics Letter A, Vol.34, PP.405-406.

189. Vorobyova. I.V & Kopnicxky. J, 2005,' MeV-atomic-ion-induced tracks on the surface of CaF2 single crystal', Nuclear Instruments and Methods in Physics Research Section B: Beam Interactions with Materials and Atoms, Vol. 237, PP. 593-601.

190. Wang. X, 2002, 'Structure-activity relationships and response-surface analysis of nitroaromatics toxicity to the yeast (Saccharomyces cerevisiae)', Chemosphere, Vol. 46, 7, PP. 1045-1051.

191. Wang. Z. G, Dufour. Ch, Paumier. E &Toulemonde. M 1994, 'The Se sensitivity of metals under swift-heavy-ion irradiation: a transient thermal process', Journal of Physics: Condensed Matter, Vol.6, PP. 6733-6750.

192. Wolfgang Bolse & Beate Schattat, 2002, 'Atomic mixing in thin film systems by swift heavy ions', Nuclear Instruments and Methods in Physics Research Section B: Beam Interactions with Materials and Atoms, Vol. 190, PP 173-176.

193. Wolfgang Bolse, 2002, 'Atomic transport in thin film systems under heavy ion bombardment', Surface and Coatings Technology, Vol. 158-159, PP 1-7.

194. Wooster. W.A, 1953, 'Physical properties and atomic arrangements in crystals', Reports on Progress in Physics, Vol. 16, PP. 62-82.

195. Wrestbrook. J.H, 1958, RL−2033 of the G.E. Research Laboratory USA Report.

Yogam. F, Vetha Potheher. I, Cyrac Peter. A, Tamilselvan. S, Leo Rajesh. A, Vimalan. M & Sagayaraj. P, 2011, 'Growth and characterization of novel semiorganic nonlinear optical crystals of L-phenylalanine hydrochloride (LPHCl) ', Advances in Applied Science Research, Vol. 2, 1, PP. 261-268.

196. Youmei Sun, Zhang, C, Zhu, Z, Wang, Z, Jin, Y, Liu, J & Wang,Y, 2004,' The thermal-spike model description of the ion-irradiated polyimide', Nuclear Instruments and Methods in Physics Research B: Beam Interactions with Materials and Atoms, Vol. 218, PP. 318-322.

197. Yvette Le Fur, Muriel Bagieu- Beucher, & Masse Rene, Jean- Francois Nicoud and Jean- Pierre Levy, 1996, 'Crystal engineering of non centrsymmetric structures based on 2- amino 5- nitropyridine and n-chloroacetic acid assemblies' Chem. Mater, 8, PP 68-75.

198. Zaccaro. J, Capelle. B, Ibanez. A, J. 1997, 'Structural characterization and crystal growth of the 2-amino-5-nitropyridinium dihydrogenphosphate /arsenate hybrid solid solution', Journal of Crsytal Growth, Vol. 180, PP. 229–237.

199. Zaccaro. J, Bagieu-Beucher. M & Espeso. J, & Ibanez. A, 1998, 'Structural characterization and crystal growth of the 2-amino-5-nitropyridinium dihydrogenphosphate/arsenate hybrid solid solution', Journal of Crystal Growth, Vol. 186, PP. 224–232.

200. Zernike and John E. Midwinter, 1973, Applied Nonlinear Optics, John Wiley & Sons Inc.

201. Zhang. X & Xue. D, 2007, 'Bond Energy Prediction of Curie Temperature of Lithium Niobate Crystals', Journal of Physical Chemistry B, Vol.111, PP. 2587.

202. Zumsteg. F.C, Bierlein. J.D & Gier. T.E 1976, '$K_xRb_{1-x}TiOPO_4$: A new nonlinear optical material', Journal of Applied Physics, Vol. 47, PP. 4980–4985.

203. Zyss Jossph, Masse Rene, Muriel Bageu-Beucher & Jean Pierre Levy, 1993, ' Quasi-Perfect Polar Alignment of Nonlinear Chromophores in a Crystalline H-Bonded Guest-Host Structure: 2-amino-5-nitropyridinium- L-monohydrogentartrate', Advanced materials, Vol. 5, 2, PP. 120-124.

204. Zyss. J & Chemla. D.S (eds.), 1987, Nonlinear Optical Properties of Organic Molecules and Crystals, Academic Press, Orlando, Florida, PP. 23.

205. Zyss. J (eds.), 1994, Molecular Nonlinear Optics: Materials Physics and Devices, Academic, New York.

206. Zyss. J , & Oudar. J.L,1982,'Relations between microscopic and macroscopic lowest-order optical nonlinearities of molecular crystals with one- or two-dimensional units', Phys. Rev. A Vol. 26, PP. 2027-2049.

207. Zyss. J, 1979, 'Hyperpolarizabilities of substituted conjugated molecules. II. Substituent effects and respective σ-π contributions', Journal of Chemical Physics, Vol.70, PP. 3341–3349.